CHARACTERIZATION OF THE SPATIAL AND TEMPORAL CONTROLS ON SOIL MOISTURE AND STREAMFLOW GENERATION IN A SEMI-ARID HEADWATER CATCHMENT

by

Christopher Jason Williams

A thesis

Submitted in partial fulfillment

of the requirements for the degree of

Master of Science in Geology

Boise State University

December 2005

The thesis presented by Christopher Jason Williams entitled Characterization of the Spatial and Temporal Controls on Soil Moisture and Streamflow Generation in a Semi-Arid Headwater Catchment is hereby approved:

James P. McNamara
Advisor

David G. Chandler
Committee Member

Mark S. Seyfried
Committee Member

John R. Pelton
Graduate Dean

ACKNOWLEDGEMENTS

This project, like most theses, includes the support and work of many more individuals than the title page reflects, and support comes in many ways. This project would not have been possible without the technical, financial, and emotional support of those individuals. For the technical support and direction, I would like to thank three primary research advisors: Dr. Jim McNamara, Dr. David Chandler, and Dr. Mark Seyfried. A particular thanks goes to Dr. Jim McNamara for serving as my primary advisor, always having an open door to hear my questions, and for consistent insight into research questions and methods. The weekly insight from Dr. McNamara was central to the success of this project. I would also like to thank the numerous faculty members of the Geosciences Department at Boise State University that offered direction during this study.

Additional technical assistance by way of research insight, field work, instrumentation, and data analysis was given by numerous graduate students at Boise State University. The list of contributors includes: Heather Best, Rick Friese, Laura Grant, Justin Huntington, Patrick Kormos, Daniella Makram-Morgos, Mike Procsal, Eric Rothwell, and Melissa Yenko. Additional technical assistance was provided by graduate students at Utah State University. Directed field assistance was also provided by Steve Newsom and Brent Newsom.

The funding for this project was largely provided by the United States Department of Agriculture Natural Research Initiative (Grant Number 2001-35102-11031). Additional funding for my studies at Boise State University was provided through graduate teaching and research assistantships through the Geosciences Department at Boise State University.

Finally, I would like to thank my wife Andrea for her undaunting support of my efforts and for consistent encouragement through the project. Her support was paramount to the production of this thesis and my success along the way. I could not have done this without her. Thank you, Andrea, for your gift of patience and for giving so much of yourself for this project. I would also like to thank my parents and my friends for encouragement and support during this journey.

ABSTRACT

In recent years, increased demands have been placed on hydrologists modeling catchment scale hydrology. Historically, it has been acceptable to predict streamflow at the catchment outlet without partitioning physical processes (lumped modeling) that control catchment scale responses. Hydrologists are now challenged with partitioning processes controlling hillslope hydrology and stream responses and distributing those processes (distributed modeling) over various scales to improve hydrologic modeling. Increased demand for distributed versus lumped hydrologic models has led to the derivation of multiple topographic and wetness indices to parameterize soil moisture patterns. Many of the commonly derived indices assume steady state flows, common in humid environments, and are poor predictors of hydrologic processes occurring in semi-arid environments. The purposes of this study are to facilitate understanding of hillslope flowpaths and streamflow initiation and cessation in the semi-arid, snow-dominated Upper Dry Creek Experimental Watershed (UDCEW) and to improve the predictive capability of terrain and wetness based indices for modeling soil moisture patterns and hillslope processes occurring in the UDCEW.

Soil moisture patterns for the UDCEW were characterized from measured near-surface (upper 30 cm of soil profile) and modeled (SHAW model) deep (up to 1.2 m) soil moisture contents. Mapping soil moisture patterns identified a saturated subsurface source area that developed near the channel head early in the fall wet-up period. Streamflow initiated as the size of the subsurface source area increased during the late

fall wet-up or early in the hydrologically wet season and ceased as the subsurface source area decreased during the late spring drydown. Streamflow generation at the site is then partially dependent on the distribution of fall (wet-up) season soil water to a saturated subsurface source area adjacent to the channel head.

Seasonal soil moisture patterns were statistically compared with site characteristics (surface and bedrock topography, soil depth, soil structure, and vegetation patterns) to determine the temporal and spatial variability of the controls on soil moisture. Results suggest that the controls on soil moisture patterns and hillslope processes at the site vary with hydrologic regime and are different from hydrologic controls commonly observed under humid, steady state conditions. Modified topographic wetness indices were created to characterize the observed hydrologic controls. Observed soil moisture patterns were more positively correlated with modified indices than indices commonly reported in literature. Performance of modified and commonly used indices exhibited seasonality. In the near surface, indices inclusive of soil depth best explained soil moisture variability during the wet-up, hydrologically wet, and drydown periods and indices that parameterized water input and evapotranspiration best explained soil moisture variability during the dry period. For deep soil moisture parameterization, indices inclusive of soil depth best explained soil moisture during the wet-up and hydrologically wet periods, and soil moisture during the dry and drydown periods was best explained by a process based index of water input and evapotranspiration. The findings suggest that, for semi-arid climates like the UDCEW, a multi-index approach to distributed modeling may be necessary to accurately simulate seasonal variation in soil moisture patterns.

TABLE OF CONTENTS

LIST OF FIGURES

LIST OF TABLES

1. INTRODUCTION

In recent years, increased demands have been placed on hydrologists modeling catchment scale hydrology. Historically, it has been acceptable to predict streamflow at the catchment outlet without partitioning physical processes (lumped modeling) that control catchment scale responses (Moore, Grayson, and Ladson, 1991). Hydrologists are now challenged with partitioning processes controlling hillslope hydrology and stream responses and distributing those processes (distributed modeling) over various scales to improve hydrologic modeling. However, there is little agreement among researchers regarding the scale of physical processes that should be represented in hillslope hydrologic models and regarding the appropriate distributed model for predicting hydrologic responses over wide ranging scales (Troch, Mancini, Paniconi, and Wood, 1993; Freer, McDonnell, Beven, Peters, Burns, Hooper, Aulenbach, and Kendall, 2002).

Interests in soil moisture patterns over various scales have increased with the development of distributed hillslope hydrologic models (Western, Grayson, Blöschl, Willgoose, and McMahon, 1999). Soil moisture exerts significant influence on water and energy balances and sustains a feedback between the land surface and atmosphere. Soil moisture partitions precipitation into infiltration and runoff, determines the extent of groundwater recharge, affects evapotranspiration by controlling water availability to plants, and affects soil pedogenic processes (Grayson, Western, Chiew, and Blöschl,

1997; Seyfried, 1998). Therefore, knowledge of spatial and temporal soil moisture variability is important in understanding and predicting hydrologic processes at the hillslope and small catchment scale.

The increased demand for distributed versus lumped hydrologic models has led to the derivation of multiple topographic and wetness indices to parameterize three-dimensional terrain effects on soil moisture distribution and hillslope hydrology (Beven and Kirkby, 1979; Burt and Butcher, 1985; Moore et al., 1991; Barling, Moore, and Grayson, 1994; and Quinn, Beven, and Lamb, 1995). Hydrology models often employ indices to predict soil moisture at the point scale and then distribute soil moisture across the hillslope. The distributed model is then used to predict stream responses to hillslope water inputs. Many of the commonly derived indices assume steady state flows, common in humid environments, and are poor predictors of hydrologic processes occurring in semi-arid environments (Grayson et al., 1997; Gómez-Plaza, Martínez-Mean, Albaladejo, and Castillo, 2001). Thus, time series soil moisture data are needed from semi-arid environments to investigate seasonal controls on soil moisture at the hillslope scale, facilitate the understanding of hillslope flowpaths, and improve the predictive capability of commonly used topographic and wetness indices through variable amendments indicative of semi-arid hillslope hydrologic processes.

1.1 Project Description

The purposes of this study are to facilitate understanding of hillslope flowpaths and streamflow initiation and cessation in the semi-arid Upper Dry Creek Experimental

Watershed (UDCEW) and to improve the predictive capability of terrain and wetness based indices for modeling soil moisture patterns in the UDCEW. The following hypotheses were tested: 1) streamflow initiation and cessation in UDCEW are controlled by soil moisture conditions within the catchment; 2) many commonly used terrain and wetness indices do not accurately depict the hillslope hydrologic processes occurring in the UDCEW.

To test these hypotheses, soil moisture patterns were measured (near-surface) using time domain reflectometry (TDR) and modeled (at the soil-bedrock interface) using the Simultaneous Heat and Water (SHAW) model (Flerchinger, Hanson, and Wright, 1996). Results were used to evaluate the spatial and temporal variability of and the controls on soil moisture patterns in the UDCEW. These patterns were coupled with hydrologic parameters (precipitation, evapotranspiration, streamflow, flow along the soil-bedrock interface, and groundwater recharge) from a water budget analysis (2003 – 2004 water year) to investigate correlations between soil moisture patterns at various depths and the timing of streamflow initiation and cessation. The UDCEW is characterized by shallow soils (average depth is 45 cm) over granitic bedrock.

Measured and modeled soil moisture data were tested for statistical correlation with commonly used topographic and wetness indices. Soil moisture patterns and basin characteristics (topography, soils, and vegetation) were statistically analyzed (standard and geostatistical methods) to determine spatial and temporal controls on soil moisture patterns at the UDCEW. The results were incorporated into terrain and wetness indices to improve predictive capability of many commonly used indices. Findings from the soil moisture distribution and streamflow research were compared against mapped seasonal

soil moisture patterns, field observations, and results from previous studies in the UDCEW to explain hillslope hydrologic processes occurring in the study area.

1.2 Scientific Background

1.2.1 Hillslope Hydrology Overview

1.2.1.1 Soil Water Movement in the Unsaturated Zone

In semi-arid climates, most processes involving soil-water interactions with plants and the atmosphere occur when soils are unsaturated. The unsaturated zone (also called vadose zone) is referred to as the area between the ground surface and the water table (Hornberger, Raffensperger, Wiberg, and Eshleman, 1998) and encompasses the capillary fringe (area above the saturated zone where pore pressure is less than the atmosphere), an intermediate zone just above the capillary fringe, and the soil water zone. Pore spaces in the capillary fringe are saturated or near saturation and pore water is held there by surface tension (capillary forces). The intermediate zone is often referred to as the zone of aeration and is the area between soil water and the capillary fringe. The upper zone is the rooting area where water losses from the soil are through root uptake or atmospheric exchange. The term volumetric moisture content or soil moisture content refers to volume of water per bulk volume of a soil sample. As soils in the unsaturated zone drain there is a quasi-stable soil moisture content at which further decreases in soil moisture are minimal. This stable state is termed the field capacity.

Flow in the unsaturated zone involves complex relations between soil water content, suction, and conductivity (Hillel, 1998). In general, flow through soil materials

results from a hydraulic potential gradient (in the decreasing direction) and is proportional to the flow gradient and the geometries of the soil/rock matrix. Water in the unsaturated zone is subject to a negative matrix or suction potential created by the cohesion of water to the soil matrix (particles and pores). The relationship between the suction pressure applied to the soil matrix and the respective volume of water per bulk soil sample retained against suction defines the moisture characteristics of the soil. Moisture characteristic curves for specific soils are plotted as pressure head (matrix potential) versus volumetric soil moisture content and provide representation of the respective soil response to changes in soil moisture content or pressure (Hornberger et al., 1998).

Flow through a soil matrix is also dependent on the conductivity of the matrix. In saturated soils, pore spaces are filled with water and hydraulic conductivity through the matrix is continuous and maximized. Under unsaturated conditions, soil pores are partially filled with air and conduction is limited by the cross-sectional wetted area. Another difference in conductivity under unsaturated versus saturated conditions is the influence of pore size. Under saturated conditions large pores maximize conductivity, but in unsaturated conditions large pores are often empty and non-conductive due rapid draining during the saturated state. Smaller pores may have a greater hydraulic conductivity under unsaturated conditions.

1.2.1.2 Rainfall/Runoff Relationships and Hydrologic Modeling

Common approaches to hydrologic modeling involve simulation of rainfall/runoff responses. As water arrives at the land-surface there are multiple vertical and lateral fluxes acting on it. These fluxes collectively define the response of a catchment to

precipitation events (rainfall/runoff response) and are parameterized in hydrologic models.

Investigations into rainfall/runoff relationships often begin with examination of the streamflow hydrograph (Figure 1.1). Streamflow response to storm events is identified on the stream hydrograph by noting changes in the shape (rise or fall over time) of the hydrograph (Dingman, 2002). Thus, stream hydrographs provide a signature of the respective stream's response to precipitation events or regimes over time and offer a comparative data source for rainfall/runoff response modeling. Understanding what governs the shape of the streamflow hydrograph allows modelers to make inferences on mechanisms controlling soil water movement and streamflow.

Streamflow response is partially the result of precipitation processing within the respective catchment. Precipitation arriving at soil-atmosphere interface either infiltrates into the soil column, ponds at the surface, or runs over the land surface depending on the infiltration rate of the soil. The infiltration rate is defined as the rate at which water enters the soil. This rate is a function of the rate at which water is arriving, the saturated hydraulic conductivity of the soil, the degree of soil saturation, the soil roughness and slope, the chemical characteristics of the soil surface, and the physical/chemical properties of the water (Dingman, 2002). If the water arrives at a rate greater than the infiltration rate saturation from above occurs and, if on a slope, overland unsaturated flow (Hortonian flow) begins. Once a soil is saturated any additional water delivery laterally or vertically to the surface produces saturated overland flow.

Water infiltrating the soil surface can follow multiple pathways depending on the head gradient. Flow through the unsaturated zone is often referred to as throughflow

(Dingman, 2002). Under simplified conditions, throughflow percolates through the unsaturated zone under tension and is either taken up by plant roots, lost to the atmosphere through evaporation, stored as soil water, or enters the saturated zone. The rate at which water moves through the unsaturated zone depends on the conductivity of the soil matrix and forces acting upon it. The general direction of movement is vertical, however, lateral distribution can occur as soil water encounters earth materials with lower conductivities in the vertical direction.

Infiltrated soil water that flows through soil fissues, root and burrow (worm holes and channels created by soil fauna) channels, and by fingering is considered flow through preferential flowpaths. Such soil features are commonly referred to as macropores. In general pore spaces larger that 1.5 mm are considered macropores. Macropores provide a pathway by which soil water can “by-pass” the soil matrix along “preferred paths”. Flow through or along preferred pathways is common where perched saturated conditions exist (saturated soils separated above the saturated zone). Flow through macropores is much more rapid than flow predicted by Darcy’s Law (common equation for prediction of groundwater flow). Preferential flow typically increases with increases in precipitation or water inputs into the soil. Flow begins in macropores once the soil matrix surrounding the macropore becomes saturated. Downslope delivery of macropore flow can be an important component of the catchment response to precipitation events.

Partitioning flowpaths and/or streamflow sources in rainfall/runoff modeling then requires understanding of the multiple pathways in which water is transported downslope. A common method employed to separate the water sources contributing to streamflow is hydrograph separation. This is done by using isotope tracers to identify new versus old

water shown by the stream hydrograph. New water is event water or water that is new to a catchment from a precipitation event. Old water typically constitutes the base flow and is the groundwater component of a catchment. New and old water have characteristic concentrations of isotopic constituents (Dingman, 2002). Approaches to separating new and old water involve mass balance equations to quantify respective contribution sources (Dingman, 2002). Clearly, understanding the sources contributing to streamflow provides insight into rainfall/runoff relationships, but hydrologists are also concerned with what controls the delivery of soil water to respective flowpaths.

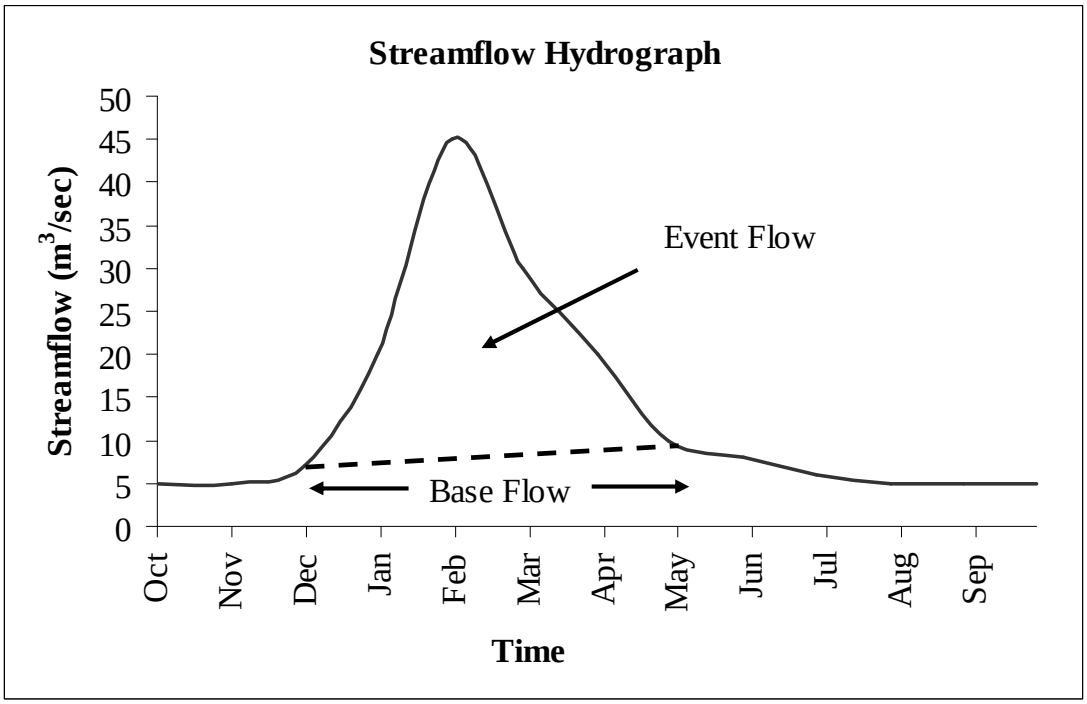

Figure 1.1. Example of a streamflow hydrograph showing streamflow versus time. Event flow (new water) is depicted in the area below the curve and above the dashed black line. Base flow (old water) is shown as the area under the curve and bounded from above by the black dashed line.

1.2.2 Controls on Soil Moisture

Soil moisture variability in time and space along a hillslope is influenced by many factors, including variations in topography, soil properties, vegetation type and density, mean soil moisture content, depth to water table, precipitation history, solar radiation, and other meteorological factors (Famiglietti, Rudnicki, and Rodell, 1998; Gómez-Plaza et al., 2001; and Chamran, Gessler, and Chadwick, 2002). Land surface slope, aspect, curvature, contributing area, and elevation all exhibit elements of control on soil moisture distribution. Steep slopes are characterized by lower infiltration rates, higher surface runoff, and more rapid subsurface drainage than gentle sloping lands (Ridolfi, D'Odorico, Porporato, and Rodriquez-Iturbe, 2003). Adding to the slope component, aspect is directly related to solar radiation and evapotranspiration, with south facing slopes having greater evaporation rates (Moore, Burch, and Mackenzie, 1988). Curvature and upslope contributing area also exert significant influences on local soil moisture. Curvature refers to the convexity or concavity of the land surface. Depressions and concave slopes tend to be wetter than convex slopes that drain more efficiently (Ridolfi et al., 2003). The upslope contributing area can control the volume of available water for lower slopes, and points with larger upslope contributing areas tend to be wetter than those with minimal contributions from upslope features (Gómez-Playa et al., 2001). Higher elevations typically receive more precipitation in the form of snow, most important for water storage on hillslopes in semi-arid regions.

Soil properties and vegetation parameters are often linked and independently and collectively influence the movement of water through the soil profile. The heterogeneity or homogeneity of soil types and textures along a hillslope influences hydraulic

conductivity, structure and complexity of macropores, surface albedo, and vegetative ground cover (Famiglietti et al., 1998). Vegetation affects soil moisture variability in many ways. Leaf area shades soils and impacts evaporation rates, canopy coverage intercepts precipitation, and roots create macropores that increase hydraulic conductivities of soils. Additionally, vegetation uses soil moisture to transpire. The amount of influence that vegetation has on soil moisture distribution varies with vegetation type and the density of ground cover. Hawley, Jackson, and McCuen (1983) and Francis, Thornes, Romero-Diaz, Lopez-Bermudez, and Fisher (1986) found that the variability of soil moisture increased with decreasing vegetative cover.

Antecedent soil moisture conditions also significantly influence soil moisture variability and distribution. Hawley et al. (1983) found that soil moisture variance increased as precipitation depth increased and as conditions became extremely dry. Other studies have posed that peak variance occurs during intermediate periods of wetting and drying (Famiglietti et al., 1998). The correlations between soil moisture and the factors that control it are often dependent on the overall moisture regime (Grayson et al., 1997). When evapotranspiration exceeds precipitation, soil moisture content is strongly influenced by hillslope aspect, vegetation, soil texture, and local topography (Grayson et al., 1997; Ridolfi et al., 2003). When precipitation exceeds evapotranspiration soil moisture is more strongly influenced by depth to the water table and the convergence of contributing areas (Grayson et al., 1997).

1.2.3 Semi-Arid Watershed Processes

1.2.3.1 Seasonal Patterns in Soil Moisture Distribution

Hydrologic processes controlling streamflow initiation and cessation in semi-arid environments are not fully understood. However, hydrologists generally agree that soil moisture content and its variability are key determinants of streamflow generation in small semi-arid catchments and that the controls on the soil moisture patterns in semi-arid environments differ from those in humid environments. Grayson et al. (1997) and Famiglietti et al. (1998) suggest that two regimes exist for soil moisture dynamics along semi-arid hillslopes: a humid regime, where unsaturated lateral flow occurs with significant spatial gradients, and a dry regime, where upslope topography does not affect the spatial distribution of soil moisture. The humid regime dominates when precipitation exceeds evapotranspiration demands. Soil moisture at a particular point during the humid regime is controlled by lateral subsurface flow mechanisms of upslope topography (non-local control). As evapotranspiration rates exceed precipitation controls on soil moisture switch to local dominance. Under local control (dry regime) soil moisture distributions reflect variations in soil properties and vegetation densities. Lateral subsurface flow discontinues, and upper slopes no longer contribute to downslope soil moisture distributions. The dry regime thus is controlled by vertical fluxes under local controls (local soils, vegetation, and evapotranspiration). Understanding these processes affecting the spatial and temporal variations in soil water fluxes facilitates understanding of hillslope flow mechanisms and respective streamflow response.

1.2.3.2 Lateral Sub-surface Flow Pathways

Lateral subsurface flowpaths have been well researched and include matrix, macropore, and bedrock flow (Freer et al., 2002), pressure wave translations (Torres, Dietrich, Montgomery, Anderson, and Loague, 1998), fracture flow (Anderson, Dietrich, Montgomery, Torres, Conrad, and Loague, 1997), and coupled preferential flowpaths (Buttle and McDonald, 2002). Although these studies are primarily from humid environments, they offer insight into potential flowpaths for semi-arid climates during fall wetting and spring snowmelt events.

Freer et al. (2002) investigated subsurface stormflow paths along a trench face in a humid, forested catchment (Georgia Piedmont, Panola Mountain Research Watershed, Stockbridge, Georgia) underlain by granitic bedrock. Their study in conjunction with chemistry analysis from Burns, Hooper, McDonnell, Freer, Kendall, and Beven (1998) demonstrated that flow from macropores along the trenchface at the study site was dilute in base cation concentrations relative to matrix flow. They suggested that macropores along the trench may be connected to a network of upslope and downslope preferential flowpaths (Freer et al., 2002). Spatial tensiometer data from the site suggested that some soil water bypassed the “bulk soil matrix” and perched at the soil-bedrock interface (Freer et al., 2002). Chemistry of the bedrock flow indicated that new water at the soil-bedrock interface laterally displaced old water (Burns et al., 1998). An end-member mixing analysis of five solutes (Na, Mg, Cl, SO_4, and H_4SiO_4) from bedrock, hillslope, and riparian water samples indicated streamflow was dominated by out-crop runoff (Burns, McDonnell, Hooper, Peters, Freer, Kendall, and Beven, 2001). The same analysis indicated the hillslope contributed 10 to 30% of the water in streamflow. Freer

et al. (2002) noted the chemistry data and tensiometer data clearly indicated that preferential flowpaths consisting of macropore and bedrock flow exist at the site and that these preferred flowpaths acted as connecting mechanisms in the generation of stormflow response.

Torres et al. (1998) used an irrigation experiment in steep sloping humid terrain (CB1 Study Catchment, Oregon Coast Range, Coos Bay, Oregon) to examine subsurface flow mechanisms and slope instability. The experiment found that hydrologic responses at the site were controlled by the soil-water retention curve (soil moisture characteristic curve) relations. Soil-water retention properties for the site yielded pressure heads in the near-zero range. Under these conditions, slight increases in water input (snowmelt or rain pulse) produced slight increases in pressure head and a corresponding rapid increase in hydraulic conductivity. These responses propagated a pressure wave and rapid release of old water from the unsaturated zone. Torres et al. (1998) indicate that, for soils with steep soil moisture characteristic curves in the near-zero pressure range, slight rainfall events on wet soil produce slight changes in pressure head, large increases in soil moisture content, and subsequent pressure wave propagation discharging stored soil water. Torres et al. (1998) suggest that such responses in wet soils may be important in developing hydrologic connection (and subsequent streamflow) between the unsaturated and saturated zones.

Investigating the same catchment (identified above) as Torres et al. (1998), Anderson et al. (1997) used sprinkler applications and tracer methods to investigate hillslope flowpaths. The study identified two key flow mechanisms at the catchment: vertical percolation in the unsaturated zone and saturated flow through and along bedrock

features. Flow through the unsaturated zone in the catchment was typically “plug flow”, old water pushed out at the base of the soil column by new water inputs (Anderson et al., 1997). During sprinkler applications, a deuterium tracer suggested “short-residence time” water moved through the unsaturated zone at a rate dependent on irrigation and/or rainfall rates. Bromide tracer injections into the bedrock at a mid-slope location identified rapid flow of old water through weathered bedrock along bedrock fractures. Anderson et al. (1997) showed that downslope thinning of fractured bedrock layers forced bedrock flow upwards near the channel head into a subsurface variable source area. At that location, old water mixed with new water from the unsaturated zone and expanded the subsurface variable source area. Streamflow generation and rates were largely dependent on the size of the variable source area. Streamflow chemistry indicated that bedrock flow contributions represented a larger portion of the flow as the stream returned to base flow levels. This occurred because the zone of mixing was small compared to the overall size of the catchment (Anderson et al., 1997). The study found that the timing of streamflow generation in the catchment was more tied to growth of the subsurface variable source area than the rate of water movement through the catchment (Anderson et al., 1997).

Buttle and McDonald (2002) examined coupled vertical and lateral flow mechanisms (vertical soil water fluxes, flow along the soil-bedrock interface, and macropore flow) in a humid, forested Canadian Shield catchment, Ontario, with thin soil cover. The study incorporated artificial irrigation, spatial soil moisture and tensiometeric data, and a 3.4 m long throughflow trench to examine macroporosity at twenty locations above the trench and to monitor slope runoff along the trench. After irrigating the site

(slightly more than average daily rainfall), rapid vertical fluxes were observed at locations with greater macroporosity. These locations exhibited vertical preferential flowpaths that were largely influenced by the rate of water applied (Buttle and McDonald, 2002). Sites with minimal macroporosity displayed vertical passing of wetting front sequentially from the upper to lower soil profiles. Event water traveled to the soil-bedrock interface at varying rates dependent on the degree of macroporosity. Event water arriving at the soil-bedrock interface mixed with pre-event water and formed an unevenly distributed saturated layer at depth. Lateral macropores at the site contributed minimally to slope discharge until connection developed with the perched saturated layer at the soil-bedrock interface. The study demonstrated that coupled preferential flowpath contributions to stormflow likely depended on soil depth, bedrock topography, and antecedent soil moisture conditions favoring extension and connection of a pre-event saturated layer above the soil-bedrock interface (Buttle and McDonald, 2002).

In a semi-arid environment, Newman, Campbell, and Wilcox (1998) demonstrated that lateral flow mechanisms in a New Mexico ponderosa pine (*Pinus ponderosa*) catchment (sandy loam soil over tuft bedrock) were similar to those observed in more humid environments. The study used natural chloride, dissolved organic carbon, and stable isotope tracers ($\delta^{18}O$ and δD) to identify flowpaths to a trench location at the base of the catchment. During three years of observation, lateral flow was episodic, with most episodes occurring during snowmelt (Newman et al., 1998). Newman et al. (1998) proposed that unsaturated macropore flow at the site occurred when the rate of water input in upper soil layers exceeded the infiltration rate of the soil matrix at the middle soil

layer. Under these conditions, a perched saturated layer developed at the middle soil layer (clay horizon) and began to travel laterally through macropores or along the clay soil horizon. For most of the year, soil moisture at the site was below 0.33 m^3/m^3 and soil water was either absorbed in the upper soil layer or by-passed the upper layer and was perched above the mid-depth clay layer (creating lateral flow). Newman et al. (1998) found that during dry periods concentrations of chloride, organic carbon, and other aqueous species accumulated in the soil profile. During snowmelt, chemistry results identified a flushing of these species and indicated the independent nature of matrix or lateral flow along the clay horizon disappears (Newman et al., 1998).

The brief review of hillslope studies above illustrates the complexity of the controls affecting hillslope flowpaths. Research on this subject continues to grow, but there are still numerous processes for which hydrologists have no adequate quantification (Freer et al., 2002). Most of the literature on hillslope flowpaths comes from humid environments. A review of the literature from humid environments is present here simply because the same processes occurring in humid landscapes occur in snow-dominated semi-arid landscapes during wet seasons. Adding complexity to the hillslope flowpath studies, plant-water dynamics in semi-arid climates are still not clearly understood.

1.2.3.3 Plant-Water Dynamics

1.2.3.3.1 Implication of Plant-Water Dynamics on Soil Water Fluxes

Even though most plant species have above ground morphological modifications to reduce transpiration losses, redistributing soil water downward and/or upward greatly improves soil water use efficiency and augments overall plant competitive strategies during water-limited periods. Such benefits are particularly important in semi-arid

environments. Numerous studies have documented how plants in semi-arid climates alter seasonal soil water fluxes (Burgess, Adams, Turner, and Ong, 1998; Caldwell, Dawson, and Richards, 1998; Sperry, Hacke, Oren, Comstock, 2002; Ryel, Caldwell, Leffler, and Yoder, 2003; and Ryel, Leffler, Peek, Ivans, and Caldwell, 2004). Plant influences on vertical and lateral fluxes thus may be an important component in hillslope hydrologic processes and should be considered in examination of the controls on hillslope soil water distributions.

1.2.3.3.2 Morphological Adaptations

Water conservation is critical in the life cycle of plants in water-limited environments. These plants employ multiple strategies to maintain physiological activity, including morphological specializations to improve water use efficiency. Often plant strategies to maximize or conserve water are considered “reactionary” (Ryel et al., 2004). This implies that plants employ some water conservation method once reduced water uptake occurs. Common reactionary strategies are stomatal control and drought leaf abscission (shedding of drought deciduous foliage). Stomatal responses involve the opening or closing of the leaf and/or stem stomates (small pores) to release moisture (transpiration) or reduce plant water loss. As soil water becomes limited, plants may sense low soil water pressure and close stomates. This process reduces transpiration (water losses) and reduces potential cavitation of xylem vessels (cell tissue responsible for water conductance) (Sperry et al., 2002). Ryel et al. (2004) provide a review of multiple studies suggesting that plants may also incorporate long-term strategies to reduce water loss. Plants may reduce root:shoot ratios (produce less foliage or root

tissue), alter leaf structure/form, and/or produce smaller xylem vessels to regulate soil water use.

Growth forms and water-use strategies differ among plant types and growth forms in semi-arid landscapes. Although water loss regulation occurs predominately in above ground leaf tissue, obtaining available water is largely a function of rooting depth, lateral root spread, and the degree of root system overlap (Schenk and Jackson, 2002). In general rooting depth simulates the above ground biomass. Grasses and forbs have shallow root systems and semi-shrubs, shrubs, and trees have increasingly deeper roots respectively. Schenk and Jackson (2002) found that there was a significant difference in semi-shrub (shrub height < 1 m) and shrub (shrub height > 1 m) root form. The study demonstrated that shrubs produced deeper root systems than semi-shrubs and that lateral spread among the two was equal to root depth and half the root depth respectively. They also noted that grasses and forbs were similar in rooting depth even though root form was fibrous for grasses and taproot for the later.

Two general underlying assumptions associated with root growth and water and nutrient uptake are: roots only extend as deep as necessary to obtain the resources for physiological requirements and that nutrient availability is greatest in the near-surface environment and when soil water content is highest. These assumptions could be extended for semi-arid landscapes to note water availability increases with depth and nutrient availability is greatest immediately following cool season precipitation. Walter (1939) and Schenk and Jackson (2002) proposed two-layered models of water use in water-limited ecosystems based on rooting depth partitioning among herbaceous and woody species. The models suggests that herbaceous and woody plant species compete

for water in the upper soil layers, but that woody plants also extend roots into deep soil layers to obtain soil moisture at depth. Such layered models indirectly suggest that resource requirements for the plant species representing each stratum are different. For example, herbaceous and annual species often senesce during the dry season and have adapted physiological strategies that use seasonal near-surface soil water during the wet periods of the year (Ryel et al., 2004). Shallow rooted fibrous plant species have thus adapted or selected strategies to grow and reproduce within short periods of high seasonal water and nutrient availability in the near-surface environment.

1.2.3.3.3 Hydraulic Lift

Deep-rooted shrub species have also adapted strategies for near-surface nutrient exchange and overall soil water use efficiencies. Richards and Caldwell (1987) introduced the concept of “hydraulic lift”. Hydraulic lift is the passive transport of water by root systems into dry soil layers from more moist soil layers (Caldwell et al., 1998). This process has been noted in at least 19 woody taxa (trees and shrubs) where root systems extend a gradient of soil water pressures and root water loss resistance is low (Caldwell et al., 1998). In the dry season, plants undergoing hydraulic lift absorb soil water from deep soil layers during evening hours when transpiration demands are low. Lifted soil water is transported upward and released to the near-surface soil (soil water pressure, Ψ_s, is less than xylem water pressure, Ψ_p) during the night. The released water is subsequently re-absorbed during the next day to meet daily transpiration demands. The volume of water lifted is largely a function of available deep soil water and the daily transpiration requirements.

Richards and Caldwell (1987) provided the first field evidence of hydraulic lift. The study examined diel (24 hour) fluctuations in Ψ_s and demonstrated that Ψ_s nightly increases and daily decreases were the result of *Artemisia tridentata* hydraulically lifting soil water. Furthermore, covering the shrub with plastic bags during daylight hours (to prevent transpiration) increased daily Ψ_s and exposing the shrub to light during the evening decreased nightly Ψ_s. This subsequent switching of diel cycles further supports that hydraulic lifting was occurring (Richards and Caldwell, 1987). The findings indicated that *A. tridentata* is capable of lifting as much as 1/3 the daily evapotranspiration requirements (Richards and Caldwell, 1987).

Literature has debated whether water should more easily move into root systems than out of root systems (Caldwell et al., 1998). Plants may exhibit such "rectifier" properties that involve physiological changes in the root tissue resulting from reduced water availability. However, these changes usually occur over periods greater than the diel fluctuations associated with hydraulic lift. In fact, several studies have shown that rewetting over diel time periods gradually increased root tissue permeability and new root growth (Caldwell et al., 1998). Additionally, Williams, Caldwell, and Richards (1993) demonstrated that hydraulic lift occurs in *A. tridentata* under very dry soil conditions (-5.0 MPa).

Hydraulic lifting clearly poses advantages for deep rooted plant species in water-limited environments. One could also pose the argument that hydraulic lift makes water available to all plants with roots in the near-surface and increases the longevity of shallow-rooted plants during dry period. This would pose conflicting resource competition for deep-rooted species sharing near-surface nutrients and lifted water.

Several studies have shown that hydraulic lift provides water allocation benefits to some shallow-rooted species (Dawson, 1993). However, most plants with shallow and fibrous roots complete seasonal physiological processes during periods of high near-surface soil water content and develop xylem cavitations during the dry season. As the near-surface environment dries out, shallow-rooted species die off and competition for near-surface soil nutrients is reduced. Deep-rooted species delaying hydraulic lift to the near-surface can then extend the growing season and, by wetting the near-surface, improve near-surface nutrient acquisition during periods of the year when competition is low (Caldwell et al., 1998).

1.2.3.3.4 Hydraulic Redistribution

Caldwell et al. (1998) proposed that in addition to hydraulic lift, the reverse of the process might also occur as Ψ_s dictates. Burgess et al. (1998) used sap flow fluxes to demonstrate that as soils wet-up following the dry season, soil water was transported by near-surface tree roots to deeper, drier soil pockets. They termed the process "hydraulic redistribution" and examined rates of soil water redistribution following pulse precipitation events. For *Grevillea robusta*, lateral root sap flow was negative during the night and at times with lower rates of transpiration. Flow rates were positive during periods of high transpiration demands, suggesting hydraulic lift. Following rain events, there was a reversal of this process. Sap flow rates then were positive in the lateral roots when the near-surface soil moisture was high. Water continued to be taken up during the evening hours. The results suggest potential reversal of lift during near-surface wetting periods and subsequent transfer of water to deeper soil layers (Burgess et al., 1998).

Burgess et al. (1998) performed the same analysis on *Eucalyptus camaldulensis* and discovered the same patterns of hydraulic redistribution (or reversal of hydraulic lift) occurred with this tree species following pulse precipitation events. The study clearly demonstrates that downward redistribution of soil water can occur when water potential gradients vary with depth (Burgess et al., 1998). In a similar study, Ryel et al. (2003) discovered that pulse rain events in a stand of *A. tridentata* delivered rain at different depths simultaneously rather than sequentially from upper to lower soil layers. This process might be expected with macropore or fracture flow, however, the arrival times at the different depths were simultaneous over a few days rather than hours as commonly reported for macropore and other preferred flowpaths.

Ryel et al. (2004) demonstrated that *A. tridentata* benefits from hydraulic redistribution downward during the wet season (fall/spring rain and over-winter snow recharge seasons) and upward (hydraulic lift) during the dry season. Downward redistribution reduces water uptake by competing plants in the near-surface, prolongs water availability during drought periods, and improves water use efficiency through uniform distribution of water through the entire soil column. This downward process stores water in deeper soil pockets and allows *A. tridentata* to reverse the process upward during times when water is limited in the near-surface.

Ryel et al. (2003) identified four advantages to downward and subsequent upward vertical redistribution of seasonal soil water. First, by redistributing soil water plant water potential remains higher throughout the summer (high transpiration rates) when water use is often limited by soil hydraulic conductance. Secondly, an even distribution of soil water in the soil column improves hydraulic conductivity between the roots and

soil and creates a more efficient use of available soil water. This may be important following over-winter recharge when soil water availability varies with conductivity through the soil column. A third benefit to redistribution is increased photosynthesis rates during warmer optimal seasons. Redistribution reduces water use during the early growing season and increases available water during the dry season. Water availability during the dry season allows for continued photosynthesis and higher transpiration rates when other plants have senesced. A fourth benefit of redistribution is the storage of water at depth, a reduction of water available to competitors in the near-surface environment.

1.2.4 Terrain and Wetness Indices

Terrain and wetness indices, herein referred to as wetness indices, in hydrologic models were originally developed to estimate the depth to a shallow water table and to predict locations of saturated source areas (Western et al., 1999). Uses of these indices have expanded to include the prediction of spatial soil moisture patterns to be included in distributed models of hillslope hydrology. The most well known wetness index, developed by Bevin and Kirkby (1979), is the $\ln(a/\mathrm{Tan}\beta)$, where a (specific catchment area) is the upslope contributing area above a contour unit divided by the length of that contour unit and β is the local slope angle. O'Loughlin (1986) modified the index – $\ln(a/T\times\mathrm{Tan}\beta)$ - to include the transmissivity (T) of a saturated soil profile. Both indices are used to predict spatial soil moisture patterns.

Derivation of wetness indices requires quantification of the representative topography. Digital terrain analysis (DTA's) software and digital elevation models (DEM's) are commonly employed to quantify basin topography. DEM's provide digital

projection of basin topography. DTA's provide a framework to calculate and analyze features projected by DEM's. Some commonly measured features include hillslope aspect, slope, curvature, convexity, and concavity. Elevation is altitude above mean sea level, aspect is the azimuth angle parallel to the steepest downhill direction, and land surface slope is the rate of change in elevation in the *x*- and *y*- directions. Convexity and concavity are used to explain the mean upward or downward curvature of the landscape. Profile curvature describes the concavity or convexity of the hillslope perpendicular to elevation contours and plan curvature refers to the curvature of the elevation contours. Mean curvature explains the average curvature tangential to flow lines. Longitudinal curvature defines curvature normal in the direction of aspect and cross-section curvature describes curvature normal and perpendicular to aspect. Negative values represent concavity and positive values indicate convexity for all measures of concavity, convexity, and curvature. Zero values represent intermediate zones, neither convex nor concave.

The use of wetness indices in distributed models infers some inherent assumptions on the processes controlling soil moisture distributions at the respective study location. The assumptions of the indices are: 1) subsurface lateral flow is the dominate control on soil moisture distributions; 2) the process occurring are at a steady state – soil moisture at any point in the catchment is influenced by lateral flow from the entire upslope contributing area (Barling et al., 1994). Hillslope analysis of soil moisture distributions predicted with topographically derived wetness indices have produced mixed results (Burt and Butcher, 1985; Moore and Thompson, 1996; Western et al., 1999; and Gómez-Playa et al., 2001) and have been criticized for being inappropriate in semi-arid climates (Grayson et al., 1997; Gómez-Playa et al., 2001). For most of the year

in semi-arid environments, soil moisture distribution is controlled by vertical, not lateral, fluxes and there is no hydrologic connection between points on a hillslope and the upslope contributing area. In these environments, lateral soil water redistribution is limited to short periods of the year (wet season) when precipitation exceeds evapotranspiration (Grayson et al., 1997).

Multiple variations of the Bevin and Kirkby (1979) index have been proposed (Burt and Butcher, 1985; Moore et al., 1988; Barling et al., 1994; Western et al., 1999; Gómez-Playa et al., 2001; and Freer et al., 2002). Moore et al. (1988) found that a multiple regression approach inclusive of the wetness index, ln(a/Tanβ), and aspect improved the prediction of soil moisture spatial variation. In a 7.5 ha catchment in New South Wales, Australia, the study found that the wetness index alone explained 26 to 33% of the variation, and the modified index explained 31 to 41% of soil moisture spatial variation. On a 1.4 ha hillslope in South Devon, United Kingdom, Burt and Butcher (1985) found that the wetness index explained less than 25% of the variance in depth to saturation. Modified indices (a × plan curvature, (a/Tanβ) × plan curvature, and a/β) improved predictions of saturation depth and slope discharge. In small semi-arid catchments in Spain, Gómez-Playa et al. (2001) investigated modified wetness indices that represented seasonal controls on soil moisture patterns in burnt and unburnt catchments. The study found that including aspect, ln((aspect × a)/Tanβ), in the wetness index improved predictions of soil moisture variability from 29 to 37%, 44 to 49%, and 32 to 38% in burnt areas during wet, intermediate, and dry seasonal soil moisture states respectively. In the unburnt areas removal of slope, ln(aspect × a), from the modified index improved predictions of soil moisture variability from 12 to 66% in the wet state;

no significant correlation was found in the unburnt zones for the intermediate and dry states.

Clearly, the uses of indices to parameterize hillslope processes require assumptions and those assumptions may not always be indicative of the processes occurring in every climate regime and for all possible variations in basin characteristics. The advent of DEM's and the increased availability of digital terrain analysis software have simplified calculations of terrain based wetness indices. However, there is still significant uncertainty in the application of specific wetness indices over varying scales and climate regimes. Furthermore, research has demonstrated that surface topography is often a poor predictor of soil moisture patterns (Freer et al., 2002). Additional uncertainty exists regarding the scale at which field data must be obtained to accurately model the influence of basin characteristics on hillslope hydrologic processes. Freer et al. (2002), Grayson et al. (1997), and Moore et al. (1991) provide reviews of multiple wetness index modifications, improved predictive capability of modified wetness indices, and trends in spatial data collection required to explain hillslope hydrologic processes depicted by wetness indices.

1.2.5 Water Balance Approaches in Semi-Arid Environments

Increasing interests in distributed hydrology models have brought scale affects of hydrologic responses to the forefront of water balance hydrologic research. Focused efforts in this area have been applied to formulate scale related concepts and equations that estimate basin characteristic responses. Such models are used to simulate average hydrologic responses at the basin scale and calibration and validation are often based on lumped hydrologic response (i.e., discharge at the outlet).

Semi-arid environments pose significant scale dilemmas for researchers and resource managers modeling hydrologic responses at the basin scale. The water balance in these environments is dominated by seasonal precipitation and evapotranspiration trends, and basin characteristics exhibits significant variability not commonly represented in hydrologic modeling (Flerchinger, Cooley, Hanson, and Seyfried, 1998). Common solutions to these problems include stratified hydrologic modeling. Such approaches break the landscape into disaggregated parcels with similar physical and vegetative conditions (Kattlemann and Elder, 1991). Water balances are computed individually for the disaggregated parcels and the final basin balance (aggregated balance) is computed by combining the inputs and outputs of the disaggregated areas (Flerchinger et al., 1998).

Flerchinger et al. (1998) compared aggregated and lumped approaches to a water balance for a 26 ha mountainous semi-arid snow-dominated catchment in the Reynolds Creek Experimental Watershed in southwest Idaho, USA. The lumped model assumed the entire catchment was uniform regarding water inputs and basin characteristics. The aggregated approach disaggregated the landscape into units based on vegetation, soil characteristics, and snow inputs.

Flerchinger et al., (1998) calculated a partial water balance for each disaggregated unit and an overall water balance by adding together (aggregating) the inputs and outputs calculated for each disaggregated unit. Precipitation was measured within each landscape unit and evapotranspiration was estimated using the SHAW (Flerchinger et al., 1996) model. The water balance for each respective year of the two year study had a discrepancy of -17 and 55 mm for the aggregated approach and 42 mm and 86 mm for the lumped approach. Flerchinger et al. (1998) noted that the largest difference between

the two approaches for both study years was the modeled evapotranspiration and that the evapotranspiration results identified the inability of the lumped approach to recognize areas where soil water was available for transpiration and areas where soil water availability was limited by high transpiration rates. The study illustrates the importance of parameterizing processes that affect basin hydrologic response.

1.2.6 Methods to Measure Soil Moisture

To this point, this introduction has focused on the need to parameterize distributed hydrologic models and has highlighted approaches (wetness indices) and problems with current methods in parameterizing hydrologic variables for modeling basin scale responses. As discussed earlier, soil moisture affects many key hydrologic processes in hillslope hydrology and patterns of soil moisture are often used to assist the understanding of hillslope responses to precipitation inputs and evapotranspiration demands and to calibrate and validate distributed hydrology models. There are multiple methods to collecting soil moisture data, including: 1) gravimetric sampling, 2) remote sensing, 3) ground penetrating radar (GPR), and 4) time domain reflectometry (TDR). Each method has positive and negative aspects regarding approach and application.

1.2.6.1 Gravimetric Sampling

Gravimetric sampling involves the removal of a soil core and determination of the moist and dry weights of the core. The moist weight is obtained by weighing the sample in the field at the time of sampling; the dry weight is determined by weighing the sample in the laboratory after drying it at 105º Celsius (°C) in an oven. The soil moisture or wetness is then calculated as the loss in mass of the core resulting from drying. Gravimetric sampling is cost effective, but there are multiple problems with the approach.

The method is time consumptive (even at the field scale) due to the large amount of time required for sampling, weighing the samples, and drying the samples in an oven. Furthermore, disturbance of the core during sampling and transport is common and core volumes are often not representative of the elementary volume of the surrounding pore-size distribution (Sherlock, Chappell, and McDonnell, 2000).

1.2.6.2 Remote Sensing Applications

Remote sensing of soil moisture data has become increasingly popular with the advent of global hydrology models used to forecast ecosystem responses to climate change. This method employs passive microwave radiometry or active radar instruments to map soil moisture over large regions (Huisman, Sperl, Bouten, and Verstraten, 2001). Remote sensing applications have low spatial resolution and can vary in footprint size from hundreds of meters to tens of kilometers. The large variation associated with this application results from averaging soil moisture variability within sensor footprints, not depicting the detail at the land surface, and is largely related to topography, microclimate, tillage, and water use by plants (Famiglietti, Deveraux, Laymon, Tsegaye, Houser, Jackson, Graham, Rodell, and van Oevelen, 1999). Thus, although remote sensing provides a labor efficient method of obtaining soil moisture information over large scales, field scale measurements are still required to provide information on the masked variation within the remote sensing footprint (Famiglietti et al., 1999; Huisman et al., 2001; Huisman, Snepvangers, Bouten, and Heuvelink, 2002).

1.2.6.3 Ground Penetrating Radar Applications

Soil moisture research using ground penetrating radar has received much attention in recent years (Huisman et al., 2001; Huisman et al., 2002). Huisman et al. (2001; 2002)

suggest that there is a “scale gap” in soil moisture research between the field scale (point, m^2) and the landscape scale (aerial estimates with remote sensing, km^2) and proposed using GPR for these “intermediate” scale applications. GPR can be applied to soil volumes 0.05 to 20 m^3 and the scale at which the measurement is taken depends on the antenna frequency and the radar configuration (Huisman et al., 2002). The method sends a high frequency electromagnetic ground wave from the source antenna through the soil profile and to the receiving antenna. The velocity at which the wave travels is well correlated with the soil dielectric properties, which are strongly related to soil moisture content (Huisman et al., 2001). The wave travel time is used to estimate the permittivity of the topsoil and the soil moisture content (van Overmeeren, Sariowan, and Gehrels, 1997).

Although GPR has applications at the field and intermediate scales, the approach is not without complication. The use of GPR requires the researcher to know the depth of the reflecting soil horizon (i.e., depth to a clay layer). This often requires drilling, which is invasive to hillslope hydrologic processes. Furthermore, the theory behind the ground wave propagation and the depth of its influence is not well understood (Huisman et al., 2001). Finally, the set-up time for GPR applications is longer than that of other methods like TDR; however, the soil volume of each individual measurement is larger with GPR than with TDR and other point methods. Therefore, there are trade offs between GPR and TDR applications. The use of GPR is increasing and GPR research is moving toward better understanding of the wave theory fundamental to its approach. The method shows promise for applications between the landscape and field or small catchment scales.

1.2.6.4 Time Domain Reflectometry Applications

Time domain reflectometry has become the most widely used technique for measuring volumetric soil moisture content for multiple reasons: 1) TDR accuracy is within 1 to 2% volumetric water content, 2) calibration methods are minimal and often not required, 3) applications are largely non-destructive, 4) radiation hazards are minimal, 4) TDR has excellent spatial and temporal resolution, and 5) use of the instrumentation is fairly simple and can be applied with multiplexing for continuous measurements (Jones, Wraith, and Or, 2002). TDR measures the apparent soil dielectric constant (*Ka*) and uses a calibration equation (Topp, Davis, Annan, 1980; Ledieu, DeRidder, DeClerck, and Dautrebande, 1986) to relate *Ka* to the volumetric water content (soil moisture content of the soil). Topp et al. (1980) demonstrated that TDR could be used with a single calibration curve to predict volumetric soil moisture contents over a range of soils and Jones et al. (2002) demonstrated that the application of the Topp equation (Equation 1.1) provides estimates of volumetric soil moisture content within an estimated error of 0.013 m^3/m^3. Ledieu et al. (1986) expanded on the work of Topp et al. (1980) and calibrated an equation that measured volumetric soil moisture content within 0.01 m^3/m^3 of the actual volumetric soil water content.

TDR instrumentation includes a TDR cable tester (waveform generator) connected via coaxial cable to a multi-rod (2 or 3 rod) probe that is inserted horizontally or vertically into the soil profile (Figure 1.2). The cable tester (TDR100, Campbell Scientific, Inc., in this study) generates an electromagnetic pulse to traverse the length of the cable and probe. The cable tester interface allows the user to specify the length of the cable and probe and then calculates the bulk dielectric constant based on the

electromagnetic pulse travel time. The dielectric constant is a function of the propagation velocity and is related to the soil moisture content using either the Topp et al. (1980),

$$\theta = -0.053 + 2.92 \cdot 10^{-2} \cdot Ka - 5.5 \cdot 10^{-4} \cdot Ka^2 + 4.3 \cdot 10^{-6} \cdot Ka^3 \qquad (1.1)$$

or the Ledieu et al. (1986) equation,

$$\theta = 0.1138 \cdot \sqrt{Ka} - 0.1758 \qquad (1.2)$$

Equations 1.1 and 1.2 are relatively insensitive to soil composition and texture and have proven results in measuring “liquid” water contents in soils (Siddiqui, Drnevich, and Deschamps, 2000; Jones et al., 2002). Jones et al. (2002) reports that both equations provide adequate estimates for soil moisture contents < 0.5 m^3/m^3, the range of values commonly investigated in mineral soil research. However, volumetric water content values greater than 0.5 m^3/m^3 are common in organic and mineral soils with high clay content. The equations are further limited to use in soils with low salinity (Siddiqui et al., 2000; Jones et al., 2002). Calibration equations have been developed for TDR applications where soil clay and organic contents and salinity are high (Siddiqui et al., 2000).

The minimal intrusive applications of TDR are attractive to researchers given the ease of use, rapid set-up procedures, and applicability to continuous data collection. There are some potential limitations to TDR applications however. Soil salinity and water content and probe and cable length and design all affect signal attenuation. Signal

deterioration can occur with cable lengths greater than 30 m (Jones et al., 2002). Thus, use of TDR in large study areas may require multiple field recording stations and require more multiplexing and data logger equipment, increasing the costs of the research.

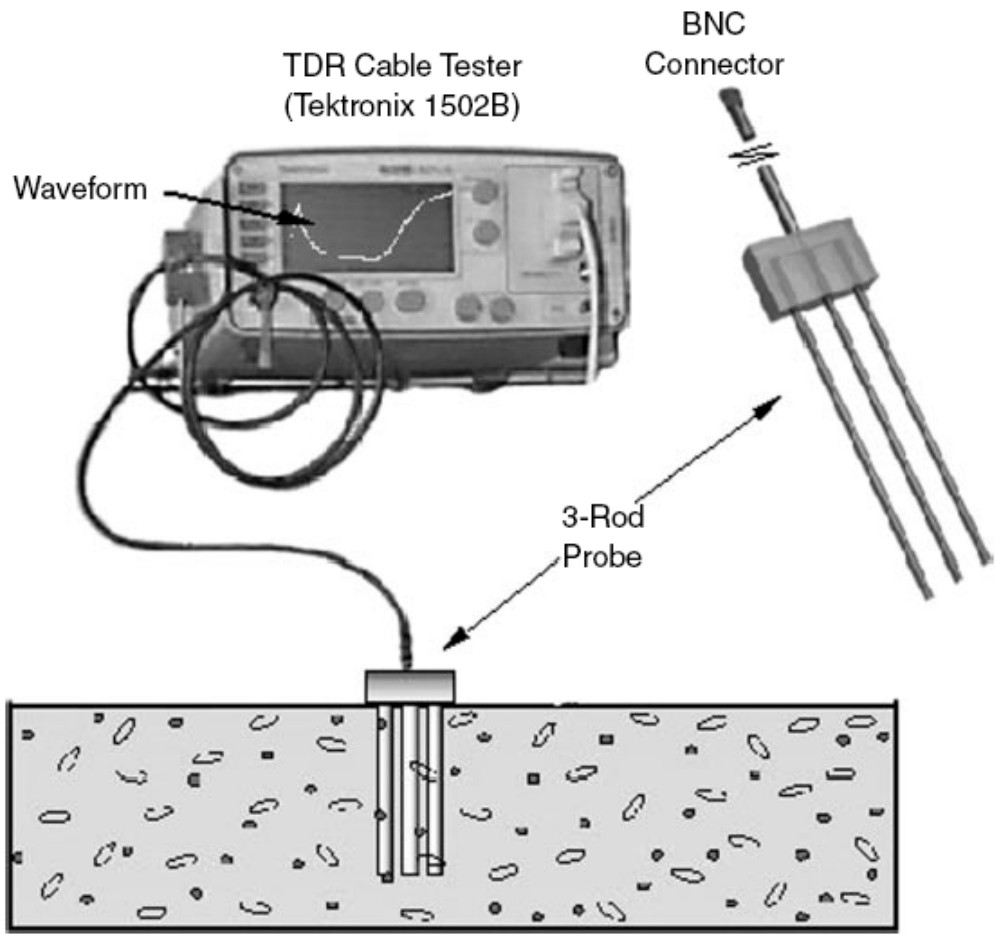

Figure 1.2. Example of possible TDR instrumentation design – cable tester (waveform generator and output interface), connection cable, and 3-rod probe vertically installed in soil column (figure from Jones et al. (2002)).

1.2.7 Time-Stability Analysis of Soil Moisture Patterns

Although distributed hydrologic modeling approaches are becoming more in demand, the data collection requirements for distributed approaches to soil moisture mapping are often too excessive for resource managers interested in soil moisture

patterns. Many resource management professionals are limited by time and funding for equipment and field personnel to collect the required data. Therefore, methodologies for determining sampling strategies that capture time-stable locations (locations representing mean soil moisture content) are of interest. Time-stability soil moisture analysis locates (through temporal ranking statistics of measured soil moisture content) specific parts of the landscape that continuously exhibit mean soil moisture contents regardless of the seasonal moisture regime (Grayson and Western, 1998). Such locations provide researchers and resource managers information on basin average responses without the requirements of numerous sampling locations.

The time-stability concept was introduced by Vachaud, Passerat de Silans, Balabanis, and Vauclin (1985) and suggests that temporal fluctuations and soil moisture contents at certain sites are consistently the same as the field average for the respective study area. Kachanoski and de Jong (1988) concluded that the underlying assumption - a linear relationship exists between soil water storage at successive sampling times across the respective study area – proposed by Vachaud et al. (1985) did not accurately depict scale dependency in soil moisture patterns. Kachanoski and de Jong (1988) expanded the concept with general linear transformations of sampling statistics and demonstrated that spatial scale dependency is related to hydrologic processes operating at different spatial scales. Kachanoski and de Jong (1988) further noted that not all hydrologic processes are scale dependent. For example, they found that soil water recharge (seasonal wet-up period) was scale dependent and that soil drying (drydown seasonal period) was scale independent.

Time-stability approaches offer insight into temporal persistence of some spatial patterns, but there is uncertainty regarding whether specific processes always exhibit the same scale dependent time-stability (Kachanoski and de Jong, 1988). Furthermore, time-stability approaches have been primarily limited to agricultural terrain and have not been widely applied to mountainous catchments with spatially diverse physical and biological characteristics (Grant, Seyfried, and McNamara, 2004). Thus, it is unclear at which scales and basin characteristics time-stability approaches are applicable. Other common approaches (like geostatistics) to analyzing soil moisture patterns often require large data sets. Time-stability methods offer an additional approach to studying soil moisture patterns when data are limited and basin characteristics are spatially consistent.

1.2.8 Geostatistical Analysis of Soil Moisture Patterns

Geostatistical analyses are commonly used to characterize the spatial variability of soil moisture and to investigate the variability of the processes that control the distribution of soil moisture over a range of scales (Grayson and Western, 1998; Western, Blöschl, and Grayson, 1998a; Western, Blöschl, and Grayson, 1998b; Skøien, Blöschl, and Western, 2003; and Western, Zhou, Grayson, McMahon, Blöschl, and Wilson, 2004). Such analyses are required for interpretation of point soil moisture data, estimation of the basin mean soil moisture content, and for distributed hydrologic modeling (Western et al., 1998a). Western et al. (1998a) provide of review of six studies of geostatistical applications to soil moisture research in small catchments.

1.2.8.1 The Variogram

The variogram (Figure 1.3) is the central concept in geostatistics and describes the variability between points as a function of their lag distance (separation distance between

points). The variability between points tends to increase with increased lag distance (points farther from one another are generally less similar). This pattern continues until the variability is stationary (the mean does not change with space); the variogram curve (Figure 1.3) flattens where the variance becomes stationary.

There are three primary components (Figure 1.3) to the variogram (Blöschl and Grayson, 2000). The first component, the sill, depicts the spatial variance of the overall pattern and represents the variogram value at which the curve flattens. The second component is the correlation length (range), a measure of the spatial continuity of measured variable. The range is the distance beyond which the correlation between points is minimal and marks the limit of spatial independence (Webster and Oliver, 2001). Large range values are indicative of smoothly varying patterns; short ranges are representative of erratically varying patterns (Blöschl and Grayson, 2000). Variograms that increase indefinitely with increasing lag distance posses neither a sill nor a range and are referred to as unbounded or stationary. The nugget is the third component of the variogram and represents the variance between points that are very closely spaced together.

The three components are representative of the processes occurring (Blöschl and Grayson, 2000). The sill represents the spatial variance in the processes; the range measures the spatial scale of the processes; and the nugget represents the sum of the two variances due to random measurement errors (non-zero nugget) or due to measurements too coarse to represent the underlying processes (apparent nugget). Non-zero nuggets indicate there is some variance even between very closely spaced points and may represent the measurement error in the variance (Blöschl and Grayson, 2000).

The variogram approach in geostatistics involves computing the sample variogram from measured data. The sample variogram is a plot of the variances of differences of the values of data pairs (*y*-axis) versus their lag distance (*x*-axis). Data pairs are grouped into lag bins and the variance between each pair within each lag bin is calculated. The maximum lag bin in variogram applications is generally set to one-half the maximum separation distance for all data pairs. The maximum lag bin is set to reduce the use of lag bins with few data pairs (there are fewer pairs with greater lag distances). The sample variogram value ($\gamma(h)$) for each lag (h) is calculated as

$$\gamma(h) = \left(\frac{1}{2N(h)}\right) \cdot \sum_{i,j} (\theta_i - \theta_j)^2 \qquad (1.3)$$

where N is the number of data pairs, θ_i and θ_j are the soil moisture at points i and j respectively, and the summation is calculated over all i,j pairs in each lag bin (Western et al., 1998a). The resultant sample variogram is then used to fit a theoretical variogram (Figure 1.3) as a smoothing function.

1.2.8.2 Modeling the Theoretical Variogram

The theoretical variogram (population variogram) is used to determine the sill, correlation length (range), and nugget, if present, for the population. There are numerous models used to fit theoretical variograms (Olea, 1999; Webster and Oliver, 2001). The most commonly applied models in soil moisture research are the exponential, spherical, and power functions (Blöschl and Grayson, 2000). Other models commonly used in geostatistical analyses include the cubic, Gaussian, and logarithmic functions (Olea, 1999). Model fitting involves visual inspection for the “best-fit” model and statistical

fitting by weighted least squares. Additional detail on model selection and fitting for this study is included in the methods section of this document.

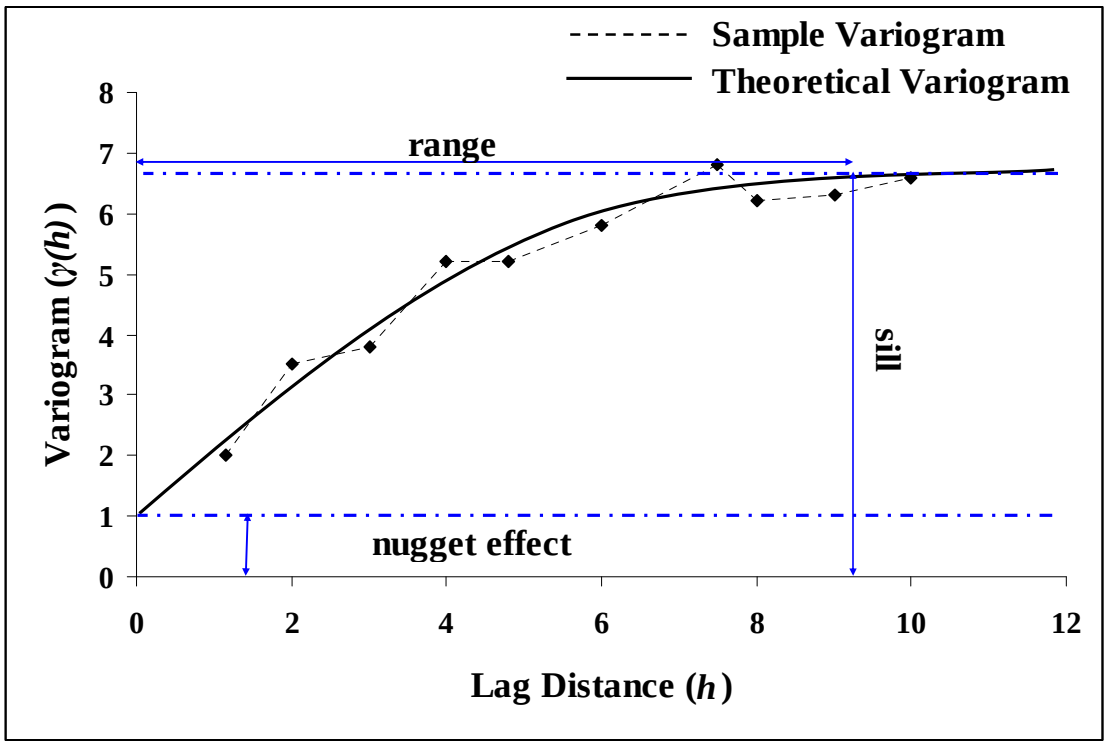

Figure 1.3. Variogram model depicting the sample and theoretical variogram and the model parameters (sill, range, and nugget).

1.2.8.3 Common Pitfalls in Variogram Analyses

Blöschl and Grayson (2000) describe three common pitfalls in geostatistical analyses of catchment hydrology. The first occurs when the nugget of the sample variogram is nearly equal to the sill and indicates that the variance between closely spaced points is no different than the variance between widely spaced points. Variograms of this form violate the fundamental assumption of geostatistics - spatial correlation is useful for spatial interpolations - and are of no use in interpolating spatial correlation of the variable of interest or the process occurring. The second pitfall occurs

when variograms are used to transpose processes across scales greater than the scale at which the data was collected. The range of a variogram is only significant for interpretation of physical processes if the data were collected closely enough to capture the process scale variability. Variograms without a clearly defined sill, range, and nugget indicate that the sampling scale is insufficient to explain the processes occurring. The third pitfall occurs where the data exhibit anisotropy (physical processes acting in preferred directions). Variograms computed from data spaced unevenly in the *x* and *y* direction commonly exhibit anisotropy. Most geostatistical software packages offer variogram computations that account for anisotropy of the sample data. Variograms generated from non-anisotropic data are omni-directional. All three pitfalls can be overcome by reducing the distance between sampling locations or by including auxiliary data in the analysis.

1.2.8.4 Mapping Soil Moisture Patterns through Kriging

The advent of geographic information systems (GIS) and digital terrain analysis software has greatly simplified the spatial mapping of geologic and hydrologic variables. These computer applications usually offer multiple algorithms to estimate values of unsampled locations based on given values at sampled neighboring locations. Spatial distributions are usually structured in one of three primary configurations: 1) triangulated irregular networks (TINs), 2) square-grid networks, or 3) contour-based networks (Moore et al., 1991). TINs are organized by surface specific-points and form irregular (triangular) networks of points based on sets of *x*, *y* and *z* values. Grid-based approaches use regular spaced geometric (square, rectangular, or triangular) grids to establish planes based on sets of *x*, *y*, and equal *z* values. With grid-based methods, an individual plane or

cell is bounded by three or four grid points to build evenly spaced triangular, square, or rectangular grid networks. Contour methods consist of digitized contour lines based on *x* and *y* coordinates positioned along lines of equal *z* values.

Computer based mapping requires interpretation of unsampled locations between known or measured locations and generally assumes values for locations at one point are closely related to the values at nearby points. Furthermore, the assumption generally follows that values for points at one location are poorly correlated with values at distant locations. Kriging (Matherorn, 1963) has become a standard method for estimating values at unsampled locations. The approach uses linear regression techniques to predict values for unsampled locations based on measured values of nearby locations and assumes the variates are not independent. There are several kriging methods available: 1) simple kriging, 2) ordinary kriging, 3) universal kriging, and 4) block kriging.

Simple kriging requires the mean to be known and assumes second-order stationarity (mean, spatial covariance, and semi-variance do not depend upon x in the random function $Z(x)$) (Davis, 2002). Ordinary kriging follows the same assumptions as simple kriging with the exception that the mean be known in advance. The approach assumes the mean of the variable of interest is constant throughout the study region. Universal kriging overcomes the shortcomings of simple (mean must be known) and ordinary (the mean is constant) kriging by allowing for drift (average or expected value of regionalized variable within a neighborhood) and residuals (difference between actual observations and drift). Kriging programs using universal kriging estimate and remove drift to create stationary residuals (krige stationary residuals for estimating residuals at unsampled locations) and combine estimates of residuals with drift to estimate the actual

surface variable. Block kriging is simply an extension of ordinary or universal kriging to include an estimate for a discrete area around an interpolation point rather that an estimation of the value solely at the point. Given the simplification of calculations and that the mean of the population is rarely known, ordinary and ordinary block approaches are the most commonly used kriging methods in soil moisture research. More detailed reviews of kriging methods and equations can be found in Olea (1999) and Webster and Oliver (2001).

2. STUDY AREA

2.1 Local Setting

The UDCEW (Figure 2.1) is a 0.02 km^2 basin in the Dry Creek Experimental Watershed (DCEW). The DCEW (Figure 2.1) is located in the semi-arid southwestern region of Idaho, USA, and is approximately 16 km northeast of the city of Boise, Idaho. The surrounding area is defined as the Boise Front and includes mountainous and foothills topography. The DCEW is delineated as the 28 km^2 northeastward trending Dry Creek drainage from the 1,000 m elevation at the junction of Dry Creek with Bogus Basin Road to the headwaters of Dry Creek near Bogus Basin. The headwaters of Dry Creek are located at an elevation of 2,100 meters in the granitic region of the Boise Front. The perennial creek flows south to southwest from its origin to its confluence with the Boise River west of the city of Boise, Idaho. The upper 11 km of Dry Creek are within the DCEW. Shingle creek is the only perennial tributary draining into Dry Creek. Numerous unnamed intermittent tributaries flow into Dry Creek within and beyond the DCEW boundary.

2.1.1 Climate

Climate in the region surrounding the DCEW results from the opposing Aleutian Low and Pacific High weather systems. The Aleutian Low controls winter weather and

delivers cool, moist air from the west and northwest. Winters in this region are moderately-cold to cold and produce abundant precipitation in the form of snow in the highlands and rain in the lowlands. The spring season begins with cool rainy months followed by drier warming trends approaching the summer months. The Pacific High system dominates the summer period and brings dry air from the Pacific Ocean to the Boise Front. Summers are typically hot and dry with occasional thunderstorm events. The autumn season is typified by clear and warm months immediately following summer and cold and moist months immediately prior to the early winter season.

There are two meteorological stations located in the DCEW: 1) Lower Dry Creek Research Site (LDCRS), 1,100 m elevation and 2) UDCEW, 1,650 m elevation. Both stations are monitored by the Agricultural Resource Service (ARS) and have periods of record from 1998 to present. The average annual precipitation at the LDCRS and UDCEW are 37.25 cm and 57 cm. Another meteorological station is located just north of the DCEW boundary at the Bogus Basin Snotel Site, also monitored by ARS. The Bogus Basin site is located at an elevation of 1,930 m and has an average annual precipitation 100 cm (1999 – present). Precipitation is greatest December through February and the average monthly temperatures are greatest in July and lowest in January. Evapotranspiration exceeds precipitation during most of the year.

2.1.2 Geology and Soils

The DCEW is located over the Atlanta Lobe of the Cretaceous aged Idaho Batholith. The Idaho Batholith is a granitic intrusion and is associated with the Mesozoic subduction zone along the western margin of North America. The Atlanta Lobe is 75 to 85 million years old and is approximately 275 km long and 130 km wide (Johnson,

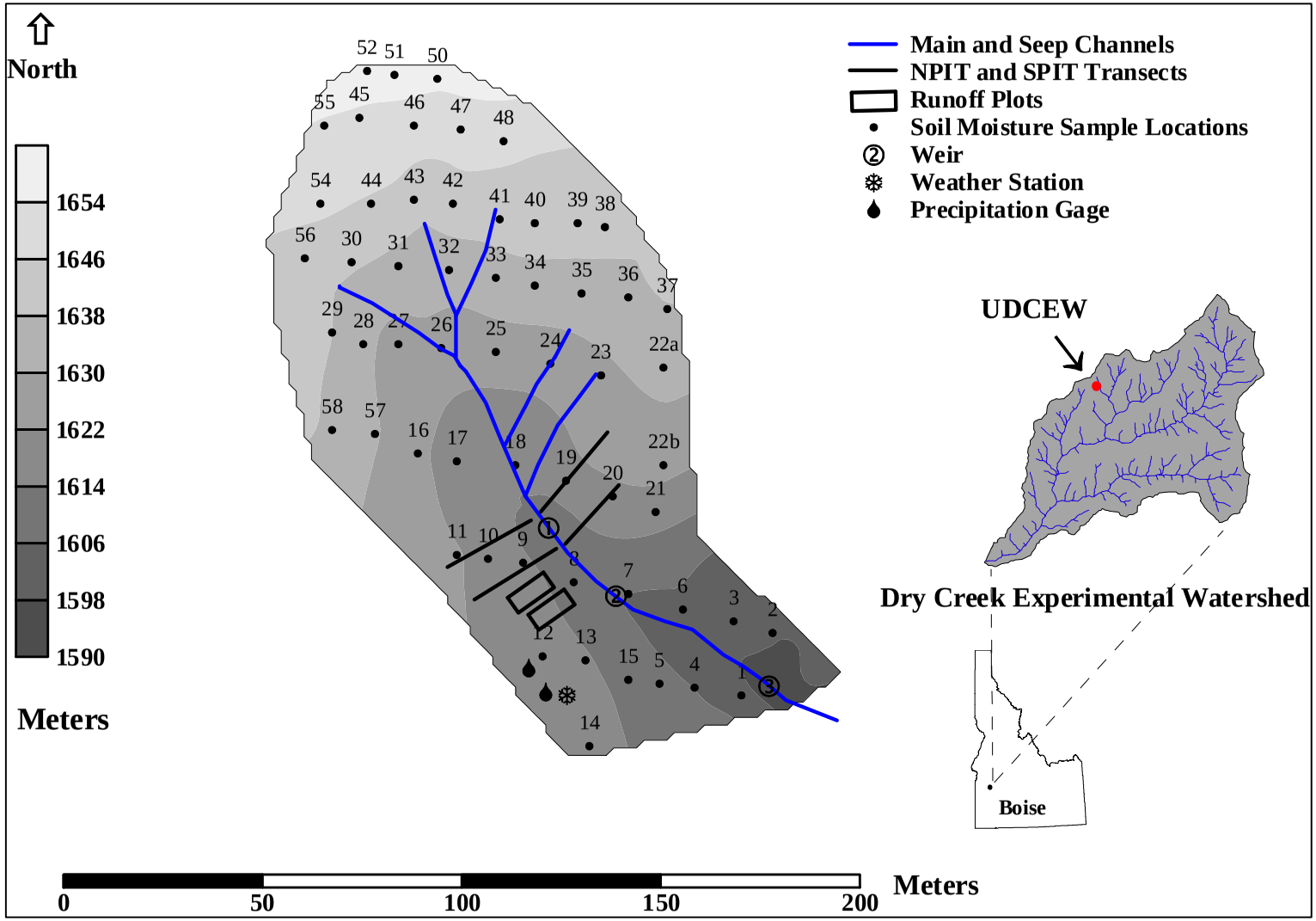

Figure 2.1. Elevation map of the UDCEW showing the study grid (soil moisture sampling locations), site instrumentation, and the regional location of the study area.

Lewis, Bennett, and Kiilsgaard, 1988). The dominant rock unit in the DCEW is biotite granodiorite (Lewis, Kiilsgaard, Bennett, and Hall, 1987). The biotite granodiorite consists of medium- to coarse-grained rocks, is light gray in color, and is composed of plagioclase, quartz, potassium feldspar, and 2 to 8% biotite (Johnson et al., 1988). The landscape in the area is typified by moderately steep slopes, and strongly dissected by streams. The local soils are derived from weathering of the Idaho Batholith and are divided into three general soil taxonomies – Argixerolls, Haploxerolls, and Haplocambids (USDA, 1997). The soils range from loam to sandy loam in texture and have high surface erosion potential. The Natural Resource Conservation's soil survey of the Boise Front (USDA, 1997) provides a more detailed description of the soils underlying the Boise Front region.

2.1.3 Vegetation

Vegetation along the Boise Front varies with elevation, geology, microclimate, soil type, and topography. At lower elevations, grass and shrublands, ponderosa pine (*Pinus ponderosa*), and Douglas-fir (*Pseudotsuga Menziesii)* occupy south and west aspects and Douglas-fir forests dominate north and east aspects. Upper elevations are dominated by ponderosa pine and Douglas-fir forest communities with patches of lodgepole pine (*Pinus contorta*) and aspen (*Populus tremuloides*). Middle elevations range from grass and shrublands to open forest communities of ponderosa pine and Douglas-fir and function as an ecotone between the sagebrush (*Artemisia spp.*) and grass dominated lowlands and more densely forested uplands.

2.1.4 Land Ownership and Activity

Land ownership in the UDCW is divided among multiple governmental entities (Boise National Forest – 42%, State of Idaho – 3%, and Bureau of Land Management – 1%) and private parties (54%). Land use in the basin includes timber harvest, cattle and sheep grazing, and recreation activities (downhill and cross country skiing, hunting and fishing, hiking, mountain biking, motorcycling, snowmobiling, ATV riding, and natural and cultural study).

2.2 Research Site

This study is restricted to the UDCEW (Figure 2.1) portion of the DCEW. The UDCEW is a 0.02 km^2 headwater basin with an outlet located immediately adjacent to and west of Bogus Basin Road at an elevation of 1592 m. The site outlet is marked at 4842066 Northing and 569395 Easting of the Universal Transverse Mercator (UTM) grid system, North American Datum of 1927 (NAD27), and is approximately 10.5 road km (along Bogus Basin Road) from the outlet of the DCEW. Precipitation to the basin is largely in the form of snow (most years), with frequent snowmelt oscillations in late winter and early spring. Rain-on-snow events are common at the site from the late fall wetting period through snowpack ablation in early spring. An ephemeral stream drains the basin and usually begins flowing in early winter following development of the snowpack. Streamflow typically continues through mid- to late-spring and concludes upon completion of snowmelt. Occasional summer thunderstorms may wet drainage

lines, but the basin is usually too dry for continuous streamflow at any time following late spring.

2.2.1 Geology and Soils

The underlying geology of the UDCEW is biotite granodiorite and is concurrent with the discussion in Section 2.1.2. A map of bedrock topography (Figure 2.2) has been constructed based on soil depth estimates at fifty-seven points along a 10 x 20 m grid (herein defined as the study grid and sample locations) in the UDCEW. Soil depth estimates were made at each sampling location by vertically pounding a metal rod through the soil horizon to refusal. Based on the fifty-seven measurements, the mean soil depth for the basin is approximately 0.46 m (range is 0.3 to 1.2 m) with the greatest and lowest depths at mid- to lower and upper-middle to upper slopes respectively.

The soil texture at the site was investigated by Yenko (2003). Yenko (2003) performed a sieve analyses (Table 2.1) on soil samples at 8 to 70 cm depth at one location in the UDCEW and characterized the soil texture as a sandy loam (72% sand, 20% silt, and 8% clay) with a weathered C horizon along the soil-bedrock interface. The average porosity for the site is 0.38 (Yenko, 2003). Additional soil samples from fifty-seven sampling locations along the study grid were examined for this thesis. Sieve analysis of those samples examined the percentages of the coarse (> 2.00 mm), sand (< 2.00 mm and > 0.05 mm), and fine (< 0.05 mm) grain fractions. The results of that analysis are shown in Appendix A and Figure 2.2.

Field observations from this study have identified a thin clay layer at the base of the soil column immediately above the soil-bedrock interface. This layer was observed at all soil sampling locations but varied in thickness by location. The thickest clay layers

Table 2.1. Grain size distribution, wilting point, and field capacity for soils at the UDCEW as measured and reported by Yenko (2003).

Soil Depth	% SAND	% SILT	% CLAY	Wilting Point	Field Capacity	Porosity
0-8 cm	77	16	7	0.07	0.16	0.38
8-26 cm	76	16	8	0.08	0.17	0.39
26-54 cm	74	17	9	0.08	0.18	0.4
54-70 cm	78	15	7	0.07	0.16	0.38
70+ cm	Granite					

were noted where soil depth was greatest (central portion of the basin and immediately south of weir one and west of weir two) (Figure 2.2). Ridge locations, upper slopes, and topographic rises between seep channels typify the coarsest and shallower soils in the UDCEW. The majority of surface rock resides in the northeastern most portion of the basin and along the eastern boundary, and the percentage of sand in the soil profile is greatest immediately upslope of the seep channel junctions in the upper third of the basin (Figure 2.2).

2.2.2 Vegetation

The UDCEW is located in a vegetation transition zone (ecotone) between the grass and shrub-lands and the forested regions of the DCEW. The primary vegetation community includes sagebrush, forbs, grasses, and scattered ponderosa pine and Douglas-fir trees; the vegetation community is classified as sagebrush-steppe. There are nineteen trees on the site, seventeen of which are ponderosa pine. Only ten of the trees have a diameter greater than 13 cm (≈ 5 in) and only six have diameters greater than 50 cm (≈ 20 in). The average crown width and crown height of the six largest trees are 12.8 m (≈ 42.0 ft) and 16.6 m (≈ 54.5 ft) respectively. During fall and winter seasons the

average percent live canopy cover is approximately 9%. Live canopy cover averages approximately 35% and 45% for the spring and summer seasons respectively (Figure 2.3).

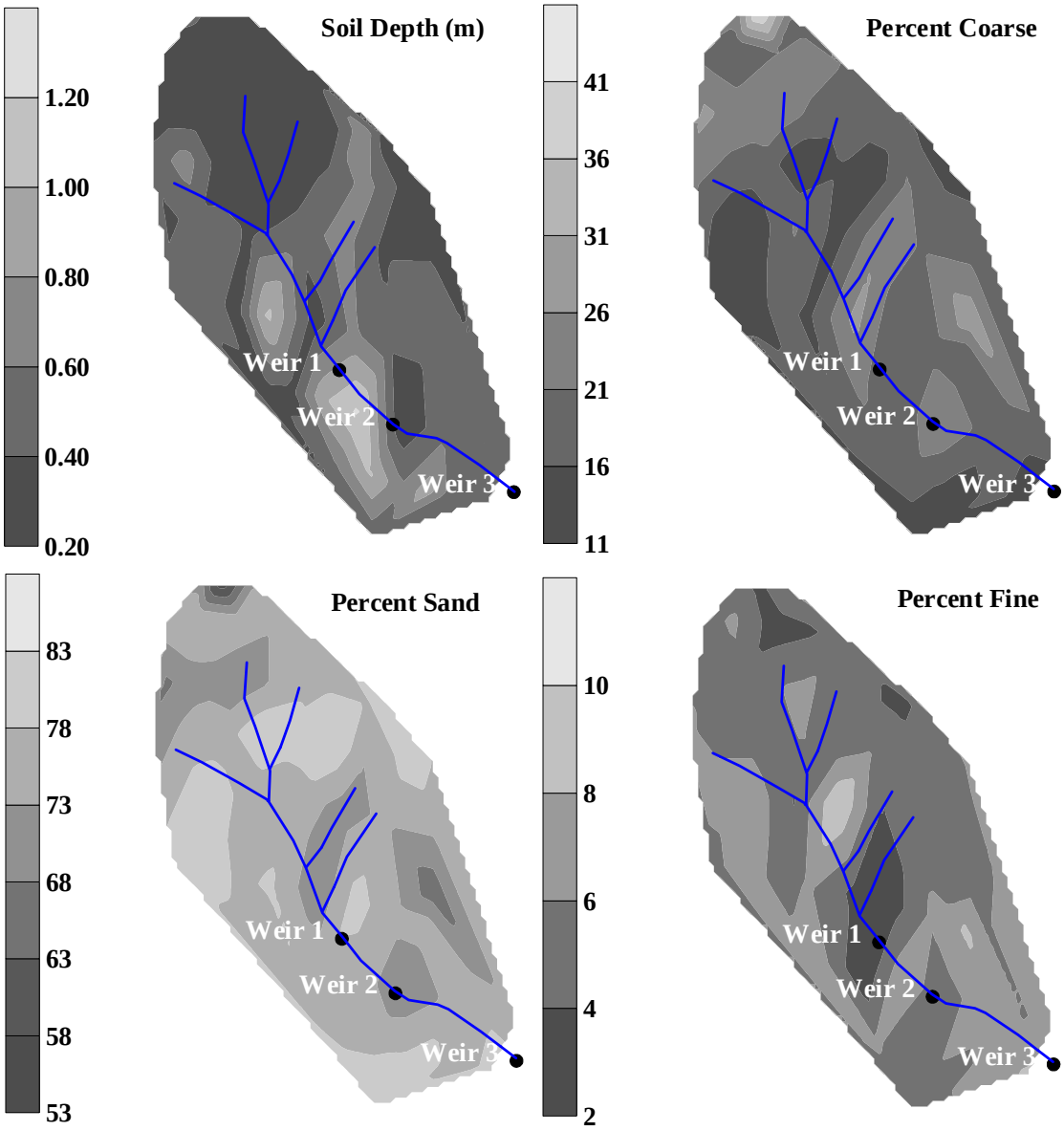

Figure 2.2. Observed soil depth and percentages of coarse (> 2 mm), sand (< 2.00 mm and > 0.05), and fine (< 0.05 mm) soil fractions at the UDCEW.

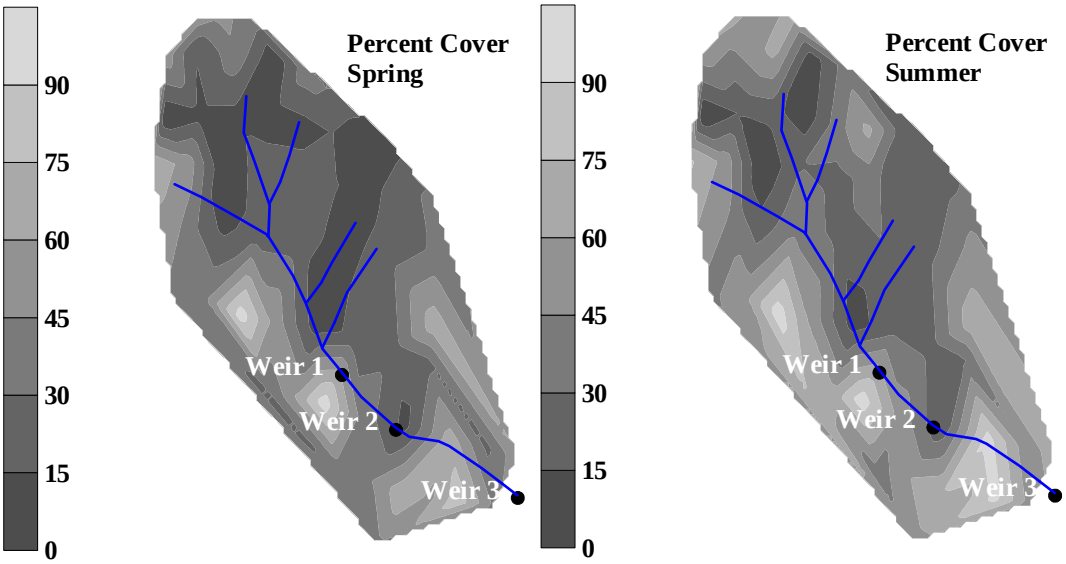

Figure 2.3. Distribution of live plant foliage (percent cover) observed at the UDCEW during the spring and summer seasons.

"Greening" up of the site generally begins in mid-March depending on the timing of snowmelt and the consistency of spring rain events. Early spring season forbs and grasses reach heights of 7 cm by late march and shrub leaves begin budding by early April. By late April grasses reach approximately 15 cm in height and overall canopy cover increases beyond 20%. By late May grasses at the site are approximately 25 cm in height and shrub cover nears its maximum. Plant cover reaches its maximum in mid-June before some species begin senescence.

Spence (1937) classified root systems for fifty species in the Boise River Watershed, southwestern Idaho. The classification system divided plants into four groups based on physical characteristics of the root systems. The same classification scheme was used in this study to group plant species at the UDCEW for later analysis and provides a functional grouping for plants at the site (Table 2.2). Spence (1937) grouped the plants as having a fibrous, semi-fibrous, semi-taproot, or taproot network and the descriptions that follow are from that study. Plants in the fibrous group had densely

organized fibrous roots in the upper 3 cm of the soil that spread laterally and downward to 40 cm depth. Roots in the semi-fibrous group consisted of 5 to 50 laterals from short (1 to 8 cm), horizontal tuberous roots and spread 40 to 60 cm horizontally and 40 to 190 cm downward. Root systems in semi-taproot plants consisted of tuberous to fibrous networks extended from a 50 to 80 cm downward growing taproot. The taproot group consisted of species with single or forked taproot systems. Roots from these species extended to depths of 200 cm and contained numerous laterals along the main taproot. Spence (1937) considered root structure and function more so than rooting depth as a grouping method. Estimated representation of each group at UDCEW in terms of percent live canopy cover for the fall and winter seasons are as follows: 0% fibrous, 2% semi-fibrous, 2% semi-taproot, and 5% taproot. During the spring season the respective canopy coverage representations are 7% fibrous, 6% semi-fibrous, 10% semi-taproot, and 12% taproot. Summer live canopy coverage includes 10% fibrous, 6% semi-fibrous, 14% semi-taproot, and 15% taproot plants.

2.2.3 Topography

The UDCEW trends northwest to southeast with the stream outlet oriented at the southeastern end of the basin (Figure 2.1). The basin represents all possible aspects and encompasses land surface slopes of 20 to 40 degrees (35 to 80%) over mostly concave and convex angles (Figure 2.4). The basin has one main ephemeral channel with five connecting seep channels. For description, the basin is divided into three approximately equal portions. The upper (NW) third contains the channel head and is much less confined and more dissected than the middle third. Hillslope lengths (from ridge to slope

Table 2.2. Plant species observed at the UDCEW and the respective growth and duration parmaters.

Common Name	Scientific Name	Growth	Duration	Water Use	Growth Period	Root Form
Arrowleaf Balsamroot	Balsamorhiza sagittata	Forb	Perennial	Med	Spring	Semi-taproot
Bitterbrush	Purshia tridentata	Shrub	Perennial	Low	Spring and Summer	Taproot
Bottlebrush Squirreltail	Sitanion hystrix	Grass	Perennial	Med	Spring	Fibrous
Choke Cherry	Prunus emarginata	Tree	Perennial	Med	Spring and Summer	Semi-Fibrous
Clarkia	Clarkia pulchella	Forb	Annual	Med	Spring	Fibrous
Death Camas	Zigadenus venenosus (var. gramineus)	Forb	Perennial	Med	Spring	Fibrous
Douglas-fir	Pseudotsuga menziesii	Tree	Perennial	Med	Spring and Summer	Taproot
Fescue	Festuca spp.	Grass	Perennial	Med	Spring	Fibrous
Lupine	Lupinus spp.	Semi-shrub	Perennial	Low	Spring and Summer	Semi-taproot
Mountain Big Sagebrush	Artemisia tridentata (ssp. vaseyana)	Shrub	Perennial	Med	Spring and Summer	Taproot
Nootka Rose	Rosa nutkana (var. hispida)	Shrub	Perennial	High	Spring and Summer	Fibrous
Parsnip Buckwheat	Eriogonum heracleoides var. heracleoides	Semi-shrub	Perennial	Low	Spring and Summer	Semi-taproot
Ponderosa Pine	Pinus ponderosa	Tree	Perennial	Med	Spring and Summer	Taproot
Sandberg's Bluegrass	Poa sandbergii	Grass	Perennial	Med	Spring and Fall	Fibrous
Scouler Willow	Salix scouleriana	Tree	Perennial	High	Spring and Summer	Semi-fibrous
Snowbrush Ceanothus	Ceanothus velutinus	Tree	Perennial	Med	Spring and Summer	Taproot
Sticky Geranium	Geranium viscosissimum	Forb	Annual	Low	Spring and Summer	Semi-taproot
Stiff Sagebrush	Artemisia rigida	Semi-Shrub	Perennial	Low	Spring and Summer	Taproot
Sulphur-flower buckwheat	Eriogonum umbellatum	Semi-Shrub	Perennial	Low	Spring and Summer	Semi-taproot
Twin Arnica	Arnica sororia	Forb	Perennial	Med	Spring and Summer	Fibrous
Wax Current	Ribes cereum	Shrub	Perennial	Low	Spring and Summer	Semi-Fibrous
Western Yarrow	Achillea millefolium L. var. occidentalis	Forb	Perennial	Med	Spring	Semi-fibrous

base) in the upper third of the basin are 60 to 75 m in length and are much longer than the hillslopes lower in the basin. The stream gradient in the upper third is approximately 26% and is greater than the middle third of the basin. Hillslope topography in the upper portion consists of steep convex and concave angles (Figure 2.5). The middle third of the basin is confined by steep convex northeast and southwest facing slopes. Slope lengths in this portion of the basin are approximately 45 to 50 m. Stream gradient in the middle third is approximately 16%, the lowest for the entire basin. The lower third of the basin starts and extends beneath the middle weir. This portion of the basin opens topographically to the west and remains confined from the southwest by a moderate to steep hillslope averaging 55 m in length from ridge to stream. The stream gradient in this portion of the basin is approximately 26%.

2.2.4 Instrumentation

The UDCEW is one of several meteorological monitoring locations in the DCEW. In collaboration with the Agricultural Research Service (ARS), a meteorological station was installed in 1999. The station measures air temperature, wind speed and direction, relative humidity, solar radiation, precipitation, soil moisture, soil temperature, and snow depth. Shielded and unshielded weighing bucket gages are used to measure precipitation in fifteen-minute intervals. The gages are mounted 1.5 meters above ground on posts just downslope from a ridge location in the southwestern portion of the basin (Figure 2.1). Volumetric soil moisture content and soil temperature at the station are measured hourly at 5, 15, 30, 45, and 65 cm depths using Campbell Scientific water content reflectometers and thermocouples respectively. Snow depth is measured by a Judd sonic depth sensor located mid-slope on a northeast facing aspect near the center of the basin. Additional

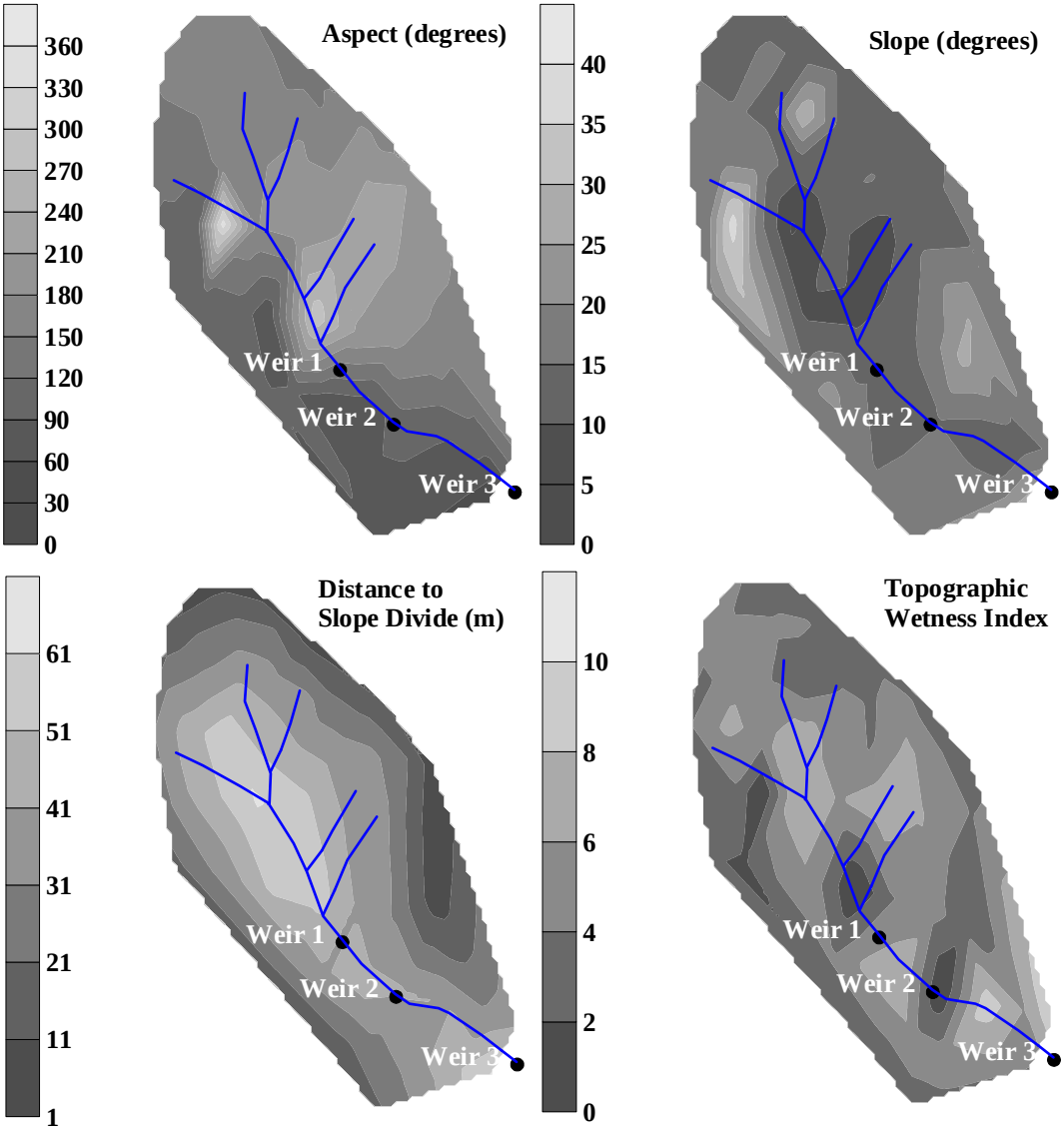

Figure 2.4. Topographic attributes of the UDCEW. The distance to the slope divide is the perpendicular upslope distance to the most immediate slope divide, and the topographic wetness index (dimensionless) is calculated as the Bevin and Kirkby (1979) topographic index.

TDR probes and tensiometers are horizontally installed at multiple depths in twenty locations (spaced along the hillslope from stream to ridgetop) in four transects on northeast and southwest facing slopes (Figure 2.1). TDR and tensiometers in these

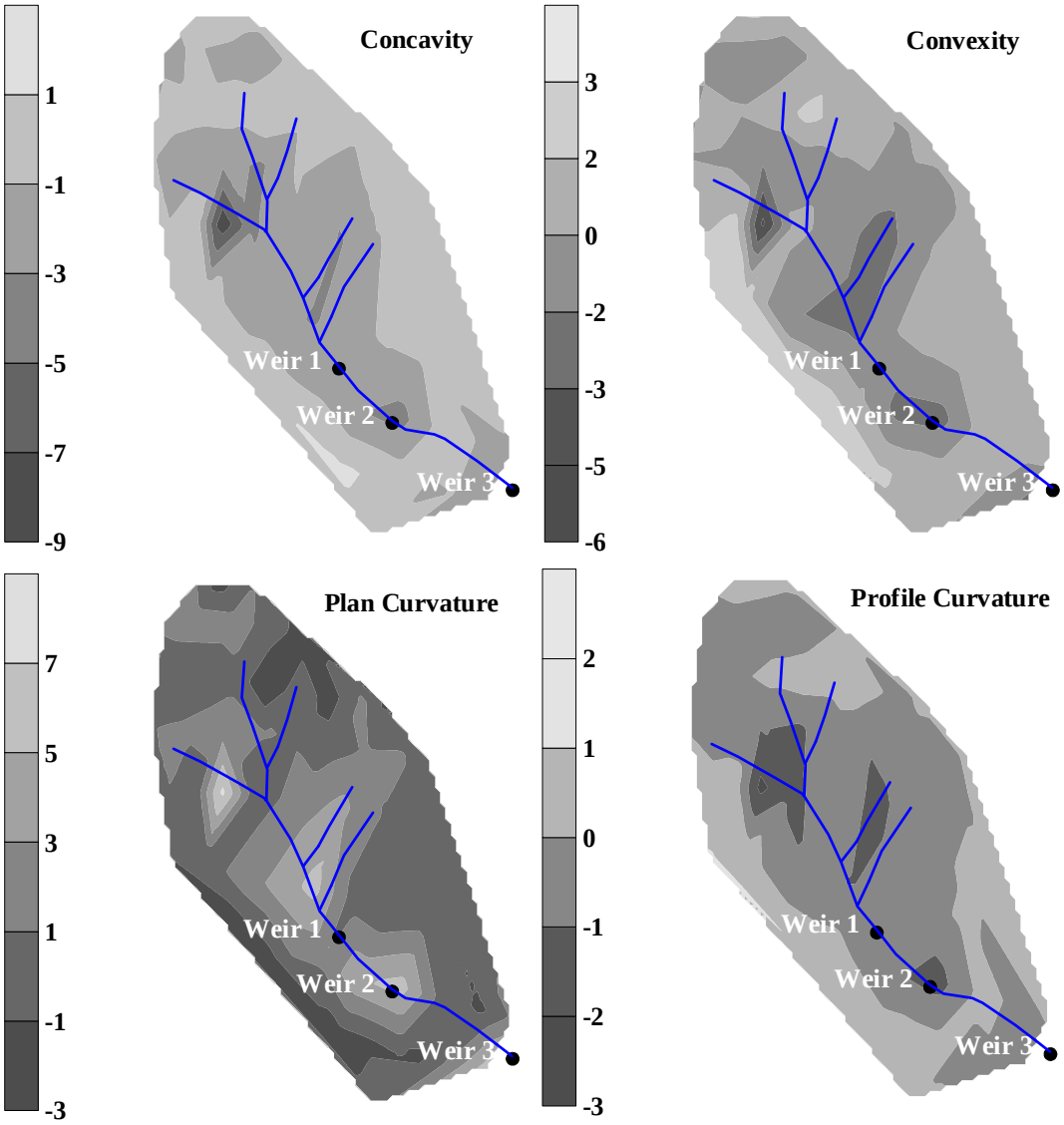

Figure 2.5. Curvature and convexity (both are dimensionless) represented by the topography at the UDCEW. Plan curvature represents the contour curvature and profile curvature depicts the slope profile curvature. Negative values represent concavity and positive values indicate convexity for all measures of concavity, convexity, and curvature. Zero values depict intermediate zones, neither convex nor concave.

locations record soil moisture and soil pore-water pressure in hourly intervals. Data from the meteorological station, TDR, and tensiometers are logged on Campbell Scientific CR10X data loggers. Overland flow collection tanks are installed on a northeast facing

slope in the southwestern portion of the basin. Overland flow has never been observed at the site. Streamflow at the site is monitored at three weir locations (Figure 2.1) using capacitance rods. The capacitance rods are frequently calibrated using the "v-notch" weirs. Spatial near-surface soil moisture measurements are recorded manually at various times along a basin wide 10 x 20 meter grid using a portable Campbell Scientific TDR 100 and wave content reflectometer.

2.2.5 Meteorological Data

2.2.5.1 Precipitation

Precipitation at the UDCEW occurs predominately as cool season rain and snow events. The site is characterized by a winter-long snowpack most years. The wetting season typically begins in early September (fall) and continues into December. Snowfall commonly begins in January (winter) and continues until mid-March. Rain-on-snow events are common at the site during late fall and early spring (March) and during warm winter weather patterns. This study used meteorological data from the October 2003 to October 2004 period, referred to herein as the 2003/2004 water year. Precipitation during the 2003/2004 water year was 72.7 cm with 42.7 cm (59%) falling as rain and 30.0 cm (41%) falling as snow. Precipitation during the study water year is summarized in Figure 2.6. Snow depth and snow water equivalent (SWE) were measured along the study grid at the time of basin average maximum snow depth and are depicted in Figure 2.7.

2.2.5.2 Temperature

Air temperature at the UDCEW meteorological station for the study period fluctuated from 28.3 °C to -11.6 °C. The mean recorded temperature for the 2003/2004 water year was 8.9 °C. The data are summarized in Table 2.3 and Figure 2.8. The maximum monthly temperature occurred in August of 2004 and the minimum monthly temperature occurred in January of 2004.

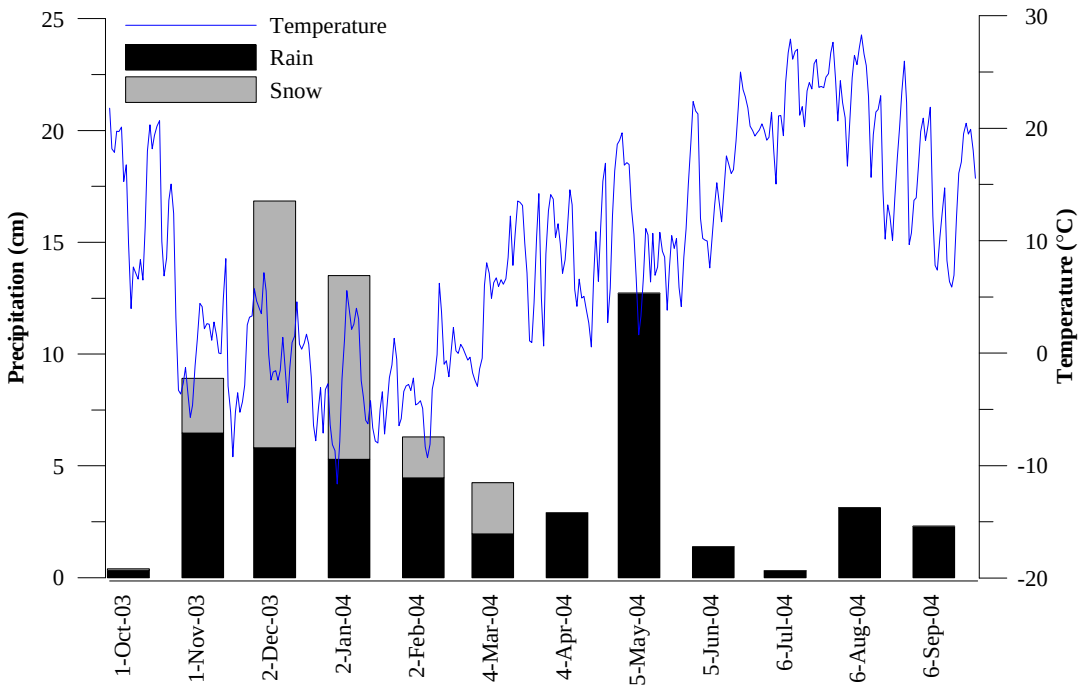

Figure 2.6. Precipitation and air temperature by month as recorded at the UDCEW meteorological station between October 2003 and October 2004.

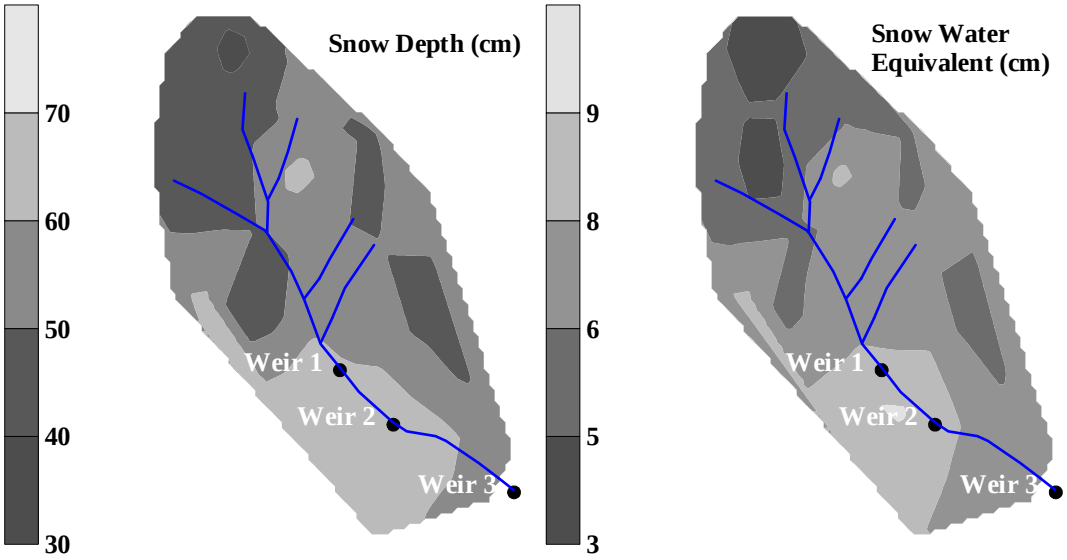

Figure 2.7. Snow depth and snow water equivalent measured at the UDCEW at time of basin average maximum snow depth.

Table 2.3. Monthly average, maximum, and minimum temperatures recorded at the UDCEW meteorological station during the 2003/2004 water year.

	Temperature (°C)		
Month	**Mean**	**Maximum**	**Minimum**
October 2003	12.57	21.79	-3.64
November 2003	-0.42	8.40	-9.21
December 2003	-0.25	7.16	-7.79
January 2004	-3.21	5.55	-11.62
Februray 2004	-2.10	6.21	-9.29
March 2004	6.03	14.19	-2.96
April 2004	8.44	16.89	0.56
May 2004	10.27	19.58	1.65
June 2004	16.86	24.99	7.58
July 2004	22.77	27.94	15.04
August 2004	20.82	28.29	10.02
September 2004	14.62	22.26	5.88
2003/2004 Year	**8.86**	**28.29**	**-11.62**

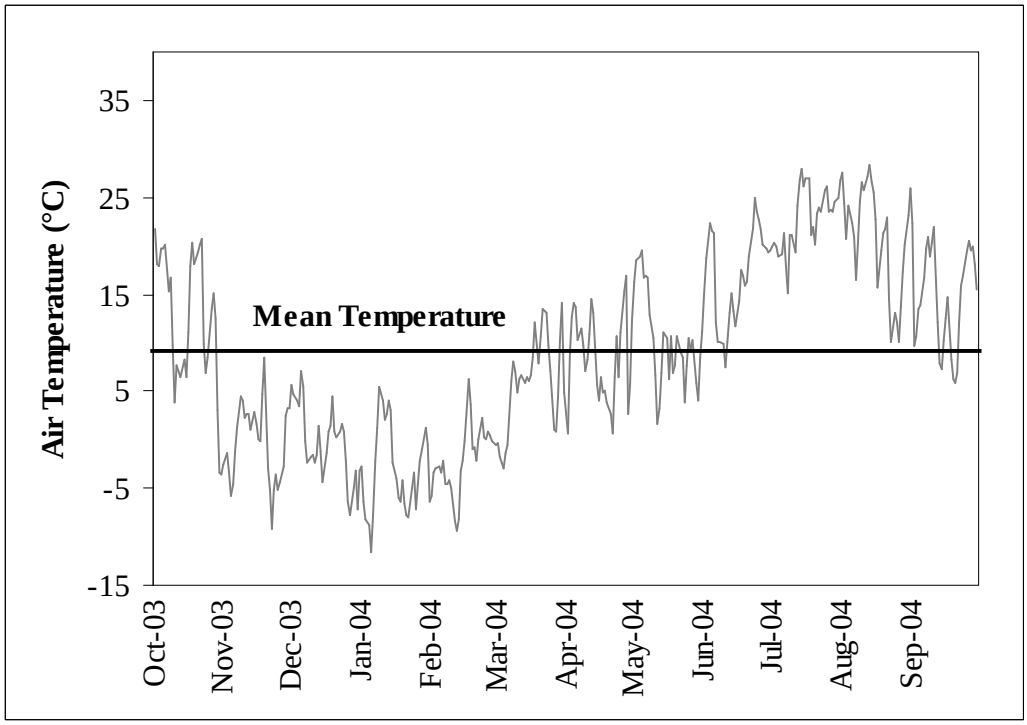

Figure 2.8. Air temperature observed at the UDCEW from October 2003 to October 2004. Mean temperature is represented by the solid black line.

2.2.5.3 Evapotranspiration

Evapotranspiration is not recorded at the study site. McNamara, Chandler, and Seyfried (2005) reported evapotranspiration estimates of 41.5 cm for the UDCEW based on a water balance study using the SHAW model (Flerchinger et al., 1996). Estimates for the 2003/2004 year were calculated for an aggregated water balance analysis of the study basin and are presented in the results section of this report.

2.2.6 Flow Components

2.2.6.1 Streamflow

Streamflow at the UDCEW is recorded at three weir locations (Figure 2.1). The upper weir (weir 1) is located centrally in the middle third of the basin approximately 55

m downstream of the main channel head. The middle weir (weir 2) is located approximately 25 m downstream from the upper weir and marks the beginning of the lower third of the basin. The lower weir (weir 3) is located approximately 16 m upstream from the outlet and 45 m downstream from the middle weir. Streamflow is recorded in fifteen-minute intervals at each weir using capacitance rods.

During the 2003/2004 water year surface water first puddled in the channel above the upper weir and disappeared approximately 2 to 3 m upstream from the middle weir. Streamflow began at the upper weir on the 2 December 2003, but was intermittent until consistent flows developed in late December. Streamflow at the middle weir intermittent until 19 December 2003. Streamflow at the lower weir was intermittent until early

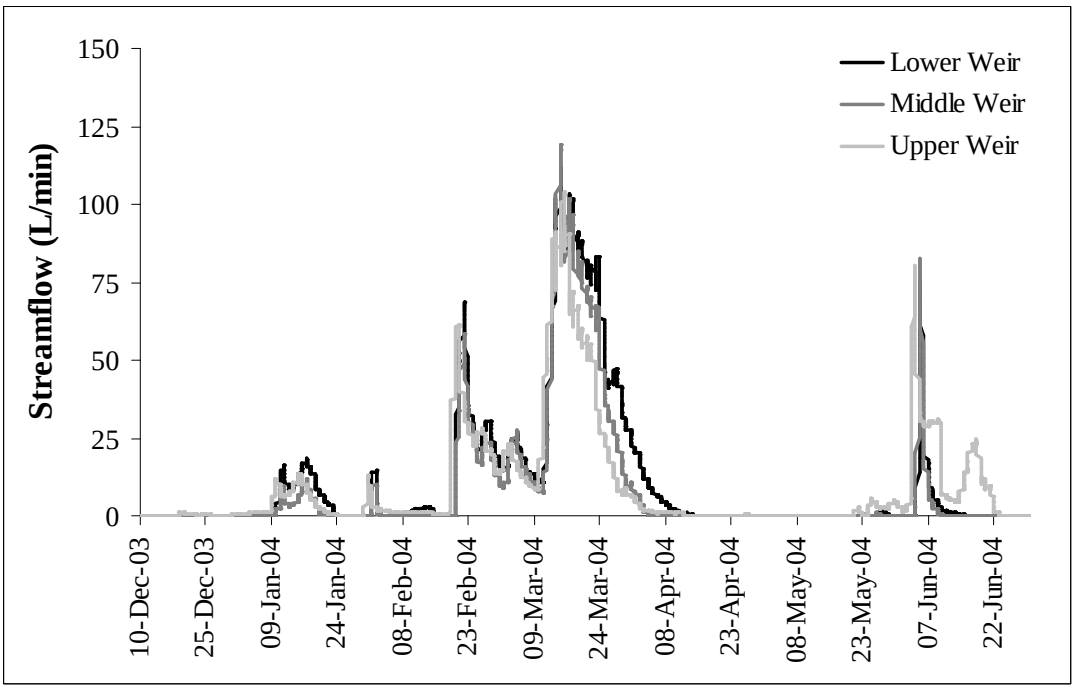

Figure 2.9. UDCEW measured streamflow at the upper, middle, and lower weirs during the 2003-2004 water year.

January when consistent flow occurred through all three weirs. Typically, the lower weir is the last station to start recording streamflow during the fall wetting period.

A hydrograph depicting streamflow for the 2003/2004 water year is shown in Figure 2.9. The 2003/2004 water year was indicative of a winter-long snowpack at the site. The snowpack was completely melted by 30 March 2004. At the conclusion of the snowmelt streamflow continued above the upper weir, disappeared 2 m downstream of the middle weir, and resurfaced midway between the middle and lower weirs. Seep channels upstream from the upper weir were saturated and puddled. By 02 April 2004, streamflow occurred between the upper weir and an area several meters upstream from the middle weir and resurfaced at the lower weir through the outlet. Streamflow ceased at the site in mid-April 2004.

Streamflow beyond mid-April occurred following precipitation events and followed a particular pattern. Late season streamflow occurred mostly between the upper and middle weir locations. Seep channels above the upper weir were saturated, but not flowing, following precipitation events. Depending on the intensity and frequency of events, streamflow would occur from the upper weir to several meters upstream or downstream of the middle weir, disappear below the surface, and then return at weir one through the outlet. By late June the stream channel was dry at all locations in the basin. For the 2003/2004 water year, peak discharge events in the basin occurred in late February, late March, and May of 2004 and correspond well with snowmelt (February and March) and rainfall events (May) during the year.

2.2.6.2 Soil Moisture

Soil moisture at the site is monitored at the meteorological station and along several transects. The patterns discussed here are solely based on soil moisture data from the meteorological station and exclude data from the TDR transects and the spatial near-surface measurements discussed earlier. Data from the TDR transects and spatial near-surface measurements are presented in the results section of this report. The 2000/2001 water year soil moisture profile from the meteorological station (for 5, 15, 30, 45, and 65 cm soil depths) is shown in Figure 2.10. Soil moisture data from the meteorological station for the 2003/2004 water year are not complete due to instrument malfunction. The 2000/2001 water year is representative of an average water year at the UDCEW. During the summer months soil moisture in the near-surface environment (5 to 30 cm) remains constant at 0.05 to 0.08 m^3/m^3, and soil moisture at depth varies from 0.08 to 0.10 m^3/m^3. Summer precipitation events occur mostly as pulse thunderstorm events and have little effect on the soil moisture at the site. Most of the summer precipitation at the site is lost to evapotranspiration.

As the fall wetting period begins, frequent rain events begin increasing soil moisture in the near-surface environment. Soil moisture from 5 to 30 cm depth increases rapidly and reaches 0.15 to 0.25 m^3/m^3. Soil moisture deeper in soil profile (30 to 65 cm) remains constant at 0.05 to 0.08 m^3/m^3 water content. Increased surface soil moisture raises the potential for infiltration to depth. Soil moisture at depth exhibits a delayed increase when compared to the near-surface environment. After the initial delay, soil moisture at 45 cm depth rises sharply to 0.15 to 0.19 m^3/m^3. Soil moisture at 65 cm depth rises more gradually from 0.15 to 0.25 m^3/m^3 as the winter snowpack develops.

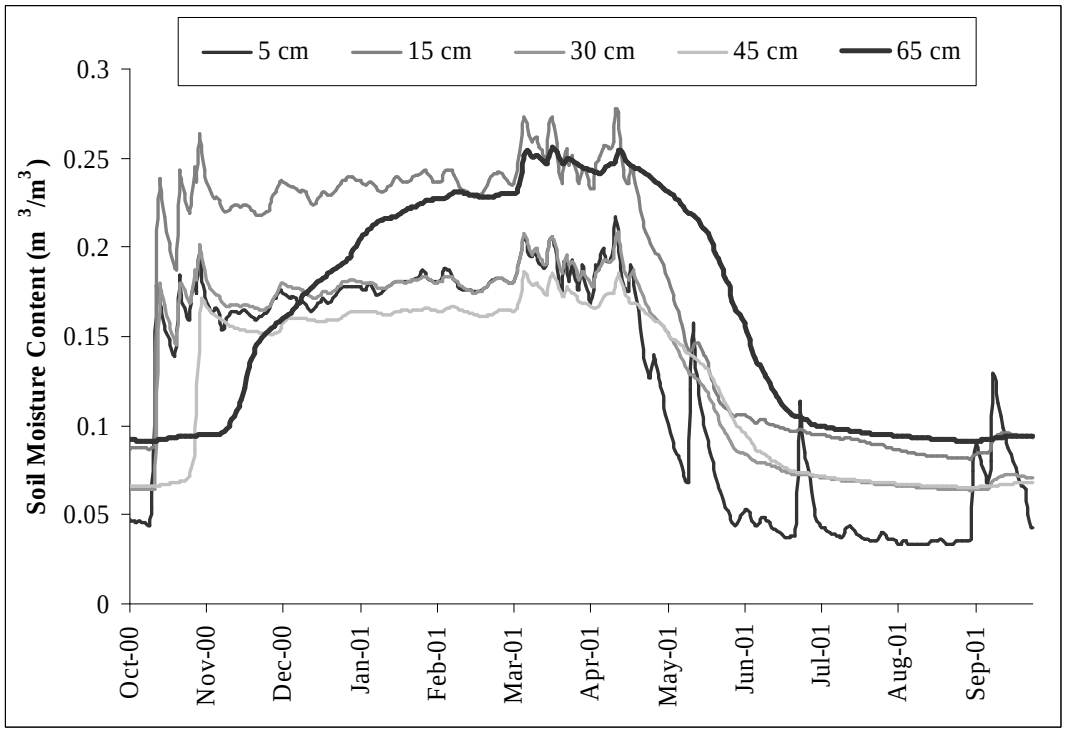

Figure 2.10. Soil moisture content at 5, 15, 30, 45, and 65 cm soil depth for the 2000/2001 water year as recorded at the meteorological station in the UDCEW.

During the late winter months, soil moisture stabilizes with near-surface slightly greater that soil moisture at depth. In spring, rapid snowmelt and pulse rain-on-snow events increase soil moisture at all depths. As summer approaches soil moisture contents in the near-surface begin to decline sharply due to reduced water input and increased evapotranspiration demands. A switching occurs in the moisture contents in the soil profile. Soil moisture is greatest at the deepest portions of the soil profile and lowest in the near-surface environment (Figure 2.10). As summer progresses, soil moisture continues to drop sharply at all depths and stabilizes at contents of 0.05 to 1.0 m^3/m^3 at depth and 0.03 to 0.08 m^3/m^3 in the near-surface.

2.2.6.3 Groundwater

McNamara et al. (2005) closed a water budget for the UDCEW based on recorded data from 2000/2001 water year and evapotranspiration and deep percolation predictions using the SHAW model (Flerchinger et al., 1996). The SHAW model estimates a *DeepPerc* component of the water balance. This *DeepPerc* component is calculated (using a darcian flux) as water lost to vertical deep percolation in the soil profile (Flerchinger et al., 1996). The *DeepPerc* component calculated for the 2000/2001 water year was 18.8 cm (McNamara et al., 2005). Discussion beyond the general estimation of deep percolation is reserved for the results section of this report.

2.2.7 Previous Research

2.2.7.1 Dry Creek Experimental Watershed Water Balance

McNamara et al. (2005) calculated a water balance for the UDCEW using the SHAW model (Flerchinger et al., 1996). The model balances water input and output by calculating precipitation (*P*); interception (*INT*); evapotranspiration (*ET*); the change in storage relative to the canopy (δS_{canopy}), snow (δS_{snow}), residue ($\delta S_{residue}$), and soil (δS_{soil}); water lost to ponding (*Ponding*); surface runoff (*Runoff*); and water lost to vertical deep percolation into the soil column (*DeepPerc*). The daily water balance equation is:

$$P - INT - ET - \delta S_{canopy} - \delta S_{snow} - \delta S_{residue} - \delta S_{soil} - Ponding - Runoff - DeepPerc + \text{Error} = 0 \quad (2.1)$$

McNamara et al. (2005) assumed, based on field observations, that the *DeepPerc* component for the UDCEW constitutes water losses to groundwater and a lateral flow component at the soil-bedrock interface. Flow along the soil-bedrock interface is a lateral flow source along a variable low permeable clay layer at the base of the soil profile. The

study substituted a bedrock flow (*BF*) component for *DeepPerc* in the daily water balance equation and calculated *BF* as:

$$BF = GW_{out} + L_{out}, \quad (2.2)$$

where GW_{out} is water lost to groundwater and L_{out} is lateral subsurface flow. The results from the balance approach are summarized in Table 2.4.

Table 2.4. SHAW calculated water balance for the 2000 water year in the UDCEW (McNamara et al., 2005).

Variable	Value (cm)
Precipitation	56.8
ET	41.5
Storage in Canopy	0.0
Storage in Snow	0.0
Storage Residue	0.0
Bedrock Flow	18.8
Streamflow	14.3
Error	-3.3

2.2.7.2 Streamflow Sources

Yenko (2003) used hydrometric and geochemical data to investigate the flow sources contributing to streamflow in the UDCEW. The study examined the chemical signature of precipitation, snowmelt, soil water (shallow – 30 cm, deep – 60 cm), and streamflow in the basin and used hydrograph separation, concentration-discharge relationships, and end-member-mixing-analysis (EMMA) to quantify flow sources in basin. Concentration-discharge relationships (Figure 2.11) explore changes (hysteresis effects) in solute concentrations at given discharges. Yenko (2003) identified a “dominant” counter-clockwise hysteresis loop and “minor” clockwise loop in the concentration-discharge relationship between streamflow and streamwater silica

concentration. Yenko (2003) suggested that the counter-clockwise loop indicates that a freshwater source (i.e., precipitation) contributes to early event flow (early streamflow) and that a more concentrated (greater silica) source (i.e., soil water) contributes to later event flow (late streamflow).

The study further examined streamflow sources through a hydrograph separation of old (pre-event) and new (event) water sources in a spring snowmelt event. The analysis found that 59% of streamflow during snowmelt was from event water (new water in the basin), and that pre-event water (older water in the basin) represented 41% of the streamflow during the snowmelt event (Yenko 2003). Yenko (2003) used an EMMA approach to further study flow sources for the snowmelt event and hypothesized that an unsampled silica source must contribute to streamflow since chemistry from deep soil water, shallow soil water, groundwater, and snowmelt could not explain silica concentrations in streamwater. Yenko (2003) assumed the silica source to be from the soil-bedrock interface (weathered in place granitic C soil horizon) and proposed a hypothesized chemical end-member representative of the soil-bedrock source (assumed silica concentration increased with depth).

Water geochemistry analysis was used to further separate the components of the streamflow hydrograph and found that 65% of streamflow during snowmelt was from event sources and that soil water and the hypothesized soil-bedrock interface sources contributed 7% and 28% of the flow respectively (Yenko, 2003). Yenko (2003) summarized that water discharge in the basin is chemically variable in the cold season and that flow sources in the basin are dependent on soil moisture conditions. The study further noted that field observations and soil moisture sensors (from mid-slope locations

in the center of the basin) indicate that the soil profile in the basin remains unsaturated throughout the year.

Yenko (2003) concluded that the timing of streamflow (initiation in late fall, cessation in early spring), duration of streamflow, and the water balance (McNamara et al., 2005) all suggest that streamflow in the basin in composed entirely of cold season precipitation. The study furthers concluded that the SHAW water balance (McNamara et

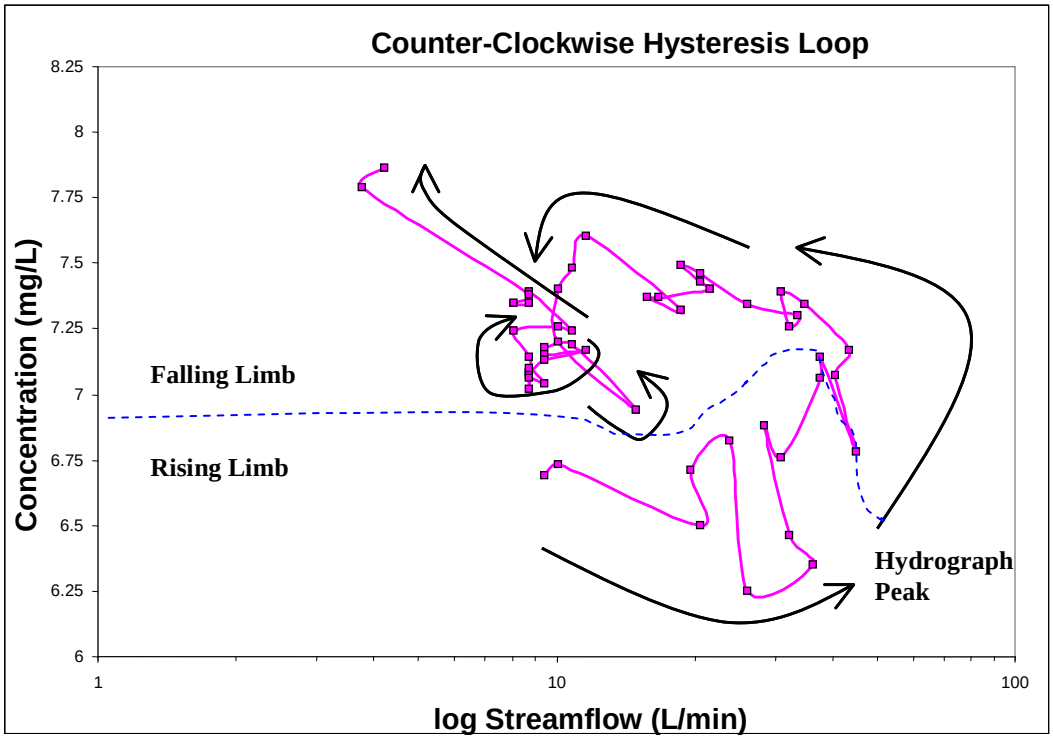

Figure 2.11. Counter-clockwise hysteresis loop (concentration decreases on rising limb of hydrograph) in a concentration-discharge relationship observed by Yenko (2003) at the UDCEW. The relationship would be reversed for a clockwise loop (concentration increases on the rising limb and decreases on the falling limb). Figure from Yenko (2003).

al., 2005) demonstrates there is no regional groundwater input required to quantify streamflow in the basin. Yenko (2003) proposed three possible explanations for the silica source contributions to streamflow:

- A localized subsurface saturated zone develops in the basin during the cold-season;
- Soil water in the analysis was not representative of the basin overall, an additional unsampled source of soil water exists elsewhere in the basin; and/or
- Formation of a localized reservoir in the fractured granitic bedrock contributes to streamflow during precipitation events.

2.2.7.3 Hillslope Connectivity

McNamara et al. (2005) used hydrometric field observations, combined one- and two-dimensional flow models, and in-stream chemical tracers to develop a conceptual model of hillslope hydrologic connectivity and the controls on streamflow initiation and cessation in the UDCEW. The study used hydrometric data and the one-dimension (1D) SHAW (Flerchinger et al., 1996) model to calculate a water balance for the 2000/2001 water year (Table 2.4). The SHAW output includes prediction of soil moisture at various depths in the soil profile. Model results and measured soil moisture data were used to define five "preferred" soil moisture states in the catchment: 1) a dry period (summer), 2) transitional fall wetting period (wet-up), 3) low flux wet period (winter), 4) high flux wet period (spring), and 5) transitional drying period (drydown) (late spring to early summer) (McNamara et al, 2005). The study suggests that transitions between the periods are the result of water balance fluctuations in rain, snow, snowmelt, and evapotranspiration and that hydrologic transitions between the dry and wet periods are not simultaneous with switches in vertical and lateral hillslope hydrologic controls (Grayson et al., 1997) commonly reported for semi-arid climates (McNamara et al., 2005).

Grayson et al. (1997) proposed that throughflow in semi-arid landscapes switches from vertical to lateral flowpaths as soil moisture conditions transition from a dry to wet state (due to increased water delivery, i.e., rainfall) and that the switch in flowpath direction and transition in soil moisture state occur simultaneously. McNamara et al. (2005) show that this is not the case for the UDCEW and that a lag in water delivery from the snowpack during the cold season lengthens the transition from dry to wet state. McNamara et al. (2005) indicate that the transition from the dry to wet state in the UDCEW results from a shift in the balance between available precipitation and evapotranspiration demands and that the timing of the switch is correlated with elevated soil moisture contents as the site progresses from the low flux to high flux wet period.

Stieglitz, Shaman, McNamara, and Engel (2003) proposed the concept of a dry connectivity barrier to hydrologic switching from vertical to lateral flowpaths. McNamara et al. (2005) evaluated the potential for dry pocket connectivity barriers at the UDCEW and proposed that such hydrologic barriers influence the switching from vertical to lateral flow at the site. The study investigated vertical and lateral flow switching mechanisms by combing the 1D water balance with a two-dimensional (2D) hillslope flow model, HYDRUS2D (Simunek, Sejna, and van Genuchten, 1999). Snowfall from the water balance was amended to represent rainfall in the 1D model and was used to simulate humid flow conditions using HYDRUS2D. The amendment of snowfall to rainfall was used to simulate water inputs directly to the soil surface rather than to winter long storage in the snowpack. McNamara et al. (2005) hypothesized that the snowpack slows delivery of cold season precipitation to the soil profile and may lead to development of dry soil connectivity barriers. Results from the 2D rainfall amended

model produced a rapid delivery of soil moisture at depth in response to rainfall input; this pattern is in contrast to observed more gradual delivery of water from the snowpack to deep soil layers (McNamara et al., 2005). The findings suggest the snowpack stores potential soil water during the winter low flux season and that the subsequent release of water during snowmelt may wet-up dry soil pocket barriers and facilitate hillslope hydrologic connectivity (McNamara et al., 2005).

McNamara et al. (2005) characterized the soil moisture patterns and subsequent controls on vertical and lateral fluxes using the defined soil moisture periods indicative of change in water input and evapotranspiration. The summary of the soil moisture periods herein are from McNamara et al. (2005). Soil moisture during the summer dry period is stable and remains around 0.05 to 0.07 m^3/m^3. During this period, evapotranspiration exceeds precipitation, vertical fluxes dominate, and the streambed remains dry. This period is consistent with the “dry” state defined by Grayson et al. (1997) (McNamara et al., 2005). The fall wetting period begins when fall rains wet-up the soil profile. Vertical fluxes still dominate and the soil profile wets-up rapidly. Precipitation exceeds evapotranspiration during this period and the wetting front progresses to the soil-bedrock interface once field capacity is reached in the near-surface environment. Soil moisture in the near-surface is erratic during this period due to fluctuating rainfall inputs. As the fall season progresses to winter, precipitation changes to snowfall and water input into the soil profile is reduced. Soil moisture contents in the near-surface stabilize, marking the beginning of the low flux wet period. McNamara et al. (2005) suggest that if the low flux season occurs early enough in the fall deep soil pockets may remain “relatively” dry during most of the winter season.

The winter wet – low flux – season is similar to the “wet” state defined by Grayson et al. (1997) with the exception that water inputs are limited by the persistent snowpack (McNamara et al., 2005). Precipitation exceeds evapotranspiration during this period, but the availability of water is limited by the snowpack energy balance. Soil moisture contents during this period are largely the result of the precipitation type. Vertical fluxes still dominate the flow of water through the soil profile. Lateral subsurface flow along the soil-bedrock interface may occur where shallow soils exist, but hillslope connectivity is likely limited by dry soil pockets in deeper soil profiles at mid-slope locations in the basin (McNamara et al., 2005). Thus, upper and lower slopes remain unconnected hydrologically. During this period, streamflow typically begins upstream from the upper weir (Figure 2.1) and is lost to the subsurface just upstream of the middle weir. McNamara et al. (2005) suggest that the losing stream contributes to a near-stream saturated wedge between the stream bottom and the soil-bedrock interface.

The spring wet – high flux – period develops as warm temperatures ripen and melt the snowpack. The rate of water input increases rapidly and the site typifies the “wet” state defined by Grayson et al. (1997). Water inputs greatly exceed evapotranspiration and the controls on subsurface flow switch from vertical to lateral fluxes. Streamflow during this period corresponds well with the rate of water input into the soil column (McNamara et al., 2005). Soil moisture at depth is at field capacity during this period and lateral flow along the soil-bedrock interface occurs. McNamara et al. (2005) note two key observations during this period: cation concentration in streamflow increases dramatically; streamflow occurs through the entire basin (no longer is lost between the middle and upper weirs). The study suggests that hillslope

connectivity develops in this period and that the increased cation concentration in the stream indicates a new source of streamwater, likely from the saturated wedge developed during the previous hydrologic period (McNamara et al., 2005). These findings are consistent with the increased silica concentration reported for the early portion of the falling hydrograph (Yenko 2003). The final period is the late spring drying period and is marked by the final snowmelt event. Soil moisture in the near-surface declines and evapotranspiration rates exceed water inputs. Streamflow continues as deep soil layers drain stored water from the previous period. McNamara et al. (2005) note that streamflow and flow along the soil-bedrock interface cease as mid-slope soil profiles dry out and that the ion concentration in streamwater is high through the remaining falling limb of the hydrograph.

In summary, the findings of McNamara et al. (2005) concur with the chemical analysis by Yenko (2003). Both studies note increases in ion concentrations following the onset of streamflow and that streamflow ion concentration remains high through the falling limb of the hydrograph. Both studies suggest that a source other than event flow and regional groundwater contributes to streamflow after the onset of snowmelt (McNamara et al., 2005). It is proposed here that both studies lack spatial examination of the basin and are limited by the use of data from few sampling locations. However, both studies incorporate substantial basin-wide field observations and concur regarding sources of streamflow in the basin. This thesis poses to add greater spatial extent to the examination of hillslope hydrology in the UDCEW and to build on the conclusions defined by Yenko (2003) and McNamara et al. (2005).

3. METHODS

It is hypothesized here that streamflow initiation and cessation in the UDCEW is controlled by seasonal fluctuations in soil moisture patterns. This study proposes investigation into spatial and temporal patterns in soil moisture and into the controls on those patterns using TDR measurement techniques and subsequent time-stability, standard and geostatistical, and soil moisture mapping applications. TDR was chosen based on the ease of its application, minimal calibration requirements, and minor site disturbance benefits. Given the uncertainty of time-stability research applications to semi-arid mountainous basins, time-stability methodology was combined with standard and variogram statistical techniques to investigate and parameterize the controls on soil moisture distributions in the UDCEW and to infer the processes controlling streamflow initiation and cessation. Ordinary block kriging was selected for the mapping applications given the need to predict soil moisture in multiple discrete areas between sample locations and the mean was unknown. Results from this study were compared with previous UDCEW studies and field observations to explain the overall governing hillslope processes occurring in the study basin.

3.1 Site Characterization

The study site was selected to coincide with additional scientific investigation into streamflow generation and cessation along the Boise Front. The UDECW is subject of multiple ongoing hydrologic studies and is well instrumented (see discussion in section 2.2). The site has been characterized in previous studies (Yenko, 2003; McNamara et al., 2005), but this study provides the most expansive spatial explanation of the site physical and biological characteristics. A 10 x 20 m study grid (57 sample locations) was established at the UDCEW specifically for this study (Figure 2.1). The site topography was surveyed using a Topcon Total Station and 213 survey points. The site characterization that follows is based on analysis of the total station survey and physical and biological data recorded at each point along the study grid.

3.1.1 Terrain Analysis

Analysis of the controls on soil moisture and the derivation and testing of terrain and wetness indices required quantification of basin topography. Data from the site survey were used to create a DEM (Figure 2.1) for the UDCEW. Elevation, aspect, and land surface slope were obtained using the site survey noted above and are shown in Appendix A. Elevation was measured as the altitude above mean sea level, aspect was recorded as the azimuth angle, from 0 to 360°, parallel to the steepest downhill direction, and land surface slope was defined as the rate of change in elevation in *x*- and *y*-directions. Digital terrain analysis software (Landserf, 2.1 [Wood, 1996]) and the site survey DEM were used to quantify land surface convexity, concavity, and profile, plan,

mean, longitudinal, and cross-section curvature (Appendix A). The program uses zero (elevation), first (slope and aspect), and second order differentials (curvature and convexity) to calculate topographic changes along the landscape; a detailed explanation of the algorithms is presented in Wood (1996).

The topographic wetness indices (Bevin and Kirkby, 1979) and upslope contributing areas for the land surface were calculated using TauDEM (Tarboton, 2003). TauDEM is a digital terrain analysis software program that interfaces with various geographic information systems (GIS). The program uses the "Dinf" (D-Infinity) (Tarboton, 1997) approach to determine the steepest downslope direction in a planar triangular facet on a block centered grid for each pixel in the DEM (Figure 3.1). The steepest downslope direction determines the flowpath to the pixel and defines the direction of upslope contributing area. The upslope area is then determined by pairing upslope pixels with correlated downslope flow directions. Tarboton (1997) provides a detailed explanation of the "Dinf" approach and a review of the improvements "Dinf" offers over previous methods of calculating upslope contributing areas.

3.1.2 Quantification of Observed Vegetation

Vegetation at the site was quantified to assess plant influence on soil moisture patterns. Percent cover was determined by estimating the percent live canopy cover of each plant observed in a 100 x 70 cm rectangular plot centered over the sample location (Daubenmire, 1959). Sampling occurred during the spring, summer, fall, and winter periods to determine seasonal fluctuations in the percent live canopy cover. Plants observed at the site were grouped by root form (Spence, 1937) for later analysis. Root

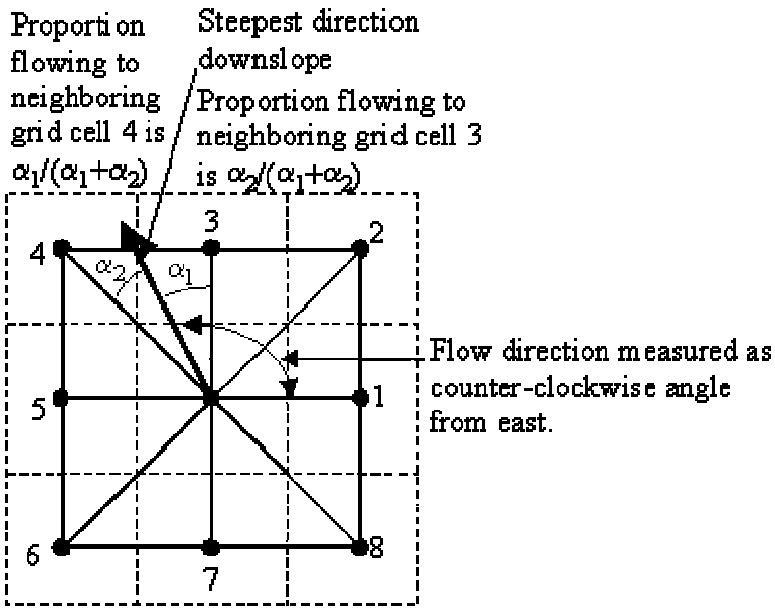

Figure 3.1. Block centered diagram illustrating the "Dinf" approach defined by Tarboton (1997). Figure is modified from Tarboton (1997).

form for each species was assumed consistent with the root forms observed by Spence 1937) in the Boise River Watershed. Root forms for plants not included in the survey by Spence (1937) were determined based on data included in the Fire Effects Information System Plant Database (FEIS Plant Database) maintained by the United States Department of Agriculture (USDA, 2005). The database provides a synthesis of literature on over 900 plant species in North America and was originally developed in the Intermountain Northwest, USA.

3.1.3 Collection and Analysis of Soils

Soil samples were taken at each point along the study grid and were sieved to quantify the coarse (> 2mm), sand (< 2 mm and > 0.05 mm), and fine (< 0.05 mm) soil fractions. Soil texture mapping was needed to quantify soil affects on soil moisture distribution at the site. The samples were collected from the soil profile using a vertically inserted split spoon sampler. Soil depth at each point along the study grid was

determined by vertically pounding a steel rod through the soil profile to refusal. Maps of the basin characteristics were created using block kriging methods within Surfer 8.0 (Golden Software, Inc.) surface mapping software and are included in the study area description (Section 2.0) of this report. Additional details on the site were obtained through field observations and are included in the study area description (Section 2.0).

3.2 Hydrometric Data Collection

3.2.1 Precipitation and Streamflow Data Sources

Precipitation data for the study period were obtained from the meteorological station at the site. Streamflow and stream stage data were obtained from ongoing streamflow measurements recorded by capacitance rods at the three weir locations within the UDCEW (Figure 2.1). Calibration of the capacitance rods is maintained by other researchers in the basin and is performed by random stream gaging at the respective "V" notch weirs. These data were required for modeling deep soil moisture distributions and to investigate catchment response to seasonal precipitation.

3.2.2 Soil Moisture Data Collection

3.2.2.1 Permanent TDR Instrumentation

Soil moisture at the study site was monitored through two methods: permanently installed TDR within soil pits and portable TDR measurements along the study grid. The meteorological station and twenty soil pit locations (see transects in Figure 2.1) in the basin are instrumented with permanently installed TDR probes and record soil moisture at varying depths in fifteen minute intervals daily. The permanent TDR transects are

perpendicular to the ephemeral stream flowing through the catchment and TDR in these locations are installed horizontally in soil pits in intervals of 5, 10, 20, 30 and 40 m along the hillslope on northwest and southeast facing slopes. The soil pits represent near stream and ridgetop locations. Data from these instruments are stored to data loggers at the site and downloaded on regular intervals. These instruments were installed prior to this study, however, data from several pit locations are considered in this analysis.

3.2.2.2 Portable TDR Measurements

Spatial soil moisture data were needed to investigate temporal and spatial variability of soil moisture at the site. Permanent TDR installations in the basin were limited to the middle and lower third of the basin. Portable TDR methods provided a cost effective method to collect soil moisture data basin wide. Point near-surface (30 centimeters depth) soil moisture data were captured using a portable TDR device along the study grid. The sampling device consisted of a TDR 100 wave generator (Campbell Scientific, Inc.), laptop computer, PC-TDR software (cable tester), RG-58 TDR connection cable, and TDR probe. The TDR 100 device generates a waveform that travels through the connection cable and soil probe and back to the TDR 100 unit. The PC-TDR software records the wave travel time, calculates the soil dielectric constant from wave travel time, and determines the respective soil moisture content (m^3/m^3) using a specified calibration equation (Topp et al., 1980; Ledieu et al., 1986). The Ledieu et al. (1986) equation was selected for this application, although both equations, Topp et al. (1980) and Ledieu et al. (1986), perform well based on laboratory observations. An overview of TDR applications and function is provided in Section 1.2.6.4 of this report.

TDR was selected for the study because it is easily adapted to a single person mobile unit, is minimally destructive to the site, accurately and consistently measures soil moisture to within 0.01 m^3/m^3 volumetric soil moisture content, and is readily available and concurrent with other instrumentation in the study basin. Calibration of the instruments was performed in the laboratory using soils obtained from the study site. Soil from the study site was dried in an oven at 105° C to a water content of 0.00 m^3/m^3. Water was added to dried soil samples in known volumes. Volumetric soil moisture contents were calculated and compared with TDR measurements over a range of volumetric soil moisture contents (Figure 3.2). TDR measurements were well correlated with the known volumetric soil moisture contents ($r^2 = 0.988$). Additionally, soil morphology at the UDCEW is well within the recommendations (for clay and organic content and salinity) (Jones et al., 2002) specified for TDR. Thus, TDR was considered an accurate and acceptable method to measure soil moisture at the UDCEW.

Point near-surface measurements along the study grid were taken by horizontally inserting the TDR probe through the upper 30 cm of the soil profile. Three measurements were taken at each sampling location on each sampling date and were averaged to determine the respective point near-surface soil moisture content. Point near-surface data along the study grid were captured on 38 occasions and occurred twice weekly (winter and spring 2004) to by-weekly (fall 2003). Sampling dates during 2003 summer months were more widely spaced, approximately twice monthly. Near-surface measurements recorded from January through February of 2004 were removed from the data set due to instrument error. The measurement period for study grid near-surface soil moisture data was April 2003 through June 2004.

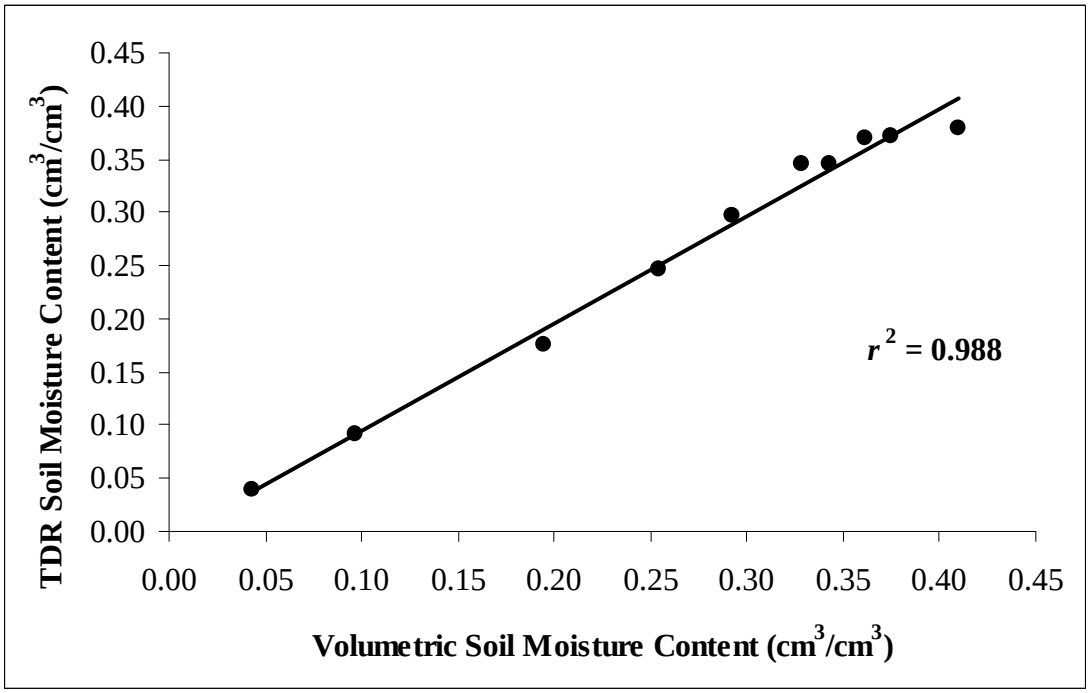

Figure 3.2. Correlation of TDR measured soil moisture content and known volumetric soil moisture content observed during laboratory calibration of TDR.

3.3 Prediction of Soil Moisture at Depth

3.3.1 Overview of SHAW Model

Near-surface soil moisture data often do not fully explain soil moisture distributions at depth. Thus, soil water at depth (at the soil-bedrock interface) was simulated using the SHAW model (Flerchinger et al., 1996). The model input parameters include initial and concluding soil temperature and water profiles, initial snow depth, hourly weather data (air temperature, wind speed, humidity, precipitation, and solar radiation), soil characteristics (depth, bulk density, saturated hydraulic conductivity, and albedo), and general site characteristics (aspect, slope, latitude, longitude, surface

roughness, percent vegetative cover, albedo, and residue thickness). The SHAW model has been shown to simulate heat and water effects on soil freezing (Flerchinger and Hanson, 1989; Flerchinger and Saxton, 1989a; Flerchinger and Saxton 1989b), soil temperature and plant water use (Flerchinger and Pierson, 1991), evapotranspiration (Flerchinger et al., 1996); and snowmelt and runoff (Flerchinger, Cooley, and Deng, 1994).

SHAW simulates a vertical 1D profile consisting of the plant canopy and snow covered upper layer, a residue layer, and a soil profile as defined by the user (Figure 3.3). Each layer is considered as a separate node in the simulation and interrelated heat, water, and solute fluxes are considered through the simulated profile (Flerchinger et al., 1996). Water and heat fluxes for each node are simulated for each user specified time step. Snow accumulation and melt is determined from a point energy and mass balance model inclusive of solar and long-wave radiation exchange, sensible and latent heat, surface transfer, and snowpack vapor transfer (Flerchinger et al., 1996). Soil freezing and thawing simulation considers freezing-induced moisture migration, solute effects on frost formation, and frozen soil runoff. Transpiration simulation considers effects of a multi-species canopy on heat and water fluxes and includes parameterization of solar and long-wave radiation, turbulent transfer of heat and water vapor, and leaf transpiration (Flerchinger et al., 1996). SHAW solves the energy, water, and solute balance at each time step and offers output inclusive of water balance, surface energy transfer, and snow and frost depth summaries. Temperature, soil moisture, and solutes profiles are generated for each time step. Flerchinger et al. (1996) provides detailed descriptions of the model components and equations.

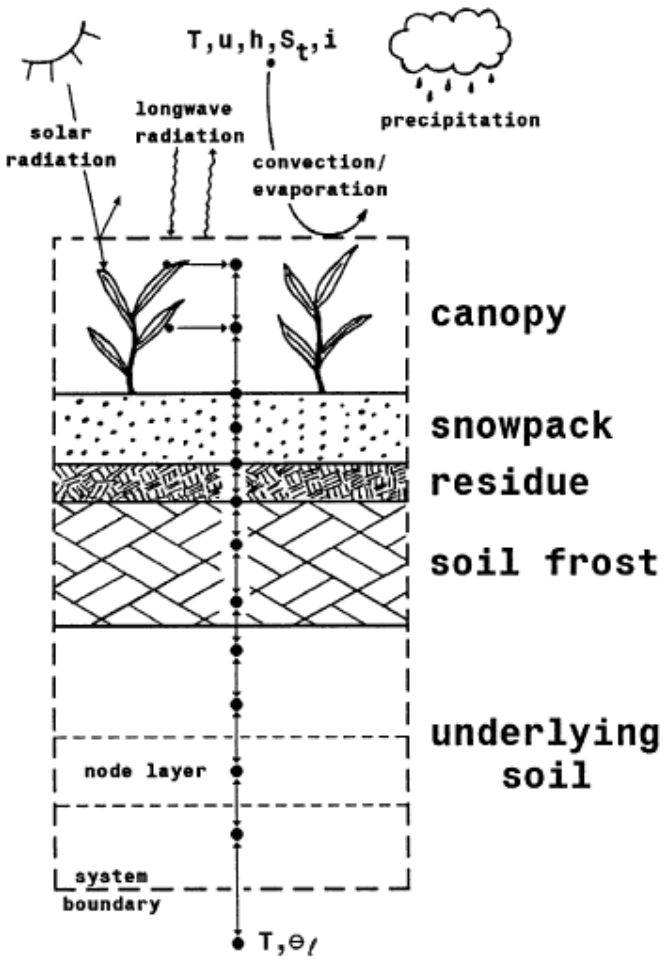

Figure 3.3. One dimensional conceptual profile simulated by the SHAW model as depicted in Flerchinger et al. (1996).

3.3.2 Input Parameters for the SHAW Model

SHAW simulations for the 2003/2004 water year were performed for each of the 57 points along the study grid. Initial and concluding soil temperature and water profiles, hourly meteorological data, and initial snow depth (0.00 m) were input based on measured values from the meteorological station at the site. The simulation year was from 1 October 2003 to 1 October 2004. The months of August and October coincide with the driest conditions at the site. Soil moisture during these months was reasonably

uniform through the UDCEW. Thus, soil temperatures and moisture contents recorded at the meteorological station were considered similar throughout the site. Precipitation was assumed uniform in the catchment given the size (0.02 km^2) and relief (65 m). Soil texture was specified for each point as obtained from the sieve analysis of soil samples from each modeled point. Elevation, aspect, slope, soil depth, and latitude for each simulated point were derived from the site survey. Values for surface roughness and wet and dry surface albedo were estimated as 5.0, 0.15 and 0.30 respectively for all simulated points.

SHAW requires the user to specify plant characteristics from the simulation area. Four plant groups were incorporated into the model representative of the plant communities observed at the site: 1) grasses and forbs, 2) sagebrush, 3) low shrubs, and 4) other shrubs. Plant height, biomass, and leaf dimension parameters were estimated for each plant group based on the site vegetative survey. Rooting depth at each point was estimated based on the rooting system classification presented by Spence (1937) and rooting depths as described in Section 2.2.3. Leaf area index (LAI) values were estimated from literature based on percent cover at the respective point and were assigned as follows: grasses and forbs, 0.48; sagebrush, 0.74; low shrubs, 0.40; and other shrubs, 0.70 (Flerchinger et al., 1996; Flerchinger and Clark, 2003). Leaf area index and plant biomass were adjusted to reflect point specific observations for each point simulation. All plant parameters estimated and the ranges of estimated LAI and biomass values are presented in Table 3.1 below.

Table 3.1. SHAW input parameters estimated for plant groups observed at the UDECW. Estimates (except LAI and biomass) are based on data reported by Flerchinger et al. (1996).

Parameter Estimated	Plant Group			
	Grasses/ Forbs	Sagebrush	Low Shrubs	Other Shrubs
Plant Albedo	0.25	0.15	0.2	0.25
Min. Transpiration Temp. (ºC)	10	7	10	10
Min. Stomatal Resistance (s/m)	200	100	100	100
Stomatal Resistance Exponent	5	5	5	5
Critical Leaf Water Potential (m)	-150	-300	-300	-300
Leaf Resistance ($m^3 s^{-1} kg^{-1}$)	38000	766000	670000	333000
Root Resistance ($m^3 s^{-1} kg^{-1}$)	77000	1700000	1600000	667000
Leaf Area Index	0.20 - 0.48	0.40 - 0.74	0.10 - 0.40	0.10 - 0.70
Plant Biomass (kg/m^2)	0.05 - 0.10	0.05 - 0.30	0.05 - 0.40	0.05 - 0.70

3.3.3 Model Calibration

The model was calibrated using measured near-surface soil moisture data from the study water year. Measured near-surface data represented the vertically averaged soil moisture in the upper 30 cm of the soil profile. Thus, SHAW predicted soil moisture was vertically averaged for the upper 30 cm of the soil profile and compared against measured data to calibrate the model. Model calibration involved adjustments to leaf area index, plant biomass, and percent sand, silt and clay. The model was most sensitive to these parameters and was easily calibrated to observed values by adjusting these specified parameters within reported ranges. Adjustments to vegetation parameters were within the ranges shown in Table 3.1. Adjustments to soil texture were within plus or minus 3% of the observed texture. Clay content was increased where the annual soil moisture simulation was low and clay content was reduced where the annual soil moisture simulation was high. Changing the vegetation parameters either reduced or increased simulated soil moisture during the late wet-high flux and drydown periods.

3.4 Water Balance Approach

An aggregated water balance (Flerchinger et al., 1998) for the UDCEW was calculated based on hydrometric data and SHAW results from the 2003/2004 water year. The SHAW model (Flerchinger et al., 1996) was used to simulate water inputs and outputs at 57 points along the study grid. Respective areas represented by each point were determined through area analysis using GIS. The respective representative areas were assumed to span 360 degrees out from the modeled point and to extend outward half the distance to the nearest adjacent modeled point. The SHAW computed *DeepPerc* component (Equation 2.1) was assumed to represent losses to groundwater and lateral flow along the soil-bedrock interface (McNamara et al., 2005) and was assumed consistent with the approach of McNamara et al. (2005) (Equation 2.2). Weighted results from each simulation were combined to form the aggregated 2003/2004 water balance model.

3.5 Investigation of the Controls on Soil Moisture

3.5.1 Definition of Soil Moisture States for the UDCEW

Soil moisture states for this study were organized for analysis consistent with those of McNamara et al. (2005). Thus, five “preferred states” were defined to represent the hydrologic regimes observed at the site (Figure 3.4): 1) summer dry (dry), 2) transitional fall wetting (wet-up), 3) low flux winter wet (wet-low flux), 4) high flux

spring wet (wet-high flux), and 5) transitional drying (drydown). Near-surface measured data were collected during all five states, but measurements during the low-flux winter wet period were not included in the analysis due to instrument error. SHAW simulated deep soil moisture data (soil moisture along the soil-bedrock interface) in this analysis were included for all five states. Point values for each state (Appendix B) were described for each point on the study grid as the mean value (for measured and simulated) observed at the respective point during the respective preferred soil moisture state. These mean preferred state point values were used to statistically analyze the controls on soil moisture

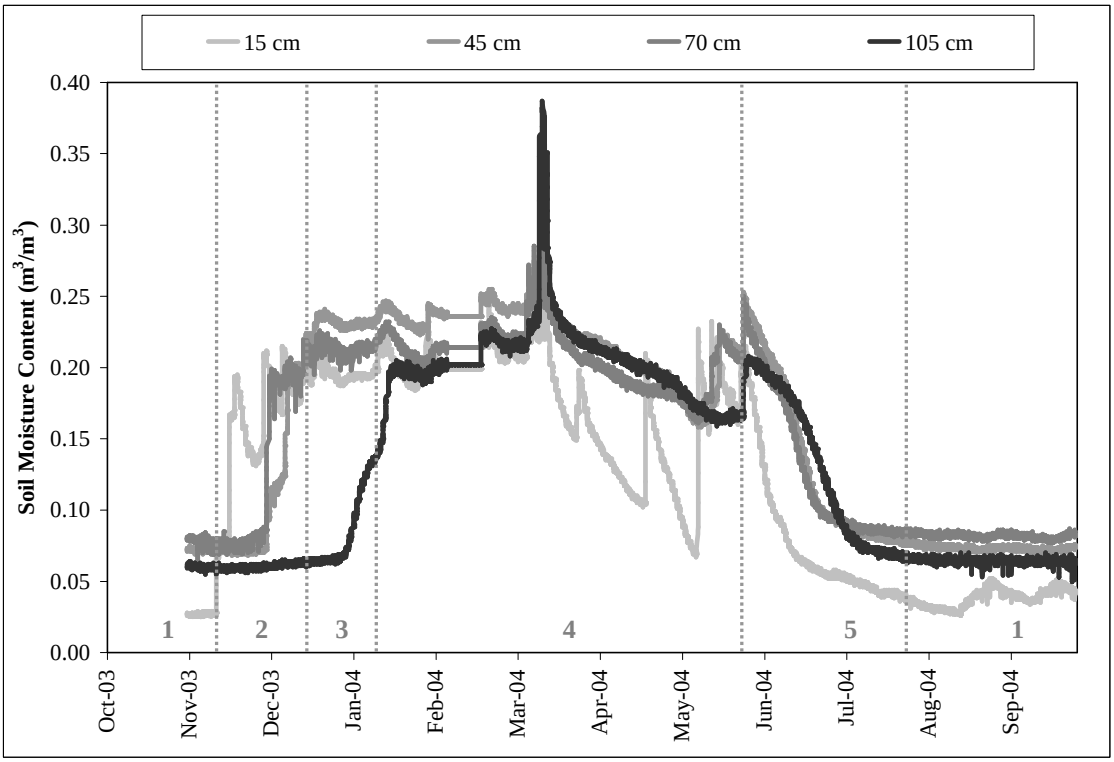

Figure 3.4. Soil moisture content observed at 15, 45, 70, and 105 cm soil depth for the 2003/2004 water year as recorded at the UDCEW. Preferred soil moisture states are illustrated by the gray captions (1 – Dry, 2 - Wet-Up, 3 – Wet-Low Flux, 4 – Wet-High Flux, and 5- Drydown) and dashed lines.

spatial variability, to quantify soil moisture distributions during each state, and to examine (through mapping) temporal variability of spatial patterns in soil moisture.

3.5.2 Standard Statistical Analysis

Correlations between soil moisture data and land surface site characteristics were tested using the Pearson correlation coefficient (Maidment, 1993). The Pearson method measures the linear association between two variables. Pearson values greater than zero indicate positive correlation (*y* variable increases as the *x* variable increases) and values less than one indicate negative correlation (*y* variable decreases as the *x* variable increases). A Pearson value of zero indicates that no correlation was observed at the sampled frequency. The point mean near-surface and deep soil moisture for each respective state were tested for correlation with the following variables: aspect; elevation; slope; distance to the divide; upslope contributing area; soil depth; percent coarse, sand, and fine soil fractions; distance to stream; plan, profile, mean, longitudinal, and cross-section curvature; concavity and convexity; percent live vegetative cover (by season); maximum snow depth; snow density @ maximum snow depth; and snow water equivalent (SWE) @ maximum snow depth.

A hypothesis test (*t* test) was conducted to test for statistical significance of the influence or control on soil moisture exerted by each of the site characteristics noted in the above paragraph. The null hypothesis was that soil moisture was not dependent on the respective tested site characteristic (the specific site characteristic exerted no control on the distribution of soil moisture at the site). The analysis required computation of a test statistic defined as:

$$t = \frac{r\sqrt{n-2}}{\sqrt{1-r^2}} \tag{3.1}$$

where t is the test statistic, r is the Pearson correlation coefficient, and n is the number of measurements (n = 57). The null hypothesis was rejected if $|t| > t_{crit}$, where t_{crit} is defined as the point on the Student's t distribution with degrees of freedom $n - 2$ and probability of exceedance equal to $\alpha/2$ (Maidment, 1993). The α value selected for this analysis was 0.05 and the resulting t_{crit} value was 2.0045. The tested variable was assumed to exert some control on soil moisture when the respective absolute value of t was greater than t_{crit}. Control was estimated in terms of the calculated Pearson correlation coefficient (r) and the percentage of variability in soil moisture explained by the respective control (r^2).

3.5.3 Temporal Stability Analysis

Temporal stability analysis was used to assess how individual sampled locations deviated from site mean soil moisture conditions during each hydrologic regime. This information provided insight into seasonal patterns in soil moisture at the site and identified sites that exhibit stability over time. Such sites could later be used to consistently monitor mean soil moisture conditions at the study basin without the investment of extensive spatial investigation. The temporal stability analysis required calculation of soil water storage (S_d) at the greatest common depth (30 cm) and the mean relative difference ($\bar{\delta}(j)$) in soil water storage observed at each sample location relative to all sampling dates. Soil water storage was calculated as

$$S_d = \sum_{i=1}^{n} \theta_i z_i \tag{3.2}$$

where θ_i and z_i represent measured near-surface soil moisture content and the thickness of the sampled soil profile (30 cm) respectively. The time average $\bar{\delta}_t(j)$ was used to describe the difference between near-surface and expected soil water storage for each seasonal hydrologic regime and for the overall 2003/2004 water year. The time average $\bar{\delta}_t(j)$ was calculated as

$$\bar{\delta}_t(j) = \frac{S_t(j) - \bar{S}_t(j)}{\bar{S}_t(j)} \tag{3.3}$$

where $S_t(j)$ is measured near-surface water storage at time *j* and $\bar{S}_t(j)$ is site mean near-surface soil water storage observed at time *j*. The time averaged values were plotted by rank for each hydrologic regime to determine which sites consistently represented basin mean soil moisture conditions.

3.5.4 Geostatistical Analysis

3.5.4.1 Computation of Sample Variograms

Variogram analyses were used to investigate temporal variation of soil moisture correlation lengths and to examine similarities in spatial variation of soil moisture and site characteristics. Sample variograms were calculated for mean near-surface and deep soil moisture (at each sample location) for each soil moisture state and for the following site characteristics: aspect; elevation; slope; distance to the divide; upslope contributing

area; soil depth; percent coarse, sand, and fine soil fractions; distance to stream; plan, profile, mean, longitudinal, and cross-section curvature; concavity and convexity; percent live vegetative cover (by season); maximum snow depth; snow density @ maximum snow depth; and snow water equivalent (SWE) @ maximum snow depth. Sample variograms of site characteristics were visually compared with soil moisture sample variograms of each preferred state to gain insight into potential controls on soil moisture patterns. Similarities in sample variograms were assumed to represent similar spatial patterns in soil moisture and the respective site characteristic and to be indicative of the respective characteristic exerting some control on soil moisture distribution at the site. The sample variograms were computed using Equation 1.3 and block kriging within the geostatistical package in Surfer 8.0 (Golden Software, Inc.) surface mapping software.

3.5.4.2 Model Fitting the Theoretical Variogram

Correlation lengths for observed and simulated soil moisture patterns at the UDCEW were modeled using omni-directional theoretical variograms (Figure 3.1). The approach provided insight into the temporal variability in spatial correlation of soil moisture patterns. The variograms were modeled using the geostatistical component of Surfer 8.0 (Golden Software, Inc.). The program calculates and plots the sample variogram based on Equation 1.3 and then allows the user to model the theoretical variogram by defining the bin and maximum lag widths, number of lag bins, degree of anisotropy, nugget effect, and the appropriate model function(s). Fine tuning of the best-fit curve is performed iteratively.

Several functions were tested in this analysis, including nested and un-nested applications of exponential, power, spherical, cubic, Gaussian, and logarithmic

approaches. Testing involve iterative best-fit plotting of the theoretical variogram through the calculated values of the sample variogram. The un-nested spherical model with a nugget effect provided the best-fit for the data and was, for consistency (Western et al., 2004), applied for all data analyzed in this study. The spherical model is explained by

$$\gamma_{sp}(h) = \frac{\sigma^2{}_0}{\sigma^2{}_P} + \left(1 - \frac{\sigma^2{}_0}{\sigma^2{}_P}\right)\left(1.5\frac{h}{a} - 0.5\left(\frac{h}{a}\right)^3\right) \quad h < a \tag{3.4}$$

$$\gamma_{sp}(h) = 1 \quad h \geq a$$

where $\gamma_{sp}(h)$ is the fitted theoretical variogram for a given lag (h), $\sigma^2{}_0/\sigma^2{}_p$ is the normalized nugget, and a is the range (Western et al., 2004).

The maximum lag distance (90 m) was set to one-half the maximum spatial extent of the data (180 m) to minimize the influence of lag bins representing few data pairs (Blöschl and Grayson, 2000). The data set included 1,596 data pairs. Lag bin width was set to 13 m to insure a minimum of 30 data pairs per lag bin. The number of bins (7) was determined by dividing the maximum lag distance (90 m) by bin width (13 m). Theoretical variograms representing near-surface and deep soil moisture were plotted for each moisture state. The quality of variogram fitting was measured by the root mean square error (RMSE) (Western et al., 2004)

$$RMSE = \left[\frac{\sum(\gamma_{sp}(h) - \gamma_s(h))^2}{n_h}\right]^{1/2} \tag{3.5}$$

where n_h is the number of lag bins in the sample variogram ($\gamma_s(h)$). Correlation lengths for near-surface and deep soil moisture were derived from the final fitted theoretical variograms and compared by moisture state to assess temporal variation in spatial soil moisture patterns.

3.5.5 Mapping of Soil Moisture Patterns

Spatial maps of near-surface and deep soil moisture were created by block kriging measured and modeled soil moisture point data with Surfer 8.0 surface mapping software. Maps were generated for each sampling date and used to visually present and analyze temporal fluctuations in soil moisture at the study site. The maps provided visual depictions of soil moisture patterns and allowed for comparison of spatial and temporal soil moisture variability with inferences made from the standard and geostatistical analyses. The maps were also compared with maps of site characteristics to visually investigate potential controls on soil moisture distributions (correlations of soil moisture contents and quantified physical and biological site characteristics).

3.6 Evaluation and Modification of Topographic and Wetness Indices

3.6.1 Evaluation of Commonly Used Indices

The following commonly used indices were tested for correlation with mean point measured and predicted soil moisture contents representative of each preferred soil moisture state:

Equation	Reference	
$\ln\left(\frac{a}{\tan\beta}\right)$	(Bevin and Kirkby, 1979)	(3.6)
$\left(\frac{a}{\tan\beta}\right)$	(O'Loughlin, 1986)	(3.7)
$\left(\frac{a}{\tan\beta}\right)\times PlanC$	(Burt and Butcher, 1985)	(3.8)
$PlanC$	(Burt and Butcher, 1985)	(3.9)
$a \times PlanC$	(Burt and Butcher, 1985)	(3.10)
$\left(\frac{a}{\beta}\right)$	(Burt and Butcher, 1985)	(3.11)
$\ln\left(\frac{a\times ASP}{\tan\beta}\right)$	(Gómez-Playa et al., 2001)	(3.12)
$\ln(a\times ASP)$	(Gómez-Playa et al., 2001)	(3.13)
$\ln(a)$	(Western et al., 1999)	(3.14)

Variables for the above equations are defined as follows: *a* represents the specific catchment area, β is the slope angle in degrees, *PlanC* is plan curvature, and *ASP* represents aspect. Values for each index above were calculated for each of the fifty-seven sampling points along the study grid. Correlations between calculated indices and near-surface and deep soil moisture for each soil moisture state were quantified using Pearson correlation analysis, inclusive of the before mentioned *t* test for significance. As with other analyses in this study, mean observed and modeled soil moisture values were used for each point during each state. The square of the Pearson correlation coefficient

was used to quantify the variability of soil moisture explained by the respective tested index during the respective soil moisture state.

3.6.2 Modification of Indices

Modified wetness indices were created to include the observed controls on soil moisture distributions in the UDCEW. The controls at the site were inferred from the before mentioned standard and geostatistical analyses of soil moisture patterns and basin characteristics. The following modified indices were tested for predictive capability:

$$\ln(a \times sdepth) \tag{3.15}$$

$$\ln(\%sand \times sdepth) \tag{3.16}$$

$$\ln(sdepth) \tag{3.17}$$

$$\ln(SWE \times sdepth) \tag{3.18}$$

$$\ln\left(\frac{ASP \times \%\ fines}{tan\beta}\right) \tag{3.19}$$

$$(a \times Convex) \tag{3.20}$$

$$(a \times LongC) \tag{3.21}$$

$$(\%smrcvr \times sdepth) \tag{3.22}$$

$$(\%spgcvr \times sdepth) \tag{3.23}$$

$$(\%wtrcvr) \tag{3.24}$$

$$\ln(WaterInput - ET) \tag{3.25}$$

where *a* is specific catchment area (m^2); *sdepth* is soil depth (m); *%sand* and *%fines* are the percentages of sand and fine grain classes respectively observed in the upper 30 cm of

the soil profile; *SWE* represents the snow water equivalent (cm) of the snowpack at the time of maximum snow depth; *%smrcvr* , *%spgcvr, and %wtrcvr* are the percent vegetative cover observed during the summer, spring, and winter seasons; *ASP* represents aspect (degrees); β is slope angle (degrees); *Convex* is slope convexity; *LongC* is longitudinal curvature; and *WaterInput* and *ET* are the mean combined rainfall (cm) and snowmelt (cm) input into and mean evapotranspiration (cm) out of the soil column respectively as determined for each point during each preferred soil moisture state. Numerous other combinations were considered. Equations 3.15 through 3.25 considered variables for observed controls and, with the exception of Equations 3.20 and 3.21 (included to test correlation with topographic curvature and convexity), provided the best combined parameterization of the observed controls. A Pearson correlation analysis, concurrent with previous applications in this study, was used to test the predictive capability of the modified indices. Significance of the parameterized relationships was tested using the before mentioned *t* test for significance.

4. RESULTS

4.1 Water Balance Simulation

The presentation of the study results begins first with the SHAW simulated 2003/2004 water balance given the remainder of the study uses the water balance parameters in the overall analysis. For the 2003/2004 water year precipitation occurred predominately during the cold season and the basin maintained a consistent snowpack during the winter months. However, the maximum snow depth (approximately 68 cm), cumulative precipitation (72.7 cm), and May rainfall (12.7 cm) were all greater than respective measurements in recent years. Additionally, the 2003/2004 water year included a significant mid-winter snowmelt event (66% reduction in snow depth) and subsequent snow accumulation period. Stream hydrograph peaks (Figure 2.9) were concurrent with snowmelt patterns observed and measured in the basin.

4.1.1 Calibration Results

The SHAW 2003/2004 water year simulation was calibrated using vertically averaged near-surface measurements from the mobile TDR soil moisture surveys at the site. Simulations were performed for each of the fifty-seven sampling locations. As discussed in Section 3.3.3, calibration of the model required adjusting leaf area index, plant biomass, and soil properties for each simulation (Table 3.1). The remainder of the site specific input parameters (aspect, elevation, latitude, and slope) were clearly defined

for each point and values for precipitation, air temperature, and soil albedo were consistent for all locations.

Representative calibration results from nine of the fifty-seven simulations are presented here due to the volume of simulations computed (Figures 4.1, 4.2, and 4.3). The nine simulations presented depict variations in the three main input parameters used during calibration (soil depth, soil texture, and vegetation). The modeled soil moisture patterns are similar to observed patterns with the following exceptions: simulated soil moisture is higher for the late December observation and remains higher slightly longer on the falling limb during the drydown period. The SHAW model simulates soil water movement in a 1D profile and does not account for lateral inflow or outflow. Modifications to the soil and vegetation properties adjusted the respective soil moisture curve to reflect seasonal variation in lateral flow components. Modifications of soil properties either increased or lowered the overall soil moisture curve for the simulation year. This approach was used when the model under predicted soil moisture for most of the year. Modifications to the vegetation properties were used to reduce over predicted soil moisture contents during the wet-low flux and drydown periods.

Calibration results are presented as observed versus simulated vertically averaged near-surface (upper 30 cm of the soil profile) soil moisture contents (m^3/m^3) at multiple sites with varying soil depths, soil textures, and vegetative communities (Figures 4.1, 4.2, and 4.3). Simulations for locations with shallow soils (< 0.40 m) and low canopy cover (< 25% annually) produced larger spikes in simulated soil moisture as water input fluctuated (Figures 4.1 and 4.3). Simulations of soil moisture for locations with greater percentages of coarse (> 2mm) and sand (< 2mm, > 0005 mm) grain fractions more

closely resembled observed soil moisture contents than simulations in locations with higher percentages of fine (< 0.05 mm) grain classes (Figure 4.2). The simulated soil moisture patterns corresponded well with the observed patterns in near-surface soil moisture. It is important to note again that the model is limited to 1D simulation and does not consider the influence of lateral flow from upslope areas.

Simulations of deep soil moisture were compared with measured deep soil moisture recorded at TDR instrumented soil pits within the study catchment (Figure 4.4). Comparisons of measured deep soil moisture and simulated deep soil moisture were only used where simulation points were in close proximity to measurement locations and where simulated and measured locations exhibited similar site characteristics (aspect, slope, vegetation, soil properties, and soil depth). Simulations from sampling location 19 (approximately 1.6 meters immediately downslope from a TDR instrumented soil pit) offered the nearest comparison point with observed TDR soil moisture data. Simulated deep soil moisture at location 19 corresponded well with observed TDR measured deep soil moisture content at soil moisture contents in the 0.07 to 0.16 m^3/m^3 range (Figure 4.4). Variability in model performance above 0.16 m^3/m^3 soil moisture content was largely attributed to 1D limitations and drift in modeled snowmelt rates. The final weighted water balance (Table 4.1), based on simulation results, is concurrent with previous research in the basin (McNamara et al., 2005), except where noted in section 4.1.1 below, and suggests that simulation results are well within reasonable limits.

4.1.2 <u>2003/2004 Water Balance</u>

The weighted aggregated water balance for the 2003/2004 water year is summarized in Table 4.1. Precipitation during the study water year fell predominately as

rainfall during the cold season, with 41% falling as snow. The water year included an early winter deep snowpack, significant mid-winter snowmelt period (66% reduction of snow depth), and late season snowpack re-accumulation period. The mid-winter melt greatly increased water input (rainfall and snowmelt) during the winter season and substantially shortened the winter-low flux season as described by McNamara et al. (2005).

McNamara et al. (2005) produced water balances for the UDCEW 1999/2000 and 2000/2001 water years using the SHAW model. Their approach simulated the respective water year balances by modeling soil water fluxes at a single point. Simulation points 8 and 9 for the 2003/2004 water year were geographically located in close proximity to the simulation points used by McNamara et al. (2005). These locations represent the deepest soil profiles observed at the UDCEW. Bedrock simulations for these points (when considered at a point scale) produced less bedrock flow (Point 8 – 24.95 cm, Point 9 – 26.45 cm) than the area weighted aggregated approach (31.28 cm) using the previously noted 57 sampling locations in the basin. This suggests that single point simulations by McNamara et al. (2005) for the 1999/2000 and 2000/2001 water years likely underestimated bedrock flow generation over the catchment scale.

A comparison of the water budgets from McNamara et al. (2005), the 2003/2004 water year, and simulation point 8 from the 2003/2004 water year is presented in Table 4.2. The 2003/2004 water year produced approximately 20% more precipitation than the water years simulated by McNamara et al. (2005). The percentage of precipitation represented by bedrock flow was greater for the aggregated 2003/2004 water budget than the water budgets derived from single point simulations by McNamara et al. (2005) and

this study for point 8. Additionally, the percentage of precipitation represented by evapotranspiration was less with the aggregated approach.

Based on the aggregated water budget for the 2003/2004 water year, evapotranspiration consumed 64.5% of the precipitation (30.1% for transpiration and 34.4% for evaporative losses) and 25.5% of the precipitation flowed out of the UDCEW as streamflow. Approximately 17.6% of the precipitation infiltrated through the soil column into groundwater storage (bedrock flow minus streamflow). The change in soil storage and error components for the 2003/2004 water year represent approximately -1.4% and -6.2% of the total precipitation respectively. Surface runoff has not been observed or recorded by runoff plots in the UDCEW since instrumentation began in the catchment in 1999. Cumulative water input and output for the 2003/2004 water balance are shown in Figure 4.5a.

4.1.3 Descriptions of Soil Moisture Periods for the 2003/2004 Water Year

4.1.3.1 Summer Dry Period

Seasonal fluctuations in available water are clearly defined by the water balance components shown in Table 4.3 and provide a framework for defining characteristic soil moisture periods at the study site. Precipitation (P) and water input (INPUT) were nearly equal to evapotranspiration (P/ET and INPUT/ET both < 1) during the dry season (10/01/03-11/11/03 and 07/29/04-10/01/04) for the 2003/2004 water year. Bedrock flow was non-existent during the dry period, suggesting that soil water was lost to evapotranspiration demands or stored in the soil profile. Soil moisture throughout the soil profile during the period ranged from 0.04 to 0.09 m^3/m^3 (Figure 4.5b). Streamflow was not observed at the site during this period.

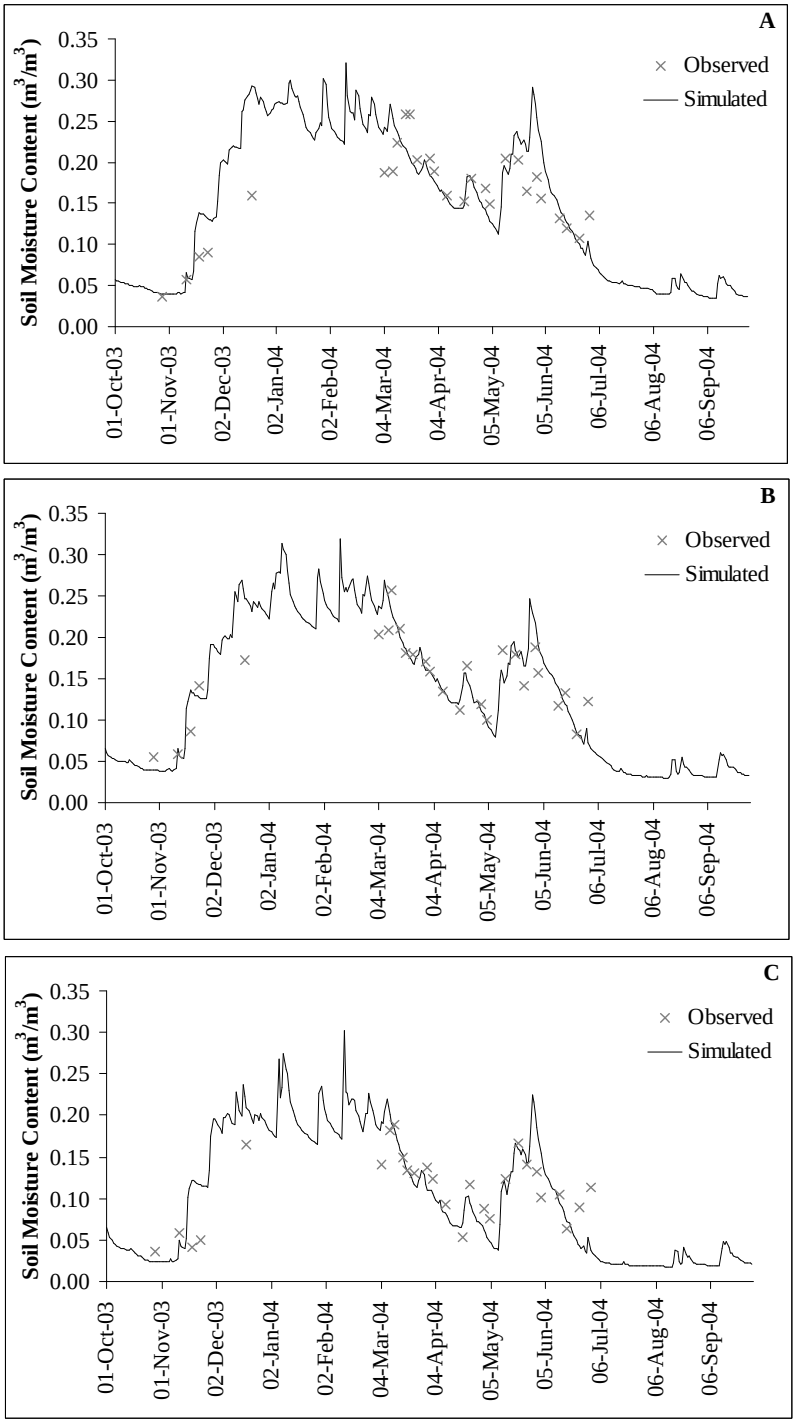

Figure 4.1. Calibration results depicting simulated and observed vertically averaged near-surface soil moisture contents for sampling points with 1.25 m (A - Point 8); 0.70 m (B - Point 30); and 0.27 m (C - Point 54) total soil depth.

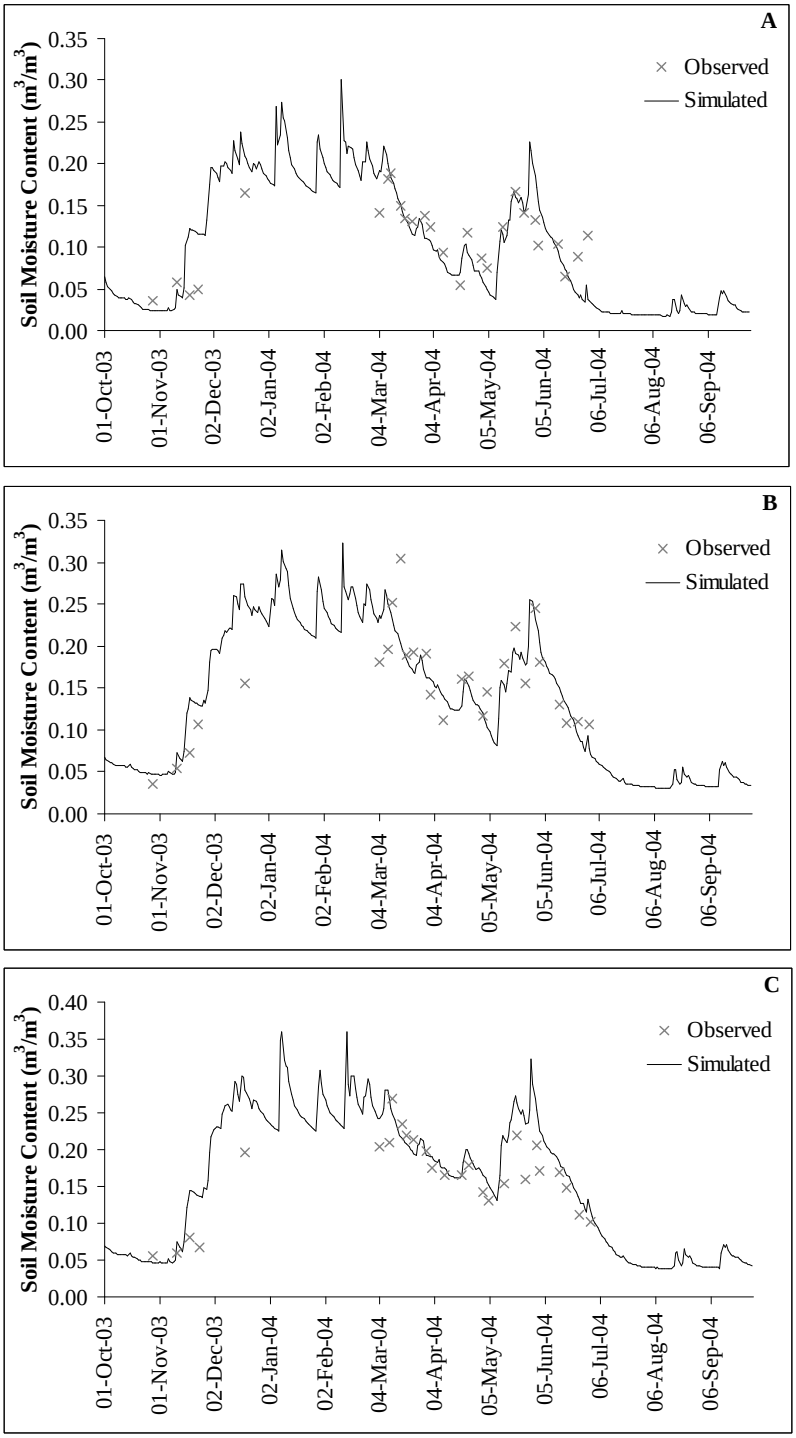

Figure 4.2. Calibration results depicting simulated and observed vertically averaged near-surface soil moisture contents for sampling points with 24% coarse (A - Point 52); 81% sand (B - Point 58); and 8% fines(C - Point 57) grain fractions.

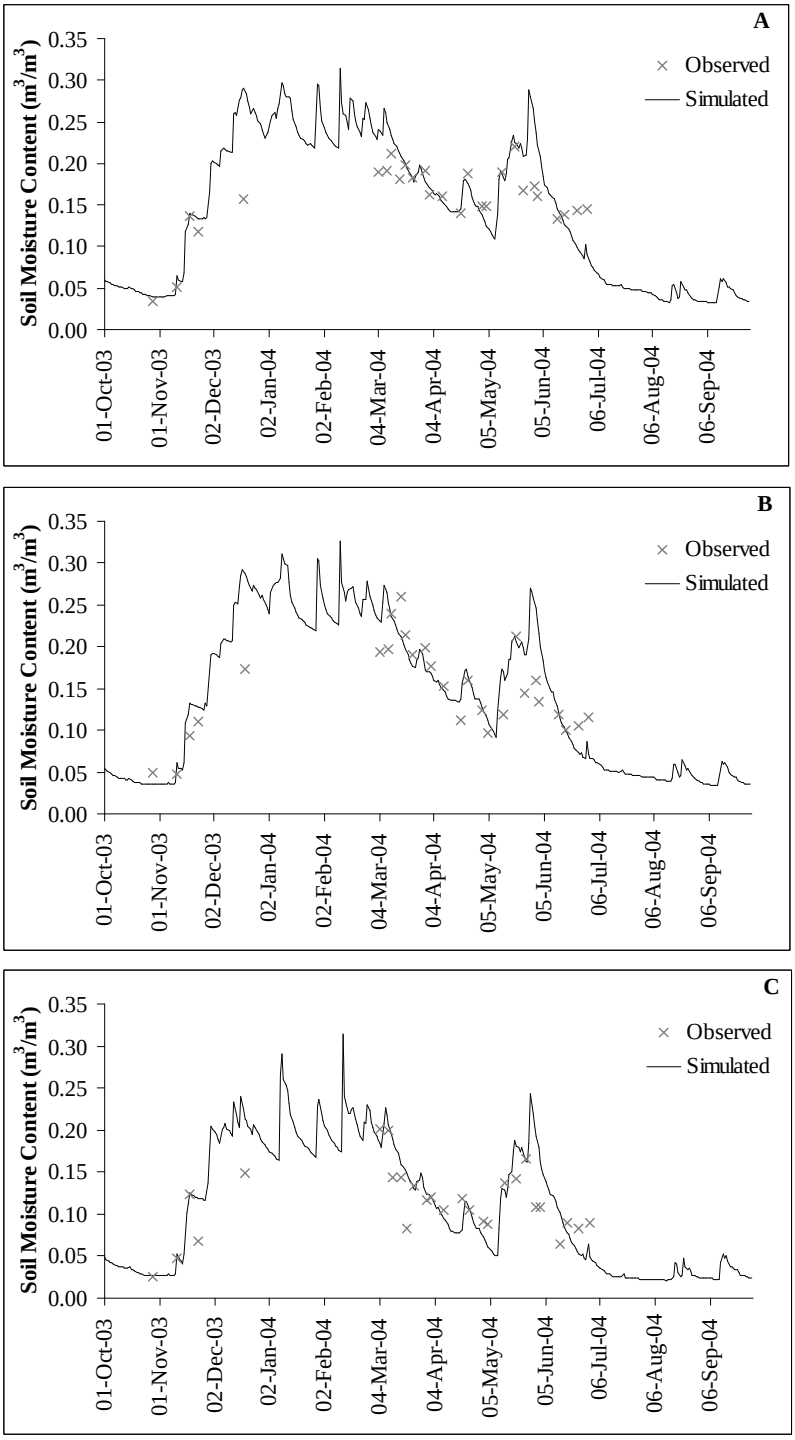

Figure 4.3. Calibration results depicting simulated and observed vertically averaged near-surface soil moisture contents for sampling points with 100% (A - Point 9); 43% (B - Point 13); and 17% (C - Point 20) annual vegetative cover.

4.1.3.2 Fall Wet-Up Period

As the fall rains commenced in December 2003, P/ET and INPUT/ET increased to 5.39 and 4.55 respectively. Precipitation and water input exceeded evapotranspiration demands and the study area began to wet-up. Near-surface (upper 30 cm) and deep (30 to 70 cm) soil moisture contents increased from 0.07 to 0.22 and 0.09 to 0.20 m^3/m^3 (Figure 4.5b). Soil moisture at the base of the deepest soil profiles (depth > 70 cm) remained near 0.07 m^3/m^3. These events define the fall wetting period (wet-up). The 2003/2004 wet-up period occurred from 11/11/03 through 12/15/03. The period marked the beginning of bedrock flow (2 cm) (Figure 4.5c), although lateral flow during the period would have been minimal given the minimal bedrock flow value. Capacitance rods at the upper and middle weirs recorded the first development of water in the channel (Figure 4.5d) as streamflow developed.

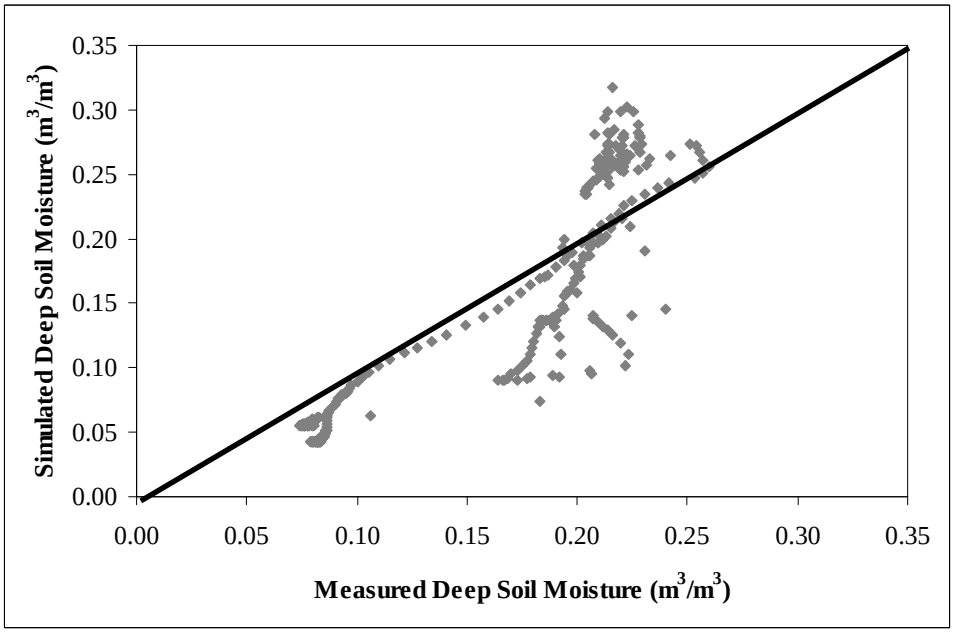

Figure 4.4. SHAW simulated deep (60 cm) soil moisture content (m^3/m^3) at sampling point 19 versus TDR measured deep (52 cm) soil moisture content (m^3/m^3) observed at an instrumented location 1.6 m immediately downslope of sampling point 19. Solid black line denotes the 1:1 line.

Table 4.1. Weighted aggregated water balance for the UDCEW 2003/2004 water year as computed using the SHAW model. The calculated values for Precipitation; Precip Intercep; ET; Plant Transp; Canopy, Snow, Residue, and Soil Storage; DeepPerc; Runoff; Ponded; and Error are weighted values based on the percent of the total catchment area (shown in column 3). The weighted values are summed to provide catchment area values, shown as the totals at the bottom of the table.

			2003 - 2004 WATER BALANCE											
							CHANGE IN STORAGE							
POINT	AREA km^2	FRACTION OF TOTAL AREA	PRECIP cm	PRECIP INTERCEPT cm	ET cm	PLANT TRANSP cm	CANOPY cm	SNOW cm	RESIDUE cm	SOIL cm	DEEP PERC cm	RUNOFF cm	PONDED cm	ERROR cm
1	0.000418	0.025	1.85	0.26	1.13	0.57	0.00	0.00	0.00	-0.03	0.86	0.00	0.00	-0.11
2	0.000218	0.013	0.97	0.12	0.69	0.35	0.00	0.00	0.00	-0.02	0.38	0.00	0.00	-0.08
3	0.000257	0.016	1.14	0.11	0.76	0.36	0.00	0.00	0.00	-0.02	0.44	0.00	0.00	-0.04
4	0.000278	0.017	1.23	0.16	0.81	0.43	0.00	0.00	0.00	-0.03	0.53	0.00	0.00	-0.08
5	0.000225	0.014	1.00	0.13	0.68	0.38	0.00	0.00	0.00	-0.01	0.37	0.00	0.00	-0.05
6	0.000340	0.021	1.51	0.19	1.08	0.57	0.00	0.00	0.00	-0.02	0.53	0.00	0.00	-0.08
7	0.000317	0.019	1.41	0.18	0.98	0.50	0.00	0.00	0.00	-0.02	0.58	0.00	0.00	-0.14
8	0.000297	0.018	1.32	0.18	0.90	0.50	0.00	0.00	0.00	-0.03	0.45	0.00	0.00	-0.01
9	0.000281	0.017	1.25	0.16	0.88	0.50	0.00	0.00	0.00	-0.03	0.45	0.00	0.00	-0.06
10	0.000259	0.016	1.15	0.15	0.78	0.40	0.00	0.00	0.00	-0.02	0.48	0.00	0.00	-0.08
11	0.000631	0.039	2.80	0.35	1.88	0.98	0.00	0.00	0.00	-0.05	1.18	0.00	0.01	-0.20
12	0.000569	0.035	2.53	0.27	1.70	0.95	0.00	0.00	0.00	-0.05	1.05	0.00	0.01	-0.17
13	0.000230	0.014	1.02	0.13	0.71	0.40	0.00	0.00	0.00	-0.02	0.37	0.00	0.00	-0.04
14	0.000362	0.022	1.61	0.20	1.06	0.55	0.00	0.00	0.00	-0.01	0.68	0.00	0.00	-0.13
15	0.000200	0.012	0.89	0.08	0.56	0.29	0.00	0.00	0.00	-0.01	0.38	0.00	0.00	-0.06
16	0.000369	0.023	1.64	0.21	1.15	0.59	0.00	0.00	0.00	-0.03	0.68	0.00	0.00	-0.17
17	0.000329	0.020	1.46	0.18	1.05	0.56	0.00	0.00	0.00	-0.02	0.51	0.00	0.00	-0.07
18	0.000374	0.023	1.66	0.08	1.03	0.41	0.00	0.00	0.00	-0.02	0.72	0.00	0.00	-0.07
19	0.000338	0.021	1.50	0.11	1.10	0.59	0.00	0.00	0.00	-0.03	0.58	0.00	0.00	-0.14
20	0.000281	0.017	1.25	0.13	0.83	0.40	0.00	0.00	0.00	-0.02	0.54	0.00	0.00	-0.11
21	0.000342	0.021	1.52	0.15	1.04	0.49	0.00	0.00	0.00	-0.02	0.63	0.00	0.00	-0.13
23	0.000376	0.023	1.67	0.22	1.15	0.56	0.00	0.00	0.00	-0.02	0.67	0.00	0.01	-0.14
24	0.000313	0.019	1.39	0.09	0.94	0.44	0.00	0.00	0.00	-0.01	0.53	0.00	0.00	-0.07
25	0.000330	0.020	1.46	0.18	1.07	0.54	0.00	0.00	0.00	-0.02	0.55	0.00	0.00	-0.14
26	0.000301	0.018	1.34	0.08	0.90	0.41	0.00	0.00	0.00	0.00	0.59	0.00	0.00	-0.16
27	0.000211	0.013	0.93	0.12	0.66	0.33	0.00	0.00	0.00	-0.01	0.39	0.00	0.00	-0.11
28	0.000198	0.012	0.88	0.11	0.61	0.31	0.00	0.00	0.00	-0.01	0.37	0.00	0.00	-0.10
29	0.000544	0.033	2.42	0.10	1.41	0.60	0.00	0.00	0.00	-0.04	1.07	0.00	0.00	-0.02
30	0.000208	0.013	0.92	0.07	0.63	0.31	0.00	0.00	0.00	-0.02	0.36	0.00	0.00	-0.05
31	0.000227	0.014	1.01	0.10	0.65	0.30	0.00	0.00	0.00	-0.02	0.40	0.00	0.00	-0.02
32	0.000221	0.013	0.98	0.07	0.64	0.28	0.00	0.00	0.00	-0.02	0.39	0.00	0.00	-0.02
33	0.000197	0.012	0.87	0.06	0.56	0.25	0.00	0.00	0.00	-0.01	0.35	0.00	0.00	-0.02
34	0.000204	0.012	0.91	0.09	0.62	0.28	0.00	0.00	0.00	-0.01	0.34	0.00	0.00	-0.05
35	0.000219	0.013	0.97	0.04	0.59	0.25	0.00	0.00	0.00	-0.02	0.42	0.00	0.00	-0.01
36	0.000232	0.014	1.03	0.06	0.62	0.24	0.00	0.00	0.00	0.00	0.51	0.00	0.00	-0.10
37	0.000142	0.009	0.63	0.02	0.36	0.13	0.00	0.00	0.00	-0.01	0.32	0.00	0.00	-0.04
38	0.000241	0.015	1.07	0.07	0.69	0.30	0.00	0.00	0.00	-0.01	0.52	0.00	0.00	-0.13
39	0.000226	0.014	1.00	0.17	0.68	0.33	0.00	0.00	0.00	-0.02	0.38	0.00	0.00	-0.04
40	0.000210	0.013	0.93	0.03	0.52	0.18	0.00	0.00	0.00	-0.01	0.47	0.00	0.00	-0.05
41	0.000180	0.011	0.80	0.01	0.37	0.07	0.00	0.00	0.00	0.00	0.43	0.00	0.00	0.00
42	0.000200	0.012	0.89	0.03	0.51	0.18	0.00	0.00	0.00	-0.01	0.44	0.00	0.00	-0.05
43	0.000203	0.012	0.90	0.03	0.52	0.18	0.00	0.00	0.00	-0.01	0.44	0.00	0.00	-0.05
44	0.000221	0.013	0.98	0.03	0.57	0.20	0.00	0.00	0.00	-0.01	0.48	0.00	0.00	-0.06
45	0.000186	0.011	0.83	0.04	0.47	0.18	0.00	0.00	0.00	-0.01	0.43	0.00	0.00	-0.07
46	0.000203	0.012	0.90	0.05	0.57	0.24	0.00	0.00	0.00	-0.01	0.46	0.00	0.00	-0.12
47	0.000198	0.012	0.88	0.03	0.50	0.18	0.00	0.00	0.00	-0.01	0.44	0.00	0.00	-0.04
48	0.000280	0.017	1.24	0.04	0.69	0.25	0.00	0.00	0.00	-0.02	0.63	0.00	0.00	-0.07
50	0.000121	0.007	0.54	0.02	0.30	0.11	0.00	0.00	0.00	0.00	0.28	0.00	0.00	-0.04
51	0.000133	0.008	0.59	0.02	0.34	0.13	0.00	0.00	0.00	0.00	0.31	0.00	0.00	-0.06
52	0.000135	0.008	0.60	0.04	0.39	0.18	0.00	0.00	0.00	-0.01	0.26	0.00	0.00	-0.04
54	0.000398	0.024	1.77	0.07	1.07	0.42	0.00	0.00	0.00	-0.02	0.86	0.00	0.00	-0.15
55	0.000305	0.019	1.35	0.14	0.85	0.35	0.00	0.00	0.00	-0.01	0.66	0.00	0.00	-0.15
56	0.000655	0.040	2.91	0.12	1.67	0.67	0.00	0.00	0.00	-0.04	1.43	0.00	0.01	-0.16
57	0.000353	0.022	1.57	0.05	0.84	0.31	0.00	0.00	0.00	-0.02	0.72	0.00	0.00	0.03
58	0.000645	0.039	2.86	0.20	1.80	0.82	0.00	0.00	0.00	-0.06	1.19	0.00	0.01	-0.06
22a	0.000223	0.014	0.99	0.10	0.70	0.34	0.00	0.00	0.00	-0.02	0.40	0.00	0.00	-0.09
22b	0.000225	0.014	1.00	0.07	0.66	0.30	0.00	0.00	0.00	-0.01	0.39	0.00	0.00	-0.04
Totals	**0.02**	**1.00**	**72.71**	**6.27**	**46.92**	**21.93**	**0.00**	**0.00**	**0.00**	**-1.04**	**31.28**	**0.00**	**0.15**	**-4.48**

Table 4.2. Comparison of the aggregated 2003/2004 water balance with the 2003/2004 water balance using simulation point 8 solely and with the 1999/2000 and 2000/2001 water balances computed by McNamara et al. (2005) for the UDCEW. Each of the balances was computed using the SHAW model. McNamara et al. (2005) simulated the 1999/2000 and 2000/2001 water balances by modeling annual soil water fluxes at one point in the basin. The aggregated 2003/2004 balance provides an area weighted approach inclusive of fifty-seven simulation points in the UDCEW.

ANNUAL WATER BUDGET	WATER YEAR			Point 8	PERCENT OF PRECIPITATION			Point 8
Parameter Measured (cm)	1999-2000	2000-2001	2003-2004	2003-2004	1999-2000	2000-2001	2003-2004	2003-2004
Precipitation	58.4	56.8	72.7	72.7	-	-	-	-
% Precip. as Snow	47	53	41	41	-	-	-	-
ET	34.9	41.5	46.9	50.0	59.8	73.2	64.5	68.8
Storage Canopy	0.0	0.0	0.0	0.0	0.0	0.0	0.0	0.0
Storage Snow	0.0	0.0	0.0	0.0	0.0	0.0	0.0	0.0
Storage Residue	0.0	0.0	0.0	0.0	0.0	0.0	0.0	0.0
Change in Soil Storage	0.0	-0.3	-1.0	-1.7	0.0	-0.4	-1.4	-2.3
Overland Flow	0.0	0.0	0.0	0.0	0.0	0.0	0.0	0.0
Bedrock Flow	Not Avail.	18.8	31.3	25.0	Not Avail.	33.0	43.0	34.4
Streamflow	Not Avail.	14.3	18.5	18.5	Not Avail.	25.2	25.4	25.4
Error	-4.8	-3.3	-4.5	-0.6	-8.2	-5.8	-6.2	-0.8

4.1.3.3 Winter Wet-Low Flux Period

As precipitation intensity increased in late December and January the hydrologic regime switched to the winter wet-low flux period (12/16/03-01/08/04). This period is typified by snowfall and the development of a winter-long snowpack at the site. Soil moisture in the upper profiles is nearly equal and soil moisture at depth, particularly at the base of the deepest soil profiles, is lower than soil moisture in the near-surface and mid-depth locations (Figure 4.5b). Soil moisture at the base of the deepest profiles rises gradually through the period (Figure 4.5b). The 2000/2001 water year produced a 117 day wet-low flux period (Table 4.3) and a persistent snowpack (McNamara et al., 2005). The 2003/2004 water year produced a brief (24 day) winter wet-low flux period followed by melting of nearly two thirds of the snowpack during the onset of the wet-high flux period (01/09/04-05/28/04). The ratios P/ET and INPUT/ET doubled during the 2003/2004 wet-low flux period, as precipitation greatly exceeded evapotranspiration.

For the 2003/2004 water year, soil moisture content during the wet low-flux period remained near 0.22 m^3/m^3 through most of the catchment. Soil moisture at the base of deep profiles increased to 0.14 m^3/m^3 (Figure 4.5b). Bedrock flow during the wet-low flux period increased three times that of the wet-up period (Figure 4.5c and Table 4.3). During the wet-low flux period streamflow at the site continued through the upper and middle weirs and began at the lower weir (Figure 4.5d).

4.1.3.4 Winter Wet-High Flux Period

The wet-high flux period is marked by a rapid increase in bedrock flow production (Figure 4.5c). Cool February air temperatures contributed to snowpack

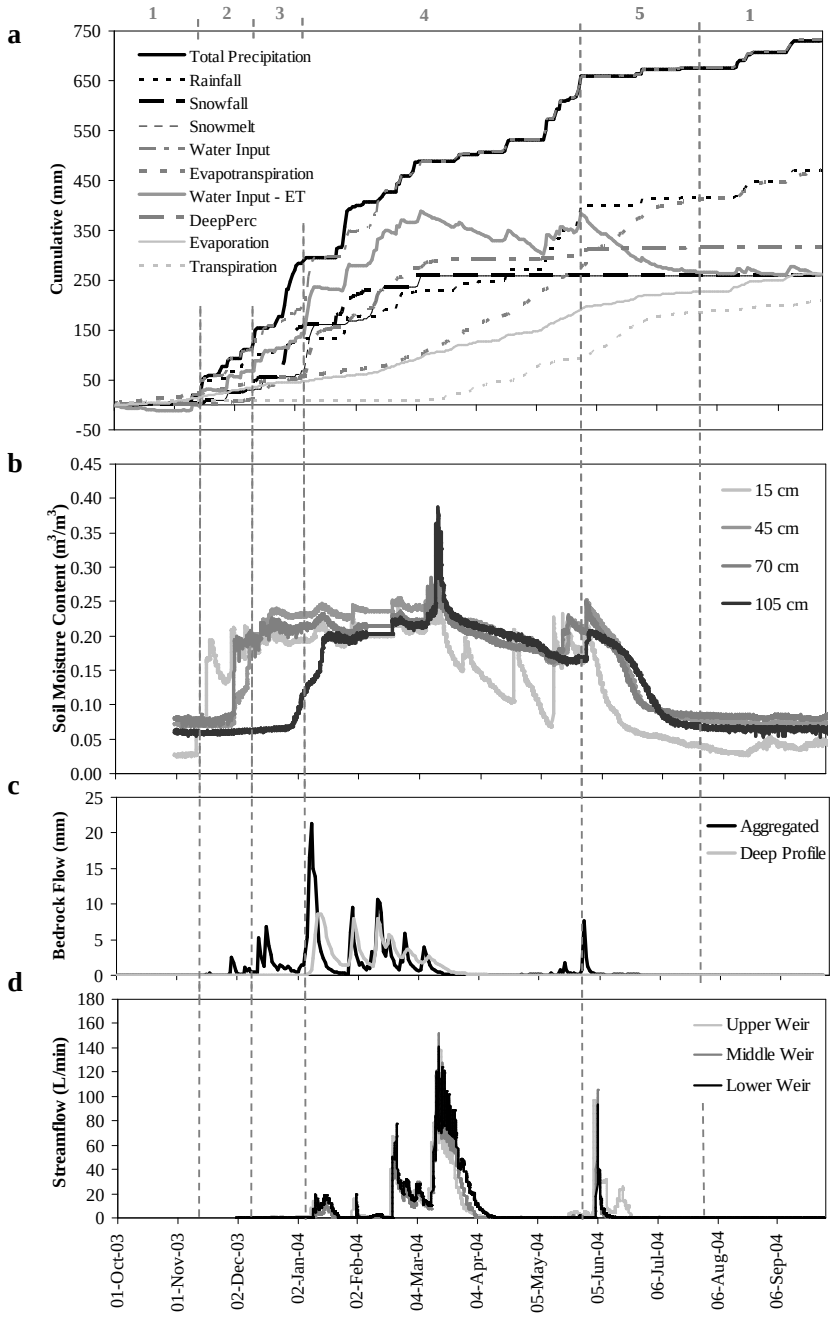

Figure 4.5. Timing of hydrologic regimes during the 2003/2004 water year: a - cumulative water gains and losses, b – soil moisture observed near simulation point 8, c – aggregated and deep soil profile bedrock flow simulated by SHAW, and d – streamflow recorded at the three weirs in the UDCEW. Timing of the water inputs and losses during the water year illustrates the soil moisture periods defined by McNamara et al. (2005): 1 – dry, 2 – wet-up, 3 – wet-low flux, 4 – wet-high flux, and 5 - drydown. The periods are delineated for the 2003/2004 water year as indicated by the dashed lines above and number headings at the top of the figure.

Table 4.3. Water balance components for the 2003/2004 and 2000/2001 (McNamara et al., 2005) water years for each of the defined soil moisture periods. Figure modified from McNamara et al. (2005) for comparison of the two respective water years. Rates for ET, precipitation intensity, and water input intensity are shown to quantify changes in water delivery to soil profile during each of the defined hydrologic regimes. P/ET and Input/ET provide quantification of the relationship between precipitation, water input, and evapotranspiration for each period.

2003 - 2004 WATER YEAR										
PERIOD	DURATION (days)	ET (cm)	PRECIP DEPTH (rain + snowfall) (cm)	WATER INPUT (rain + snowmelt) (cm)	BEDROCK FLOW (cm)	ET (mm/day)	PRECIP INTENSITY (mm/day)	WATER INPUT INTENSITY (mm/day)	P/ET	INPUT/ ET
1 - Dry	105	8	8	8	0	0.75	0.72	0.72	0.96	0.96
2 - Wet-up	34	2	13	11	2	0.73	3.95	3.33	5.39	4.55
3 - Wet-Low Flux	24	1	14	12	6	0.50	5.85	5.09	11.70	10.18
4 - Wet-High Flux	141	22	36	40	23	1.56	2.57	2.86	1.64	1.83
5 - Drydown	61	13	2	2	1	2.18	0.28	0.28	0.13	0.13
2000 - 2001 WATER YEAR										
1 - Dry	104	6	3	3	0	0.57	0.29	0.29	0.50	0.50
2 - Wet-up	29	3	13	13	0	1.10	4.53	4.53	4.33	4.33
3 - Wet-Low Flux	117	3	24	6	1	0.28	2.07	0.52	8.00	2.00
4 - Wet-High Flux	51	6	12	27	23	1.10	2.42	5.22	2.00	4.50
5 - Drydown	64	17	4	4	0	2.71	0.63	0.63	0.24	0.24

development as winter precipitation exceeded evapotranspiration demands during the wet-high-flux period. As the period progressed into March of 2004, air temperatures increased above 0˚C and precipitation began falling predominately as rainfall. Evapotranspiration demands during the wet-high flux period increased from 0.5 mm/day to 1.56 mm/day by the conclusion of the period (Table 4.3). Bedrock flow peaked as snowmelt and rainfall contributions increased water input (Figure 4.5c).

The snowpack was completely melted by mid-March and water input decreased (Figure 4.5a). Streamflow spiked to 80 L/min in early February and peaked at approximately 160 L/min in mid-March following melting of the snowpack (Figure 4.5d). Streamflow returned to near 0 L/min for the duration of the wet-high flux period. By late May water input at the site decreased dramatically while evapotranspiration demands remained high. Near-surface soil moisture content peaked near 0.24 m^3/m^3 in late March and dropped to 0.07 m^3/m^3 in late May before returning to 0.22 m^3/m^3 at the end of the wet-high flux period (Figure 4.5b). Deep soil moisture during the period peaked in mid-March at 0.35 m^3/m^3 and gradually declined before rising again to 0.20 m^3/m^3 near the end of the period (Figure 4.5b).

4.1.3.5 Drydown Period

The drydown period (05/29/04-07/28/04) began immediately after near-surface and deep soil moisture contents spiked at the end of the wet-high flux period in late May. P/ET and INPUT/ET decreased below 1.0. Bedrock flow during the drydown period decreased to 0.16 mm/day (1 cm for the entire drydown period) before ceasing in mid-June. Streamflow at the site spiked briefly (to 25 to 80 L/min) at the onset of the drydown period due to unusually high rainfall during the month of May and then ceased

in late June (Figure 4.5). By the end of the drydown period (07/28/04) near-surface soil moisture content fell sharply to 0.05 m^3/m^3 and deep soil moisture decreased to 0.08 m^3/m^3 (Figure 4.5b).

4.2 Temporal Stability

The standard deviation in soil moisture at the UDCEW increases as the site average soil moisture content increases (Figure 4.6). The mean relative difference (Equation 3.3) in near surface soil water storage (Equation 3.2) for each of the fifty-seven sampling locations was determined for the dry, wet-up, wet-high flux, and drydown soil moisture periods. The values were ranked from highest to lowest for the respective periods to investigate how individual points deviate from the mean (Figure 4.7). The wet-low flux period was excluded from this analysis because no near-surface soil moisture measurements were available for that period. The values appear reasonably symmetric about the mean for all investigated periods, with slight deviations on the wetter end of the curve for the wet-up and wet-high flux periods. In general, individual points display some variability in rank from period to period, but most points maintain similar ranks through the year. Some ranks varied dramatically from dry to wet periods and may represent locations near preferred flowpaths. For example, points 24 and 26 exhibit the greatest mean relative difference during the wet and drydown periods, but point 26 represents near and below mean conditions during the wet-up and dry periods.

Additionally, points showing the highest positive mean relative difference - wettest points relative to the mean – (19, 23, 24, 25, 26, and 41) during the wet and drydown

periods represent central basin locations. These locations are visible on spatial soil moisture maps (Appendix C and Appendix D) as locations with the highest soil moisture contents for the water year and concur with simulated deep soil moisture patterns for the wet and drydown periods.

Cumulative probability plots of soil water storage were constructed to locate points representative of mean basin hydrologic conditions and to locate sites that were consistently ranked one standard deviation above (representing conditions near the site maximum) or below (representing conditions near the site minimum) the mean (Figure 4.8). Sampling location 43 was consistently near the mean soil water storage for the 2003/2004 water year (Figure 4.8). Point 43 provides a sample location for obtaining mean basin hydrologic data throughout most of the year. The variability in basin hydrology is best described by points 19 and 47. Point 19, mean rank of 54, was consistently (with exception of dry period) one standard deviation above the mean and point 47, mean rank of 5, was consistently (with exception of wet-up period) one standard deviation below the mean for all periods of the study year. Points 19 and 47 provide insight into the basin maximum and minimum values for each period of the year. However, soil water storage at point 19 was near the mean for the dry period and soil water storage at point 47 was closer to the mean for the wet-up period. Thus, use of temporal stability monitoring sites in the UDCEW offers improvements over randomly selected monitoring locations; however, variability at the site cannot be completely assessed through time-stability inferred sampling locations. The time stability approach provided insight into locations of possible variable saturated subsurface source areas

centralized in the basin during the wet-up and hydrologically wet season. These locations are possible sources to streamflow initiation at the site.

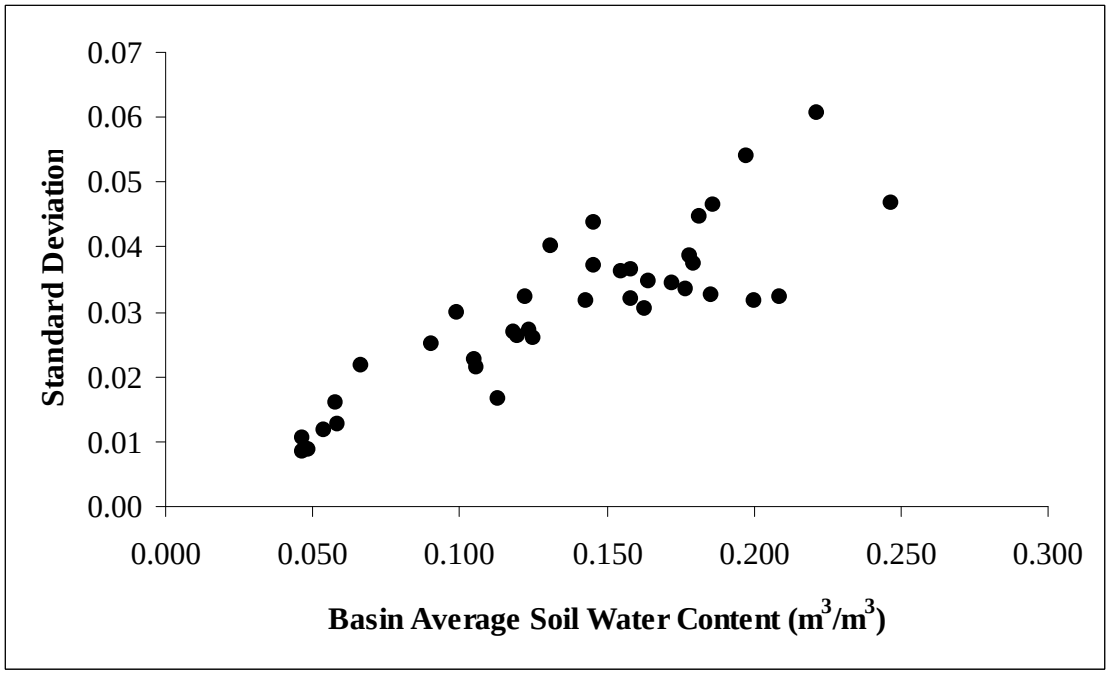

Figure 4.6. Measured basin average near-surface soil moisture content versus standard deviation of measured observations for the 2003/2004 water year.

4.3 Analysis of Controls on Soil Moisture

4.3.1 Variogram Analysis

Sample and theoretical variograms of near-surface (Figure 4.9) and deep soil moisture (Figure 4.10) were calculated to examine the temporal variation in soil moisture correlation lengths and to infer controls on the temporal variation. Variograms of near-surface data are not presented for the wet-low flux period due to missing data. Variograms for deep soil moisture during the wet-low flux period were calculated but are not presented because the general form of the variogram was not appropriate for making

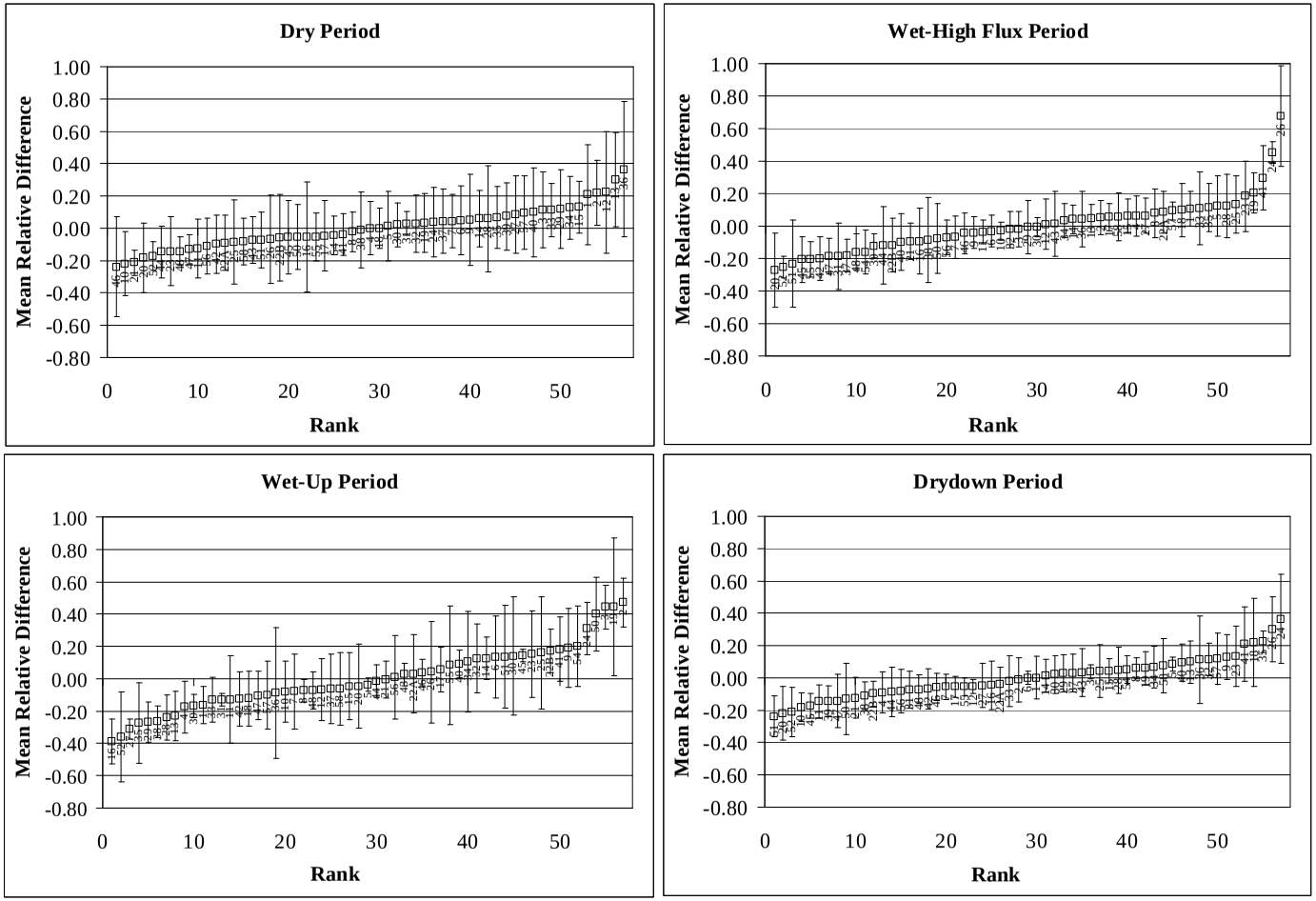

Figure 4.7. Mean relative difference in near-surface soil water storage observed at each point for the dry, wet-up, wet-high flux, and drydown periods of the 2003/2004 water year. Error bars indicate the standard deviation for the respective point during the period of interest.

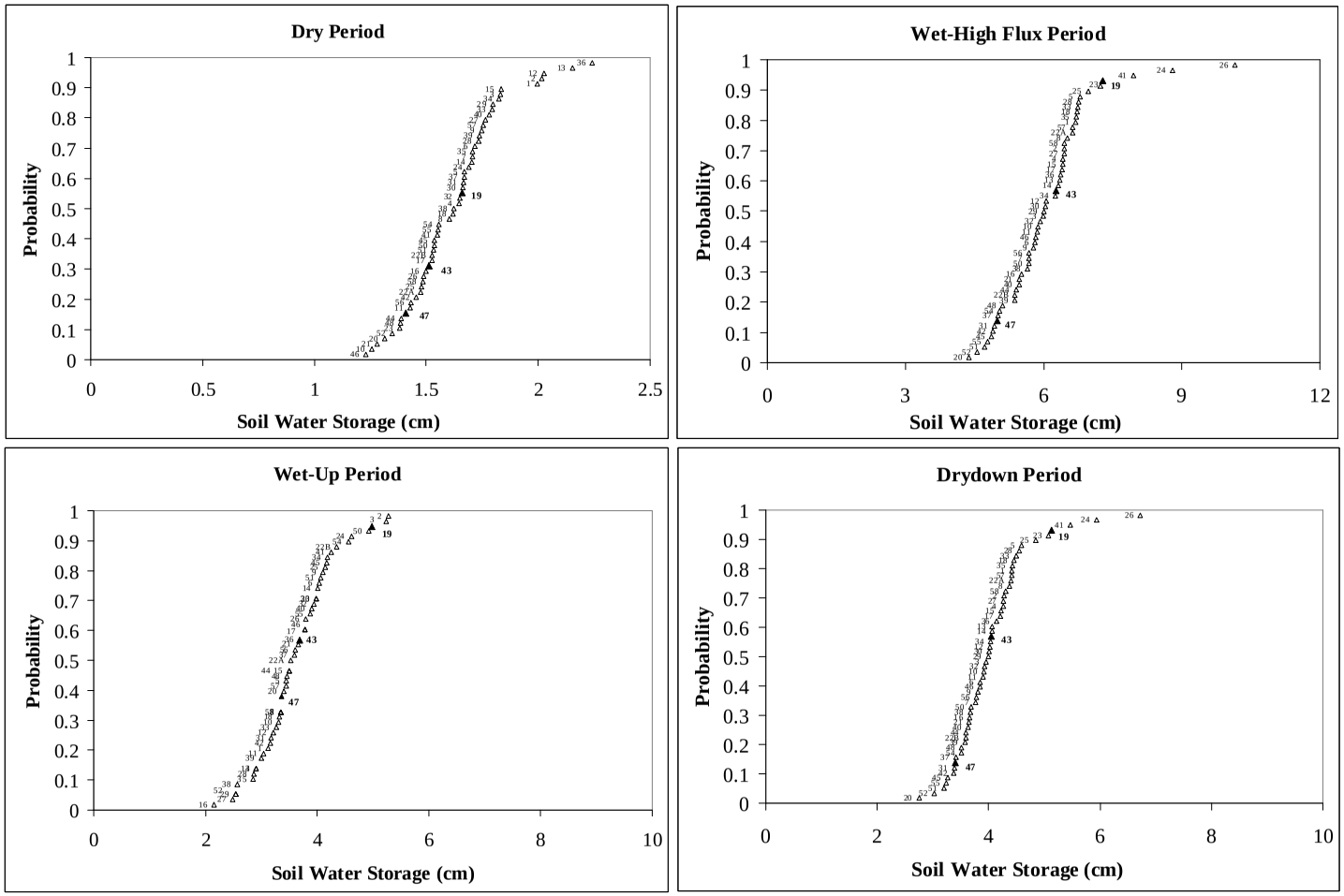

Figure 4.8. Cumulative probability of near-surface soil water storage (cm) at each sampling location during the dry, wet-up, wet-high flux, and drydown soil moisture periods. Sites consistently near the mean (Point 43), and one standard deviation above (Point 19) and below (Point 47) are indicated in bold text right of the respective plotted point.

inferences. The mean, correlation length, nugget, sill, variance, and root mean square error (RMSE) for each variogram are presented in Table 4.4.

4.3.1.1 Assessment of Variogram Quality

The quality of the variograms was measured by the RMSE (Equation 3.5) and analysis of observed nugget effects. The variogram error is assumed zero where the RMSE equals zero. The RMSE for all variograms presented was below 1.0. Overall, RMSE values were less for the near-surface variograms and indicate the near-surface data better fit the spherical model than the simulated deep soil moisture data. However, the majority of the data are well fitted to the spherical model (as evident by the low RMSE values) and are stationary with the exception of deep soil moisture data for the wet-low flux period. Thus, the spherical model is appropriate for the near-surface and simulated deep soil moisture data and for this analysis.

Non-zero nuggets were noted for all variograms except the deep soil moisture wet-low flux model. Non-zero nuggets indicate variance exist at points in very close proximity and suggest possible measurement error or grid spacing too coarse to quantify all processes. The largest nugget values for near-surface data were noted for the wet-up and wet periods. This coincides with the wettest periods of the year and may be indicative of TDR measurement errors. TDR measurements during these periods may include error associated with measuring through thin (< 1 cm) snow layers or frozen soil near the soil surface. This type of error would be within the 0.01 m^3/m^3 reported for TDR by Jones et al. (2002). The higher nugget values for the wet-up period may also be associated with the grid scale given the values are higher for the wet-up period in both the

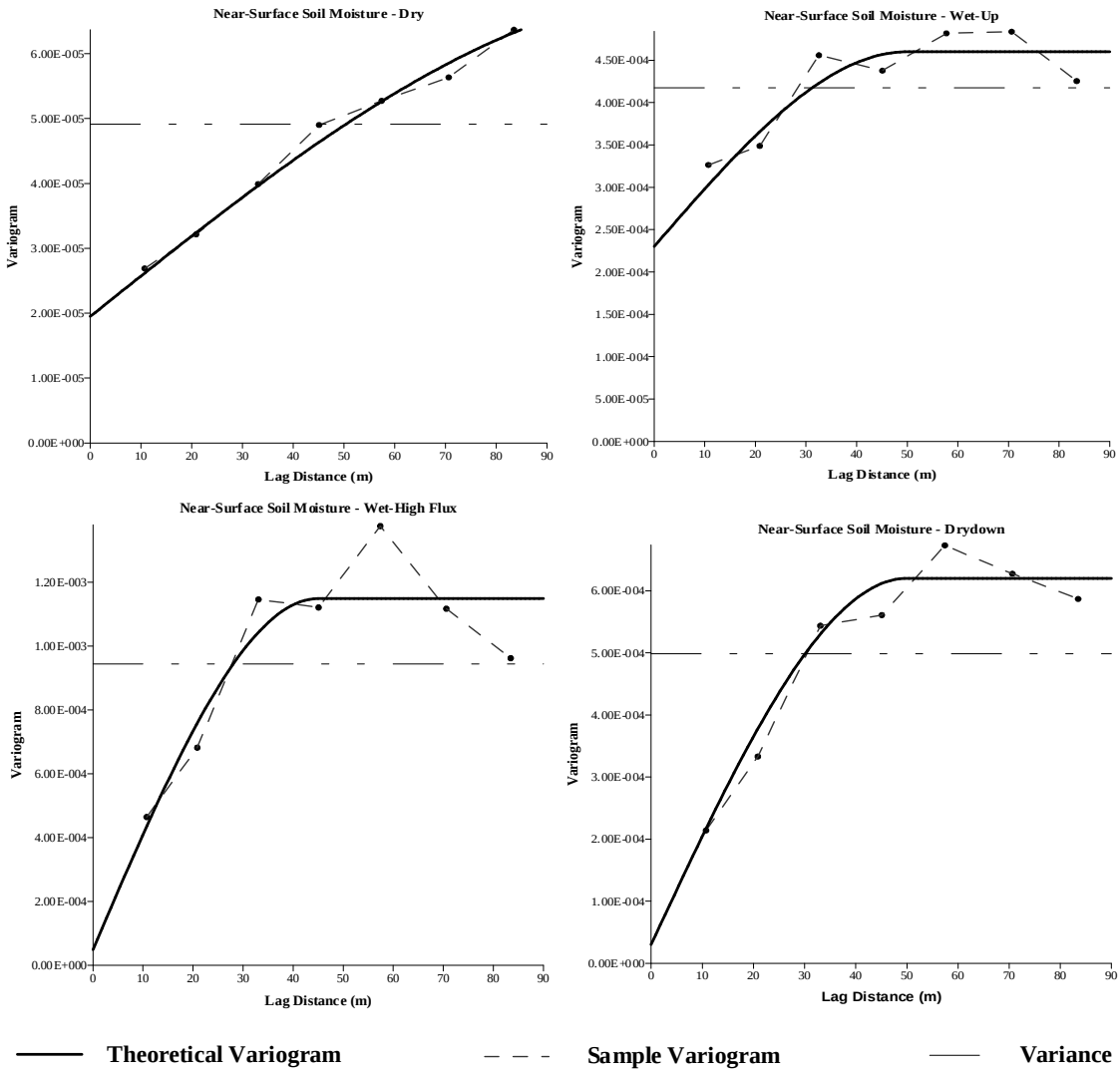

Figure 4.9. Sample and theoretical variograms of near-surface soil moisture content measured during the dry, wet-up, wet-high flux, and drydown soil moisture states during the 2003/2004 water year at the UDCEW. Theoretical variograms were modeled using the spherical model (Equation 3.4).

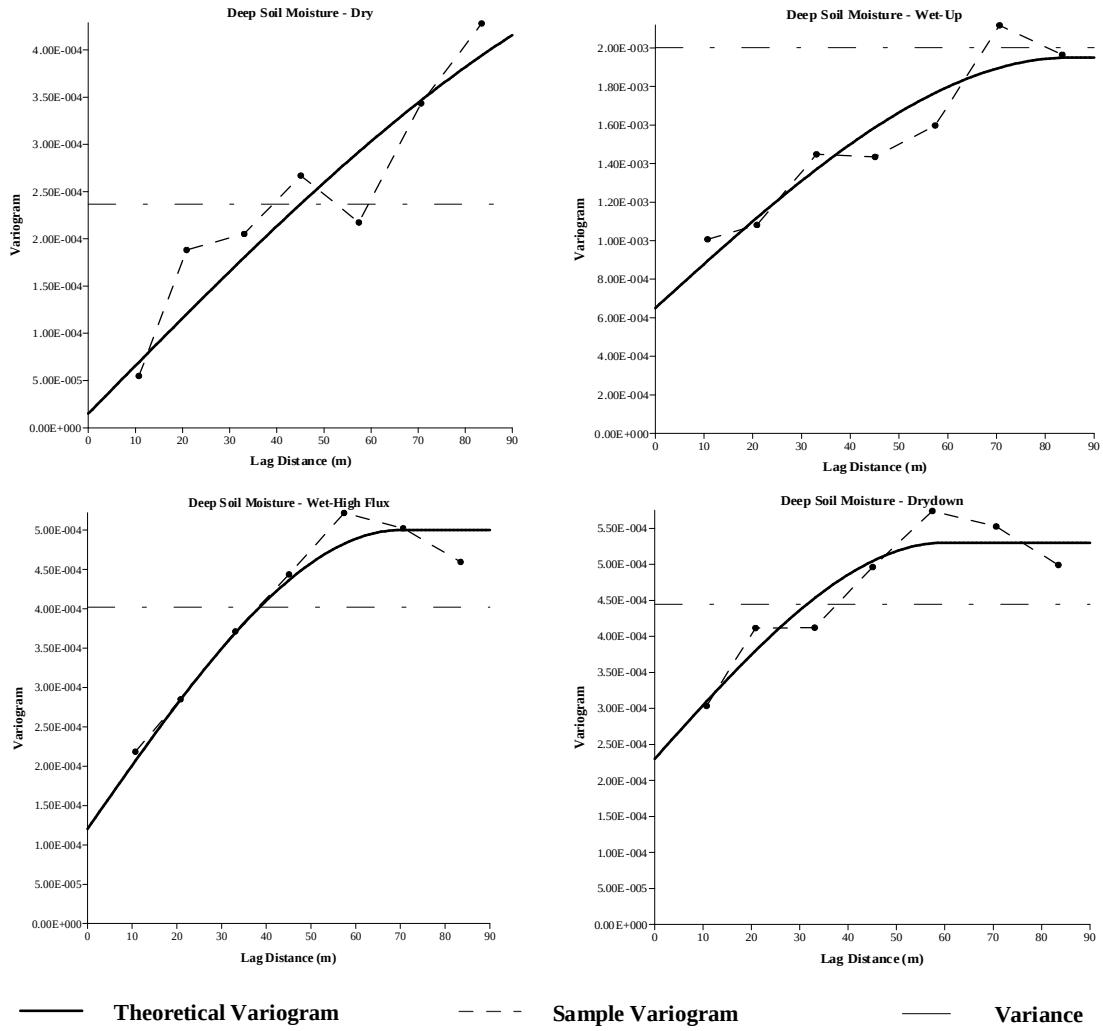

Figure 4.10. Sample and theoretical variograms of deep soil moisture measured during the dry, wet-up, wet-high flux, and drydown soil moisture states during the 2003/2004 water year at the UDCEW. Theoretical variograms were modeled using the spherical model (Equation 3.4).

Table 4.4. Descriptive statistics and variogram parameters calculated for near-surface and deep soil moisture variograms of the 2003/2004 water year.

Near Surface Soil Moisture Content						
State	**Mean (m^3/m^3)**	**Correlation Length (m)**	**Nugget**	**Sill**	**Variance**	**Root Mean Square Error**
Dry	0.054	120	0.00002	0.00007	0.00005	0.00723
Wet-Up	0.137	50	0.00023	0.00046	0.00042	0.02406
Wet-Low Flux	-	-	-	-	-	-
Wet-High Flux	0.178	45	0.00005	0.00115	0.00094	0.03322
Drydown	0.140	50	0.00003	0.00593	0.00050	0.02003
Deep Soil Moisture Content						
State	**Mean (m^3/m^3)**	**Correlation Length (m)**	**Nugget**	**Sill**	**Variance**	**Root Mean Square Error**
Dry	0.052	220	0.00002	0.00050	0.00024	0.01594
Wet-Up	0.130	85	0.00065	0.00130	0.00200	0.04111
Wet-Low Flux	-	-	-	-	-	-
Wet-High Flux	0.197	70	0.00012	0.00038	0.00040	0.02022
Drydown	0.110	60	0.00023	0.00030	0.00044	0.02308

near-surface data and the simulated bedrock flow. The study grid may be too coarse to accurately quantify all of the processes occurring at fine scales during the wet-up period. However, nugget values reported for this study are within the values commonly reported in similar studies of soil moisture patterns over large and small catchment scales (Western et al., 2004) and are not large enough to negate the relationships indicated.

4.3.1.2 Controls on Soil Water Correlation Lengths

Near-surface soil moisture correlation length decreased as the mean near-surface soil moisture content increased. The maximum correlation (120 m) length occurred during the dry state. The shorter correlation lengths during the wet-up, wet-high flux, and drydown periods are the result of multiple processes affecting the distribution of soil moisture at the site and suggest the influence of non-local controls (lateral fluxes) on soil moisture distributions. Longer correlation lengths in the dry period reflect the limited

availability of near-surface water throughout the basin and basin-wide similarities in the processes acting on the near-surface environment.

Correlation lengths for deep soil moisture were highest (220 m) during the dry period. The explanation for the maximum correlation during the dry period is concurrent with the discussion above for the near-surface. With exception of the dry period, correlation lengths for deep soil moisture were greatest (85 m) during the wet-up period and were nearly equal (60 to 70 m) for the wet-high flux and drydown periods. Bedrock flow peaked during the wet-high flux period. However, bedrock flow during the wet-up period is typically due to rainfall and results from uniform distribution of water input. Bedrock flow during the wet-low and wet-high flux periods results from snowmelt and rainfall water input. Snow depth typically is not uniform throughout the site due to differences in wind patterns and solar radiation. Water input from snowmelt is not uniform and may result in variation of water availability for bedrock flow generation. Resulting correlation lengths for deep soil moisture during the wet-up period may have been greater than that of other periods due to the uniform availability of water input. Additionally, evapotranspiration demands are low during the wet-up period, reducing the demand on water input.

The shorter correlation length for deep soil moisture during the drydown period occurs because bedrock flow is not spatially correlated except during the wetter periods of the year when water is readily available. Bedrock flow is essentially non-existent during the drydown period. However, deep soil moisture contents during the dry and drydown periods are higher than soil moisture contents in the near-surface environment during the same periods. The near-surface environment receives minimal water input

during the dry and drydown periods and losses water to evaporative demands and rapid deep soil infiltration of brief dry season rain events. Water input that does occur during the driest periods is rapidly lost from the near-surface by deep percolation and/or evaporation. The amount of water available at the soil-bedrock interface is likely dependent on local transpiration demands and infiltration rates (varying local controls).

4.3.2 Controls Inferred from Pearson Correlation Analysis

A Pearson correlation analysis was performed on near-surface and deep soil moisture to determine correlations between site characteristics and measured soil moisture and simulated deep soil moisture. The statistical significance of the correlations was determined by a *t*-test (Equation 3.1) for significance ($\alpha = 0.05$). Correlations were considered significant (soil moisture is dependent on the site characteristic) where the calculated *t* value was greater than the critical *t* value (from the student's *t* distribution, $n - 2$, $n = 57$) (Maidment, 1993). The calculated critical *t* value for all correlations was 2.0045. Results from the near surface and bedrock flow analyses are summarized in Tables 4.5 and 4.6. Positive Pearson coefficients (positive correlation) indicate that soil moisture increases as the value of the respective site characteristic increases; negative Pearson coefficients (negative correlation) indicate soil moisture decreases as the value of the respective site characteristic increases. A Pearson value close to 1.0 indicates a strongly positive correlation and Pearson values close to -1.0 indicate a strongly negative correlation. Values near 0.0 are indicators of weaker correlation. The square of the Pearson correlation coefficient (r^2) is presented (Tables 4.5 and 4.6) to show the percentage of soil moisture variability that is explained by each site characteristic. Significant Pearson and r^2 values in Tables 4.5 and 4.6 are shown in bold font.

4.3.2.1 Controls on Near-Surface Soil Moisture

The percentage of variability explained by the different controls varied with hydrologic seasonality. During the dry period near-surface soil moisture was positively correlated with soil depth, % sand, and snow water storage (snow depth and SWE at maximum snow depth) and was negatively correlated with aspect, convexity, and % coarse. Variability during the dry period was best explained by maximum snow depth (15.8%). Near-surface soil moisture during the wet-up period was solely correlated (+) with aspect (explained 11.8% variability). For the wet-high flux period, positive correlations were found with soil depth, slope, distance to the divide, % sand, and snow water storage variables; distance to the stream and % coarse were negatively correlated. Distance to the divide (28.2%) and snow water storage variables (averaged 19.9%) explained the most variability during the wet-low flux period. Near-surface soil moisture in the drydown period was positively correlated with soil depth, distance to the divide, % sand, and snow water storage variables. Variability during the drydown period was most explained by distance to the divide (18.5%) and snow water storage variables (averaged 9.9%). For the 2003/2004 water year, near-surface soil moisture was positively correlated with variables representing snow water storage, soil depth, % sand, and the distance to the stream divide and was negatively correlated with distance to the stream channel and % coarse. Variables for snow water storage (averaged 49.5%) explained the most variability in near-surface soil moisture during the water year.

4.3.2.2 Controls on Deep Soil Moisture

Controls on deep soil moisture (SHAW simulated) were derived from a Pearson correlation analysis of deep soil moisture data from the 2003/2004 water year and site

characteristics of the UDCEW. The analysis was consistent with that of near-surface soil moisture (Section 4.3.2.1). Deep soil moisture during the dry period was positively correlated with soil depth and snow water storage; soil depth and snow water storage explained 11.2% and 9.4% of the variability respectively. The controls on deep soil moisture during the wet-up period were diverse, with the strongest correlations occurring with soil depth (-), distance to the stream (+), snow water storage (-), aspect (+), and distance to the divide (-). Variability during the wet-up period was best explained by soil depth (43.2%), snow water storage (26.9%), and distance to the stream and divide (27.2% and 18.0%). The significant controls on deep soil moisture during the wet-low flux period were soil depth (-) and contributing area (-), with soil depth explaining 19.0% of the variability and contributing area explaining 6.8% of the variability. Controls on deep soil moisture during the wet-high flux were as diverse as the wet-up season, and represented both local and non-local variables. Distance to the divide (+), snow water storage (+), aspect (-), convexity (-), and soil properties (soil depth and %sand) (+) exerted the greatest influence on deep soil moisture variability during the wet-high flux period and explained 23.0%, 12.8%, 8.0%, 7.1%, and 7% of the variability respectively. Deep soil moisture during the drydown period was most influenced by distance to the divide (+), snow water storage (+), and slope (+). The variability during the drydown period was best explained by distance to the divide (17.8%) and snow water storage (9.9%). On the annual scale (2003/2004 water year), distance to the divide was the sole statistically significant influence on deep soil moisture, explaining 9.7% of the variability in deep soil moisture.

Table 4.5. Pearson correlation coefficients and variability explained (r^2) by the respective coefficients for measured near-surface soil moisture and site characteristics at the UDCEW. Data from all measurement dates were used to determine correlation relationships for all dates of measurement, the 2003/2004 water year, and the soil moisture periods shown. No data were available for the 2003/2004 wet-low flux period. Significant values (α = 0.05, critical t = 2.0045, n = 57) are indicated in italics.

Near-Surface Soil Moisture	Pearson Correlation Coefficient						Variability Explained (r^2)					
Correlation With:	All Dates	03-04 Water Year	Dry	Wet-Up	Wet-High Flux	Drydown	All Dates	03-04 Water Year	Dry	Wet-Up	Wet-High Flux	Drydown
Soil Depth	***0.385***	***0.374***	***0.301***	-0.053	***0.336***	***0.267***	***0.148***	***0.140***	***0.090***	0.003	***0.113***	***0.072***
Wetness Index	0.140	0.136	0.176	-0.036	0.064	0.104	0.020	0.018	0.031	0.001	0.004	0.011
Aspect (Degrees)	-0.025	0.010	***-0.260***	***0.344***	-0.014	0.109	0.001	0.000	***0.068***	***0.118***	0.000	0.012
Profile Curvature	-0.207	-0.190	-0.217	0.026	-0.168	-0.136	0.043	0.036	0.047	0.001	0.028	0.018
Plan Curvature	0.121	0.083	0.099	0.024	0.040	0.127	0.015	0.007	0.010	0.001	0.002	0.016
Mean Curvature	-0.203	-0.172	-0.203	0.078	-0.152	-0.139	0.041	0.029	0.041	0.006	0.023	0.019
Longitudinal Curvature	-0.193	-0.172	-0.224	0.071	-0.153	-0.111	0.037	0.030	0.050	0.005	0.024	0.012
X-Sec Curvature	-0.132	-0.094	-0.074	0.055	-0.082	-0.127	0.018	0.009	0.005	0.003	0.007	0.016
Concavity	-0.092	-0.052	-0.030	0.055	-0.067	-0.024	0.009	0.003	0.001	0.003	0.004	0.001
Convexity	-0.242	-0.223	***-0.286***	0.078	-0.182	-0.193	0.059	0.050	***0.082***	0.006	0.033	0.037
Slope (Degrees)	0.258	0.235	-0.021	-0.012	***0.310***	0.236	0.067	0.055	0.000	0.000	***0.096***	0.056
Contributing Area	0.113	0.073	0.107	0.100	0.020	0.072	0.013	0.005	0.011	0.010	0.000	0.005
Distance To Divide	***0.532***	***0.508***	0.247	-0.081	***0.531***	***0.430***	***0.283***	***0.258***	0.061	0.007	***0.282***	***0.185***
Distance To Stream	***-0.326***	***-0.300***	0.019	0.001	***-0.319***	-0.177	***0.106***	***0.090***	0.000	0.000	***0.102***	0.032
% Coarse	***-0.352***	***-0.331***	***-0.325***	0.184	***-0.352***	-0.227	***0.124***	***0.110***	***0.106***	0.034	***0.124***	0.052
% Sand	***0.362***	***0.349***	***0.345***	-0.170	***0.347***	***0.284***	***0.131***	***0.122***	***0.119***	0.029	***0.120***	***0.080***
% Fines	0.074	0.042	0.033	-0.100	0.123	-0.111	0.006	0.002	0.001	0.010	0.015	0.012
% Cover Summer	0.060	0.027	0.065	0.083	0.011	-0.071	0.004	0.001	0.004	0.007	0.000	0.005
% Cover Spring	0.011	-0.034	0.034	-0.018	-0.045	-0.103	0.000	0.001	0.001	0.000	0.002	0.011
% Cover Winter	0.025	0.008	0.041	-0.079	-0.073	0.035	0.001	0.000	0.002	0.006	0.005	0.001
Maximum Snow Depth	***0.454***	***0.446***	***0.398***	-0.084	***0.370***	***0.293***	***0.206***	***0.199***	***0.158***	0.007	***0.137***	***0.086***
SWE @ Max Depth	***0.518***	***0.517***	***0.373***	-0.075	***0.454***	***0.328***	***0.268***	***0.267***	***0.139***	0.006	***0.206***	***0.107***

Table 4.6. Pearson correlation coefficients and variability explained (r^2) by the respective coefficients for simulated deep soil moisture and site characteristics at the UDCEW. Data from 2003/20004 water year were used to determine correlation relationships for the 2003/2004 water year and each of the soil moisture periods shown. Significant values (α = 0.05, critical t = 2.0045, n = 57) are indicated in italics.

Deep Soil Moisture	Pearson Correlation Coefficient						Variability Explained (r^2)					
Correlation With:	03-04 Water Year	Dry	Wet-Up	Wet-Low Flux	Wet-High Flux	Drydown	03-04 Water Year	Dry	Wet-Up	Wet-Low Flux	Wet-High Flux	Drydown
Soil Depth	0.014	***0.334***	***-0.658***	***-0.436***	***0.265***	0.132	0.000	***0.112***	***0.432***	***0.190***	***0.070***	0.018
Wetness Index	0.060	0.181	-0.230	-0.055	0.107	0.092	0.004	0.033	0.053	0.003	0.011	0.008
Aspect (Degrees)	-0.083	-0.145	***0.458***	0.121	***-0.283***	-0.162	0.007	0.021	***0.210***	0.015	***0.080***	0.026
Profile Curvature	-0.148	-0.186	0.254	0.002	-0.228	-0.171	0.022	0.035	0.065	0.000	0.052	0.029
Plan Curvature	-0.003	0.012	***-0.276***	-0.001	0.127	0.020	0.000	0.000	***0.076***	0.000	0.016	0.000
Mean Curvature	-0.142	-0.157	***0.283***	-0.022	-0.248	-0.154	0.020	0.025	***0.080***	0.000	0.062	0.024
Longitudinal Curvature	-0.163	-0.181	0.238	-0.025	-0.238	-0.176	0.027	0.033	0.056	0.001	0.057	0.031
X-Sec Curvature	-0.041	-0.044	0.237	-0.008	-0.156	-0.046	0.002	0.002	0.056	0.000	0.024	0.002
Concavity	-0.060	-0.003	0.172	-0.055	-0.154	-0.066	0.004	0.000	0.030	0.003	0.024	0.004
Convexity	-0.173	-0.235	***0.305***	0.006	***-0.266***	-0.186	0.030	0.055	***0.093***	0.000	***0.071***	0.035
Tan(Slope)	0.088	-0.102	0.026	0.005	0.129	0.170	0.008	0.010	0.001	0.000	0.017	0.029
Slope (Degrees)	0.156	-0.030	-0.101	0.029	***0.238***	***0.251***	0.024	0.001	0.010	0.001	***0.057***	***0.063***
Contributing Area	-0.064	0.132	-0.226	-0.261	0.034	-0.055	0.004	0.017	0.051	***0.068***	0.001	0.003
Distance To Divide	***0.312***	0.144	***-0.424***	0.168	***0.479***	***0.422***	***0.097***	0.021	***0.180***	0.028	***0.230***	***0.178***
Distance To Stream	-0.013	-0.151	***0.522***	0.081	-0.179	-0.143	0.000	0.023	***0.272***	0.007	0.032	0.021
% Coarse	-0.158	-0.114	0.238	-0.137	-0.239	-0.158	0.025	0.013	0.057	0.019	0.057	0.025
% Sand	0.198	0.153	-0.204	0.150	***0.265***	0.169	0.039	0.023	0.042	0.022	***0.070***	0.029
% Fines	-0.081	-0.089	-0.178	0.002	-0.009	0.012	0.006	0.008	0.032	0.000	0.000	0.000
% Cover Summer	-0.056	0.146	***-0.291***	-0.246	0.052	-0.009	0.003	0.021	***0.085***	0.060	0.003	0.000
% Cover Spring	-0.116	0.077	***-0.329***	-0.232	0.015	-0.051	0.013	0.006	***0.108***	0.054	0.000	0.003
% Cover Winter	0.044	0.179	-0.246	-0.159	0.129	0.071	0.002	0.032	0.061	0.025	0.017	0.005
Maximum Snow Depth	0.174	0.258	***-0.454***	-0.082	***0.325***	***0.264***	0.030	0.067	***0.206***	0.007	***0.105***	***0.070***
SWE @ Max Depth	0.203	***0.307***	***-0.519***	-0.067	***0.357***	***0.314***	0.041	***0.094***	***0.269***	0.005	***0.128***	***0.099***

4.3.3 Controls Inferred by Spatial Mapping of Near-Surface and Deep Soil Moisture

The final investigation into potential controls on soil water distribution is presented in spatial maps of measured near-surface soil moisture (Appendix C) and simulated deep soil moisture (Appendix D) projected for various dates during the 2003/2004 water year. The maps were generated by block kriging in the Surfer 8.0 mapping software package. Maps for dates in each period (no data for wet-low flux near-surface) show the temporal variation in the spatial distribution of near-surface and deep soil water for the 2003/2004 water year. The maps were compared with spatial maps of site characteristics (Figures 2.1 - elevation, 2.2 – soil properties, 2.3 – vegetative cover, 2.4 – topography, 2.5 – curvature and convexity, and 2.7 – snow distribution at maximum depth) to infer controls on soil moisture during the water year.

4.3.3.1 Spatial Patterns of Near-Surface Soil Moisture

The chronology of spatial mapping at the UDCEW demonstrates the seasonal variability in the spatial distribution of near-surface soil moisture. The maps for the dry period most closely resemble maps of soil depth, with the higher soil moisture occurring in areas with deeper soils. Similar patterns are noted with maps of the % coarse and sand grain fractions. Soil moisture during the dry period was greater with lower % coarse and greater % sand grain fractions.

Spatial mapping of the wet-up period was best matched by maps of aspect. Soil moisture during this period was greater along the northeastern to eastern half of the basin, where aspect was more southeasterly. These sections in the basin experience oscillating melt periods of shallow early-season snowpacks. By the conclusion of the wet-up period near-surface soil moisture was highest in the central portion of the catchment near the

main channel head. No maps are presented for the wet-low flux period due to missing data.

Soil moisture early in the wet-high flux period was greatest in the central portion of the catchment near the channel head and just above the upper weir. This area maintained the highest near-surface soil moisture content for the duration of the wet-high flux period. The spatial maps of near-surface soil moisture for the wet-high flux period most resemble spatial maps of profile and plan curvature, concavity and convexity, distance to the divide, slope, and the Bevin and Kirkby (1979) wetness index. Near-surface soil moisture content during the wet-low flux period was greatest where slope is gentle, plan curvature is positive, and profile curvature is negative. These features are consistent with the area near the channel head and along the main channel immediately upstream of the upper weir. These locations were the first sites to display saturation of the stream channel and development of stream stage early in the water year. The increased influence of topography (local control) during the wet-low and wet-high flux periods suggests a switch from non-local to local control as the site progresses from the wet-up to winter wet periods.

Spatial mapping of the early drydown period most closely matches spatial maps of hillslope curvature, convexity, and concavity. Near-surface soil moisture during this period remained greatest near the channel head and just above the upper weir, where the topography is concave. The late season drydown maps are similar to the map of soil depth, with near-surface soil moisture being greater where deep soils exist.

In summary, the spatial mapping time series suggests that near-surface soil moisture during the dry period is uniform, with higher soil moisture contents occurring in

locations with deep soils (vertical control). As the basin wets up, near-surface soil moisture content is greatest near the channel head and the upper weir. This pattern continues through most of the year and suggests that these areas may be source areas for streamflow generation. Aspect (vertical - local control) exerts the most influence during the wet-up period. This supports the Pearson correlation analyses in Section 4.3.2. Topographic controls (lateral, non-local) appear to exert more influence on the distribution of near-surface soil moisture during the wet-high flux period than other periods of the year. The spatial patterns of near-surface soil moisture in the early drydown period are similar to the late wet-high flux period. As drydown continues, the controls switch from topography (non-local) to vertical controls (local control) due to evaporative demands and lack of water input from the atmosphere and lateral soil water delivery. This switch is evident by the similarities in the maps of soil depth and middle to late drydown near-surface soil moisture maps.

4.3.3.2 Spatial Patterns of Deep Soil Moisture

The time series spatial maps of deep soil moisture identified similar seasonality to the controls on soil water distribution at the UDCEW. Maps of the dry period deep soil moisture illustrate near uniform conditions in deep soil moisture, with higher soil moisture contents in deep soil pockets. The wet-up period began with bedrock flow generation (based on SHAW results) in the north and northeastern parts of the catchment where the shallowest and coarsest soils exist. Soil moisture contents in deep soil locations, centralized in the basin, maintained moisture contents similar to dry period conditions. As the period continued, bedrock flow increased throughout the basin, but was greatest where the % sand was the highest. This is evident by the similarities in the

12/19/03 map of deep soil moisture and the map of % sand for the site. Additionally, the 12/19/03 deep soil moisture map plots nearly as the inverse of the soil depth map, indicating that deep soil moisture for this date was less where deep soils exist.

Spatial maps of deep soil moisture during the wet-low flux period are inversely similar to maps of soil depth and spring vegetative cover. This suggests that deep soil moisture during the wet-low flux season was greatest where soils are shallow and vegetative cover is minimal. The map of aspect also appears to simulate deep soil moisture projections for the wet-low flux period. As the period progressed into January of 2004, deep soil moisture was centralized in the catchment and was greatest near the channel head and upslope of the upper weir. This pattern is similar to the near-surface soil moisture pattern discussed in Section 4.3.3.1 and identifies the development of a subsurface variable source area near the main channel head and the upper weir.

Maps of deep soil moisture for the wet-high flux period demonstrate the complexity of processes acting during this period. Early wet-high flux maps (01/08/04) resemble maps of aspect, soil depth and % coarse. Deep soil moisture and bedrock flow during high water input periods was greatest where shallow coarse soils exist along southeasterly exposures. By mid-winter deep soil moisture maps were more correlated with maps of maximum snow depth and snow water equivalent. The switch was due to a more uniform coverage of snow and reduced water input. Deep soil moisture during this period was largely a function water input from the snowpack. As the wet-high flux period progressed into late May, water input from rainfall increased and deep soil moisture was again greatest on southeasterly aspects where soils are shallow and coarse.

Deep soil moisture during the drydown period was minimal. Early drydown maps show the influence of the maximum snow depth. As the period progressed, deep soil moisture distributions most closely resembled maps of aspect and % spring cover. Deep soil moisture in the drydown period was influenced by transpiration of deep soil water and evaporation of near-surface soil moisture. Water input during this period was minimal and the controls on soil water distributions became more vertical than lateral. This is indicated by the similarity of deep soil moisture maps to aspect and inverse correlation with increasing spring cover.

Clearly, the time series spatial mapping of near-surface and deep soil moisture indicates a seasonal switch in the controls on soil water distribution. The findings of the mapping analyses are consistent with the variogram and Pearson correlation analysis and suggest that the seasonal controls switch from vertical (local) fluxes during the late drydown, dry, and early wet-up periods to a combination of lateral (non-local) and vertical (local) fluxes during the late wet-up, wet-low flux, wet-high flux, and early drydown periods. Soil depth appeared to exert the greatest influence on soil moisture patterns on an annual basis. The observed seasonal switching of controls is not commonly parameterized in wetness indices to predict basin hydrologic responses. Investigation of these limitations in commonly used wetness indices is presented in Section 4.4.

4.4 Analysis of Commonly Used Wetness Indices

Many commonly used topographic and wetness indices do not represent the controls observed at the UDCEW and in other semi-arid environments. Yet, these indices are often employed by researchers to predict catchment hydrologic responses to precipitation events. Numerous commonly used indices were calculated for the UDCEW and compared against measured near-surface soil moisture and simulated deep soil moisture to evaluate the predictive capability of the indices. The correlation analysis was consistent with all other Pearson correlation analyses presented in this thesis. The indices tested are identified in Section 3.6.1 as Equations 3.6 through 3.14. The results of the analysis are presented in Table 4.8.

4.4.1 Correlation of Indices with Measured Near-Surface Soil Moisture

Only two of the commonly used indices tested were found to be significantly correlated with measured near-surface soil moisture at the UDCEW. The ln($a \times aspect$) index (Gómez-Playa et al., 2001) explained 8.8% of the variability in near-surface soil moisture content for all dates of measurement. The index was also significantly correlated with near-surface soil moisture for the wet-high flux and drydown periods, explaining 8.2% and 8.8% variability respectively. Results from the analyses of the controls on soil moisture at the site suggest that aspect exerts significant control on soil moisture during the wet-up and dry periods. Thus, it is not surprising that an index inclusive of this control demonstrates significant correlation. However, the correlation is

quite low and the index is only significant for two of the four soil moisture periods tested (wet-low flux not tested due to missing data). The ln(a) index (Western et al., 1999) also was significantly correlated with all dates and the wet-high and drydown periods. The index explained 10.1%, 10.4%, and 7.9% of the near-surface soil moisture variability at the UDCEW for the all dates, wet-high flux, and drydown periods. Pearson correlation analysis of the controls at the UDCEW failed to find significance in correlation of the specific catchment area (a) and near-surface soil moisture contents measured at the site and sample frequency selected for this study. However, the controls that vary with elevation (indirect contributing area, contributing area increases with decreases in elevation) – soil depth, soil texture, distance to the divide, distance to the stream – were significant for the 2003/2004 water year and for the wet periods. This could explain why the index was significantly correlated with the wet-high flux and drydown periods.

4.4.2 Correlation of Indices with Simulated Deep Soil Moisture

None of the commonly used indices tested were significantly correlated with deep soil moisture for the 2003/2004 UDCEW water year. Statistically significant correlations among commonly used indices and simulated deep soil moisture were found in the wet-up and wet-low flux periods only. O'Loughlin's (1986) index ($a/\tan\beta$) significantly explained 7.6% of deep soil moisture variability for the wet-low flux period. Burt and Butcher's (1985) indices (($a/\tan\beta$) × *plan curvature*) and (a/β) significantly explained 9.1% and 7.6% of the deep soil moisture variability for the wet-low flux period respectively. Burt and Butcher's (1985) index (*plan curvature*) was significantly correlated with deep soil moisture, explaining 7.6% of the variability in deep soil moisture content for the wet-up period. In addition, the ln(a) index by Western et al.

(1999) was positively correlated with deep soil moisture for the wet-up period. The index ln(*a*) explained 7.8% of deep soil moisture variability for the wet-up period.

4.4.3 Overall Performance of Common Wetness Indices

The indices tested were more correlated with deep soil moisture than near-surface soil moisture. The positive correlations noted with deep soil moisture were exclusively during the wet-up and wet-low flux periods when lateral fluxes (non-local controls) are occurring. Thus, the hydrologic processes during those periods are more similar to the processes occurring in humid landscapes (where wetness indices perform well). The overall performance of the indices was poor, and correlations were much lower than those reported in studies from humid climates (Western et al., 1999 for review). These findings support the assumption that many of the commonly topographically based wetness indices are poor predictors of seasonal fluxes in soil moisture patterns represented in semi-arid landscapes like the UDCEW.

4.5 Performance of Modified and New Wetness Indices

Modified indices (Equations 3.15 through 3.25) were developed for this study that were inclusive of the controls observed at the UDCEW. The indices were calculated and tested for correlation (Pearson correlation analysis) with measured near-surface and simulated deep soil moisture data from the UDCEW (Table 4.9). Numerous indices were derived, but those presented (Equations 3.15 through 3.25) most accurately incorporated the observed controls.

4.5.1 Correlation of Modified New Indices with Measured Near-Surface Soil Moisture

The modified indices offered significant improvements over the commonly used indices (Equations 3.6 through 3.14) (Table 4.8). However, the variability explained by significant correlations was still quite low (below 25%). The greatest improvement in predictive capability was achieved with the index ln(*SWE* × *soil depth*). This suggests that parameterization of available water and soil water storage capability may provide the best explanation of soil moisture patterns in snow dominated semi-arid headwater catchments. The ln(*SWE* × *soil depth*) index explained 21.5% of the all dates variability and 11.5%, 23.1%, and 9.7% of the variability during the dry, wet-high flux, and drydown periods. Indices incorporating variables for curvature and topography performed poorly, but the index ln(*a* × *soil depth*), natural log of contributing area and soil depth, was significantly correlated with measurements for the dry (explained 8.4% variability) and wet-up (explained 9.4% variability) periods. Including soil depth in indices improved predictability for all periods.

The strongest correlations for significant indices was found in the wet-high flux period. Soil moisture conditions during the wet-high flux period in the UDCEW more closely resembles steady state conditions that wetness indices were originally derived for. A process (representing available water and evapotranspiration demands) based index, ln(*water input* – *ET*), explained 12.7% of the variability in near-surface soil moisture observed for all dates of measurement and was significantly correlated soil moisture conditions during dry and wet periods of the year. The variation in index performance across different periods highlights the complexity of processes occurring and the poor

Table 4.7. Variability in measured near-surface soil moisture and simulated deep soil moisture at the UDCEW explained by commonly used wetness indices. Significant values (α = 0.05, critical t = 2.0045, n = 57) are indicated in bold font; negative correlations are shown in italics.

Near-Surface Soil Moisture Correlation With:	Variability Explained (r^2)					
	03-04 Water Year	Dry	Wet-Up	Wet-Low Flux	Wet-High Flux	Drydown
$\ln(a/\tan\beta)$	0.038	0.020	0.001	-	0.040	0.022
$(a/\tan\beta)$	0.005	0.001	0.005	-	0.004	0.001
$(a/\tan\beta) \times PlanC$	0.002	0.001	0.005	-	0.002	0.000
PlanC	0.022	0.002	0.012	-	0.016	0.033
$a \times PlanC$	0.004	0.001	0.005	-	0.016	0.001
(a/β)	0.005	0.001	0.005	-	0.003	0.001
$\ln((a \times aspect)/(\tan\beta))$	0.032	0.006	0.002	-	0.030	0.028
$\ln(a \times aspect)$	***0.088***	0.000	0.005	-	***0.082***	***0.088***
$\ln(a)$	***0.101***	0.010	0.000	-	***0.104***	***0.079***

Deep Soil Moisture Correlation With:	Variability Explained (r^2)					
	03-04 Water Year	Dry	Wet-Up	Wet-Low Flux	Wet-High Flux	Drydown
$\ln(a/\tan\beta)$	0.004	0.033	0.053	0.003	0.011	0.008
$(a/\tan\beta)$	0.011	0.011	0.052	***0.076***	0.000	0.010
$(a/\tan\beta) \times PlanC$	0.016	0.009	0.049	***0.091***	0.000	0.015
PlanC	0.000	0.000	***0.076***	0.000	0.016	0.000
$a \times PlanC$	0.012	0.011	0.048	***0.087***	0.016	0.011
(a/β)	0.011	0.012	0.052	***0.076***	0.000	0.009
$\ln((a \times aspect)/(\tan\beta))$	0.001	0.022	0.018	0.001	0.002	0.003
$\ln(a \times aspect)$	0.010	0.029	0.027	0.001	0.014	0.020
$\ln(a)$	0.016	0.044	***0.078***	0.004	0.040	0.037

overall performance suggests that index parameterization of controls on near-surface soil moisture may not be an effective tool in predicting soil water distribution.

4.5.2 Correlation of Modified and New Indices with Simulated Deep Soil Moisture

Results from the Pearson correlation analysis of deep soil moisture and modified and new wetness indices indicate predictability of wetness indices in semi-arid climates can be improved through substitution of variables indicative of the processes occurring. The most significant improvement was found with the index ln(*water input – ET*). This index was significantly correlated with simulated deep soil moisture for all periods and for the entire 2003/2004 water year. The index explained 28.0% of the variability of deep soil moisture on the annual scale. The inclusion of soil properties (*soil depth* and *% sand*) in indices offered improved predictive capability by parameterizing the vertical flux influences (local control) of evapotranspiration and soil water storage.

Deep soil moisture during the dry season was best explained by ln(*Water Input – ET*) (20.0% of the variability). The most significant correlation during the wet-up period was found with ln(*SWE* × *soil depth*). The predictability of this index (explained 53.9% variability) for the wet-up season is somewhat surprising, as *SWE* (measured at maximum depth) measurements were from the wet-high flux period. The index ln *(% sand* × *soil depth*) also performed well (explained 50.1% variability) for the wet-up period, illustrating the influence of soil texture during the fall wetting period. Deep soil moisture during the wet-low flux period was well correlated (nearly 50% variability explained) with multiple indices that included *soil depth*. The index ln(*Water Input – ET*) explained 50.7% of the variability during the wet-low flux period. The wet-high flux period was well best explained by ln(*SWE* × *soil depth*) (explained 12.9% variability) and the

Table 4.8. Variability in measured near-surface and simulated deep soil moisture at the UDCEW explained by modified and new wetness indices indicative of the observed controls on soil moisture at the UDCEW. Significant values (α = 0.05, critical t = 2.0045, n = 57) are indicated in bold font; negative correlations are shown in italics.

Near-Surface Soil Moisture	Variability Explained (r^2)					
Correlation With:	03-04 Water Year	Dry	Wet-Up	Wet-Low Flux	Wet-High Flux	Drydown
$\ln(a/\tan\beta)$	0.038	0.020	0.001	-	0.040	0.022
$\ln(a \times \textit{soil depth})$	0.002	***0.084***	**0.094**	-	0.010	0.009
$\ln(\%\textit{sand} \times \textit{soil depth})$	**0.171**	**0.085**	0.002	-	**0.182**	**0.092**
$\ln(\textit{soil depth})$	**0.151**	**0.068**	0.000	-	**0.159**	**0.082**
$\ln(\text{SWE} \times \textit{soil depth})$	**0.215**	**0.115**	0.000	-	**0.231**	**0.097**
$\ln((\textit{aspect} \times \%\textit{fines})/\tan\beta)$	0.042	0.000	0.007	-	0.042	0.057
$(a \times \textit{convexity})$	0.050	0.010	0.003	-	0.049	0.035
$(a \times \textit{longitudinal curvature})$	0.052	0.023	0.005	-	0.055	0.018
$(\%\textit{summer cover} \times \textit{soil depth})$	0.035	0.032	0.000	-	0.039	0.008
$(\%\textit{spring cover} \times \textit{soil depth})$	0.012	0.023	0.000	-	0.015	0.001
$\%\textit{winter cover}$	0.004	0.010	0.001	-	0.002	0.009
$\ln(\textit{Water Input - ET})$	**0.127**	**0.134**	0.009	-	**0.145**	0.044

Deep Soil Moisture	Variability Explained (r^2)					
Correlation With:	03-04 Water Year	Dry	Wet-Up	Wet-Low Flux	Wet-High Flux	Drydown
$\ln(a/\tan\beta)$	0.004	0.033	0.053	0.003	0.011	0.008
$\ln(a \times \textit{soil depth})$	0.008	0.017	**0.170**	0.019	***0.081***	0.028
$\ln(\%\textit{sand} \times \textit{soil depth})$	0.004	**0.105**	***0.501***	***0.072***	**0.100**	0.036
$\ln(\textit{soil depth})$	0.001	**0.099**	***0.505***	***0.093***	**0.084**	0.030
$\ln(\text{SWE} \times \textit{soil depth})$	0.013	**0.130**	***0.539***	0.061	**0.129**	0.067
$\ln((\textit{aspect} \times \%\textit{fines})/\tan\beta)$	0.045	0.011	0.027	0.006	***0.106***	***0.070***
$(a \times \textit{convexity})$	0.008	0.012	0.068	0.002	0.037	0.017
$(a \times \textit{longitudinal curvature})$	0.025	0.020	0.036	0.000	0.047	0.044
$(\%\textit{summer cover} \times \textit{soil depth})$	0.002	**0.095**	***0.304***	***0.263***	0.032	0.002
$(\%\textit{spring cover} \times \textit{soil depth})$	0.004	0.062	***0.255***	***0.223***	0.022	0.001
$\%\textit{winter cover}$	0.006	**0.073**	***0.091***	***0.087***	0.039	0.011
$\ln(\textit{Water Input - ET})$	***0.280***	***0.200***	***0.272***	***0.507***	***0.116***	***0.151***

ln(*Water Input – ET*) process index (explained 11.6% variability). The influence of soil depth was noted in this study, but the effect of curvature was expected given the influence of topography during the wet period of the year. Deep soil moisture variability during drydown was best explained by index ln(*Water Input – ET*), explaining 15.1% of the variability. Although modified indices offered improved correlations with measured and simulated deep soil moisture contents, the overall poor performance (over 50% variability still unexplained with most indices) of commonly used and modified indices indicates that index approaches to predicting soil moisture patterns in semi-arid climates are complex and, although efficient as shortcut approaches, may not be effective methods for simulating hillslope processes in semi-arid landscapes.

5. DISCUSSION

The primary purposes of this study were to provide insight into the hillslope processes that govern streamflow initiation and cessation at the UDCEW and to apply that insight into the testing of new and modified wetness indices that accurately depict the processes occurring. Yenko (2003) demonstrated through hydrograph separation and concentration-discharge relationships (Section 2.2.8.2) that streamflow sources at the UDCEW are dependent on soil moisture conditions in the catchment. McNamara et al. (2005) further demonstrated that the soil moisture patterns that govern streamflow at the site are the result of seasonal fluxes in vertical (local) and lateral (non-local) controls on soil moisture. Both studies were based on data from a few points in the basin. Therefore, a more complete spatial analysis was needed to examine the controls on soil moisture at the site and to explain the processes governing streamflow generation and cessation.

5.1 Seasonal Controls on Soil Moisture

5.1.1 Seasonal Controls on Near Surface Soil Moisture

Variogram, Pearson correlation, and spatial mapping analyses of near-surface and deep soil moisture patterns identified seasonal variation in the controls on soil moisture at the UDCEW site. At the UDCEW, near-surface soil moisture content during most of the year is well correlated with variables representing distance to the divide, soil depth, soil

texture, and snow water storage. Soil depth at the study site is shallowest near ridge locations, soil texture is coarser on southeast aspects of upper slopes, and snow depth typically increases with distance from the divide. Thus, the similarities in Pearson correlations (Section 4.3.2) of near-surface soil moisture patterns and distance to the divide, soil depth, soil texture, and snow water storage are likely the result of correlations between the respective variables and could be explained using one of these three site characteristics. Snow water storage at the site is significantly correlated with all soil moisture periods except wet-up. This seems logical, as the wet-up season marks the beginning of a new water year and near-surface soil moisture during that period should be more correlated with new precipitation than precipitation from the pervious water year. Snow water storage however appears to be an important control on near-surface soil moisture for most of the year. This is expected given precipitation at the site falls mostly during the cool season. The snowpack serves as storage for cool season precipitation, slowly releasing water to the soil column.

Water input during the summer dry period is minimal and the distribution of soil water is controlled by evaporation from the near-surface and plant use (transpiration) of deep soil water. The dominant controls on near-surface soil moisture during the dry period are soil depth, % coarse and sand grain fractions, and aspect. These controls are representative of vertical (local) controls on soil moisture. Aspect dictates the amount of solar radiation received at the surface and influences evaporation. Soil texture influences near- surface soil moisture as coarse soils provide greater hydraulic conductivity during the wet season and are well drained following the wet-high flux season. Thus, it is expected that soils with a lower percentage of coarse grains would maintain a higher soil

moisture content during the dry season. Shallow soils at the site would also be well drained following the wet-high flux period and would lose remaining soil moisture to evaporative losses during the dry summer. Thus, locations with deeper soils maintain higher soil moisture during the dry season.

Water input during the fall wet-up period exceeds evaporative and transpiration demands. High water input delivers water vertically through the soil column (local flux). Shallow soils maintain high soil moisture contents until the moisture content reaches a threshold for lateral flow generation (non-local control). Soil water movement through deep soil profiles is slower (greater vertical travel distance) and the timing of lateral flow is delayed. Near-surface soil water movement during the wet-up period is dominated by aspect, soil texture, and slope. The combined vertical and lateral controls for this period demonstrate the variation in the timing of the vertical to lateral switch. Locations receiving higher solar radiation (southerly aspects) likely receive more water input in the form of snowmelt than due areas with northerly exposures. Northerly aspects often develop a shallow snowpack in the wet-up period that delays water input. Therefore, aspect provides some vertical control on water input. Soil texture offers a combined influence of vertical and lateral control through varied infiltration (vertical) and lateral conductivity rates. Topographic slope provides the lateral influence as soils wet-up beyond the vertical control threshold. Discussion regarding the transition from the fall wet-up to the wet-low flux period is reserved for deep soil moisture discussion given the lack of near-surface moisture content data for that period.

The controls on near-surface soil moisture during the wet-high flux period are similar to the wet-up period and are represented by vertical - local - (soil properties and

snow water storage) and lateral - non-local - (slope and hillslope shape) controls. Water input during the wet-high flux period greatly exceeds evaporative and transpiration demands and flow through the soil column is maximized (Figure 4.5c). The spatial patterns in near-surface soil moisture at the UDCEW during the wet-high flux period are largely dictated by topography and vertical and lateral conductivity of soil column.

The drydown period is marked by increased evapotranspiration rates, decreased water input, and a resulting switch from combined lateral and vertical influences to vertical fluxes. The soil profile dries out vertically, with the near-surface losing water to evaporative demands. Deep soils store water from the wet-high flux period and provide water for plant transpiration. As the drydown period progresses, soil texture exerts even more vertical (local) control on near-surface soil moisture as represented in the dry period.

5.2.1 Seasonal Controls on Deep Soil Moisture

The controls on deep soil moisture, like those in the near-surface, at the UDCEW exhibit seasonality. On an annual scale, deep soil moisture at the UDCEW is largely controlled by snow water storage (dictates timing of water input) and soil properties (soil depth and porosity). Deep soil moisture during the dry period is controlled by the capacity of soil water storage (soil depth and porosity) and transpiration of deep soil water. The variogram, spatial mapping, and indices analyses suggest that plants at the study site have more influence on deep soil moisture than on the near-surface. This study does not investigate whether hydraulic lift by plants occurs at the UDCEW, but it is assumed that most of the plants transpiring in the dry season are deep rooted species using deep soil moisture.

Deep soil moisture patterns during the wet-up period are largely related to aspect (vertical control) and the type (rainfall or snowfall) and quantity of fall precipitation. During the fall season, southerly aspects receive water input from oscillating snowmelt events (northerly exposures accumulate snow) and deliver water vertically through the soil profile. Shallow and coarser soils at the site more rapidly conduct fall season water input through the profile to the soil-bedrock interface. As the deep soil moisture contents reach field capacity in shallow soil locations, the influence of lateral controls (topographic, non-local control) develops. The timing of the combined vertical and lateral control during the wet-up period depends on the amount of water input (dependent on the type – rainfall or snowfall - and quantity of precipitation) and ceases with the onset of the wet-low flux period (water input reduced due to storage in developing snowpack).

The wet-low flux season is typically marked by the development of a winter long snowpack. Water input (rainfall and snowmelt) defines the length of this period. Cold and wet winters produce long wet-low flux periods and warmer wet winters produce short wet-low flux periods. McNamara et al. (2005) suggested that the switch from vertical to lateral controls on soil moisture in the UDCEW is slow due to the gradual release of winter precipitation in the form of snowmelt. Grayson et al. (1997) defined preferred states in soil moisture distribution for semi-arid landscapes and suggested the change from the dry to wet season includes a rapid transition from local (vertical fluxes) to non-local (lateral fluxes) controls on soil moisture. It is proposed here that the transition from vertical to lateral controls at the UDCEW is dependent on the length of the wet-low flux season. Vertical controls dominate the site during the wet-low flux period, but, if early winter air temperatures support rainfall and rapid snowmelt, a short

duration winter low-flux period results and causes a rapid transition from vertical to lateral controls on near-surface and deep soil moisture. The timing of streamflow peaks at the study site is largely related to the length of wet-low flux season (Figure 4.5).

The conclusion of the wet-low flux season marks the beginning of the switch from vertical to lateral dominance of soil moisture fluxes. Water input during this period greatly exceeds evapotranspiration demands and bedrock flow is maximized (Figure 4.5c). The controls on deep soil moisture distribution at the UDCEW during the wet-high flux period are similar to annual controls in humid climates, but also include vertical controls. Soil moisture patterns during the wet-high flux period are largely dictated by topography (curvature, concavity, contributing area) and the available water in the remaining snowpack. The wet-high flux period is then controlled laterally (non-locally) by topography and lateral hydraulic conductivity (soil properties) and vertically (locally) by the available of water input and infiltration rates.

The drydown state begins as water input decreases below evapotranspiration rates (Figure 4.5). As drydown progresses, a switch in the controls on deep soil moisture occurs. Deep soil water moisture during this period is controlled by evapotranspiration demands and precipitation. As water availability declines the vertical fluxes (evapotranspiration) dictate the upward or downward movement of the remaining water in the soil profile and lateral controls cease. Hydrologic connection between upper and lower slopes discontinues and streamflow ceases.

5.2 Streamflow Initiation and Cessation

Streamflow initiation and cessation during the 2003/2004 water year was well synchronized with timing of seasonal changes in soil moisture controls. Bedrock flow began early in the water year (middle of the wet-up period) (Figure 4.5c). Precipitation during this period was mostly rainfall and rapidly infiltrated to the soil-bedrock interface. Oscillating snowmelt events during the early wet-low flux period resulted in an early switch from vertical to lateral controls as indicated by spatial mapping of near-surface (Appendix C) and deep (Appendix D) soil moisture. The onset of streamflow near the channel head early in the wet-up period indicated a response to bedrock flow in the near-stream environment. However, lateral flow was not sufficient to connect upper and lower slopes and generate streamflow to the middle weir. Two possible explanations exist: upper and lower bedrock flow sources were disconnected, or bedrock flow was channeled into fractures or a deep soil source area near the stream channel.

McNamara et al. (2005) proposed that dry pockets in mid-slope deep soils at the site may act as a disconnect on lateral flow from upper slopes during the wet-low flux season. For the 2003/2004 water year, soil moisture data from a TDR instrumented soil pit in a mid-slope deep soil location was used to investigate the concept of deep soil barriers to lateral flow (Figure 5.1). Soil moisture content at the base of the soil profile in the soil pit lagged behind soil moisture contents in the upper and middle portions of the soil profile (Figure 5.1). In early March, soil moisture contents throughout the soil profile were nearly equal, with soil-bedrock interface having the highest soil moisture

content. The hydrograph peak for the 2003/2004 water year (Figure 2.9) corresponds with the point on the graph in Figure 5.1 where near-surface, mid-depth, and deep soil moisture contents become nearly equal.

Additional insight into soil moisture movement in deep soil profiles was gained by plotting bedrock flow generation in deep and shallow soil locations (Figure 5.2). Bedrock flow generation in shallow soils (Figure 5.2b) occurs earlier in the year and is greater than bedrock flow generation in locations with deep soil profiles (Figure 5.2a). It is proposed here that an unquantified component of wet-up period bedrock flow from upper slope shallow soils (northern portion of the catchment, Figure 5.3) flows laterally downslope into deep soil locations and increases soil moisture contents in the middle portion of deep soil profiles. Further lateral delivery of soil moisture from or through deep soil profiles is delayed until soil moisture contents throughout the deep soil profile are nearly equal at all depths (Figure 5.1). This typically occurs at the UDCEW at the onset of the wet-high flux, when bedrock flow is maximized (Figure 4.5).

Spatial mapping of soil moisture during the wet-up (near-surface, Figure 5.4a) and wet-low flux (deep soil, Figure 5.4b) periods identified the development of a variable subsurface source area near the channel head and immediately upstream from the upper weir. Anderson et al. (1997) noted a similar source area responsible for streamflow initiation in a steep unchanneled basin in the Oregon Coast Range. The study identified bedrock flow through a weathered bedrock layer along the soil-bedrock interface. Lateral flow through the bedrock layer intersected soil water infiltrating vertically in the soil profile near the channel head. The combined flowpaths developed a variable subsurface source area that dictated streamflow generation.

This study proposes that bedrock flow generated in the UDCEW from shallow coarse soils in the northeastern portion of the basin (Figure 5.3) during the wet-up and wet-low flux period fuels the development of a subsurface source area near the channel head above the upper weir. Early season streamflow initiates with the growth of the source area as lateral flow develops with the switch from vertical to lateral controls in shallow soil locations during portions of the wet-up period. For the 2003/2004 water year, this occurred in late December to early January. Below the upper weir streamflow was delayed due to deep soil dry pocket barriers (to lateral flow) noted in mid-slope locations in this region of the basin. Therefore, streamflow through the upper and middle weirs is dependent on the development of the subsurface source area above the upper weir and the subsequent hillslope connection of upper and lower slopes adjacent to the channel between the upper and middle weirs.

Yenko (2003) used stream chemistry analyses to identify a counter-clockwise hysteresis loop of silica concentration in stream water at the study site (Figure 5.1). The results demonstrated that silica concentration in stream water at the UDCEW were lower on the rising limb of the hydrograph than on the falling limb. Yenko (2003) suggested that this indicates activation of a flow source with greater silica concentration as snowmelt progresses and catchment soil moisture contents increases. Yenko (2003) further suggested that the silica increases in streamwater on the falling limb were linked to flow along the soil-bedrock interface. It is proposed here that the source may also be from stored water in the variable source area near the channel head or from the saturated wedge (between the upper and lower weirs) identified by McNamara et al. (2005). In either case, the stream chemistry supports the concept of a subsurface variable source

area near the channel head that is fueled by bedrock flow from upper slopes during the late wet-up and early wet-low flux periods.

Growth of the subsurface source area during the wet-low flux period coincides with increases in bedrock flow and streamflow (Figures 2.11, 4.5c and 4.5d). However, the significant rises in the stream hydrograph lag behind the bedrock flow hydrograph (Figure 5.5). Freer et al. (2002) and Buttle and McDonald (2002) demonstrated that controls on coupled flowpaths (vertical and lateral) may vary with water input. Both studies determined that preferred vertical and lateral flowpaths increased the rate of water delivery downslope, but that the lateral delivery was dependent first on the vertical connection. At the UDCEW, the vertical connection develops first in the northeastern

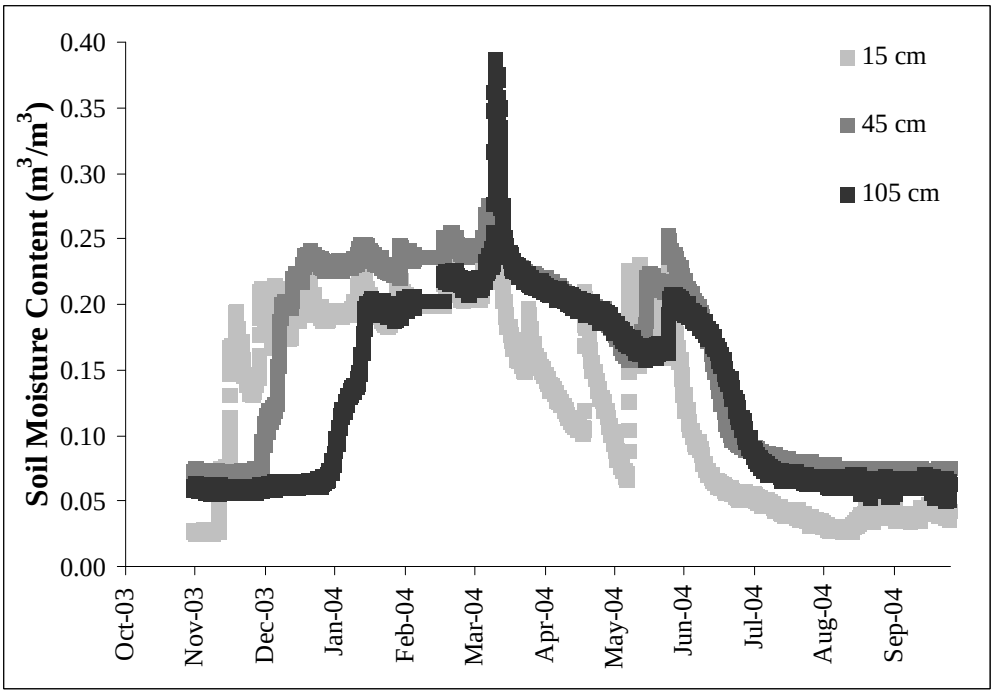

Figure 5.1. Soil moisture content (m^3/m^3) measured at 15, 45, and 105 cm depth in a TDR instrumented pit on the northwest facing slope between the upper and middle weirs at the UDCEW. The location is representative of the deep soil region between soil moisture sampling points 5, 13, and 8 (Figure 2.1). Figure illustrates soil moisture patterns (dry soil pockets described by McNamara et al. (2005)) that occur at various depths in deep soil profiles between the upper and middle weirs.

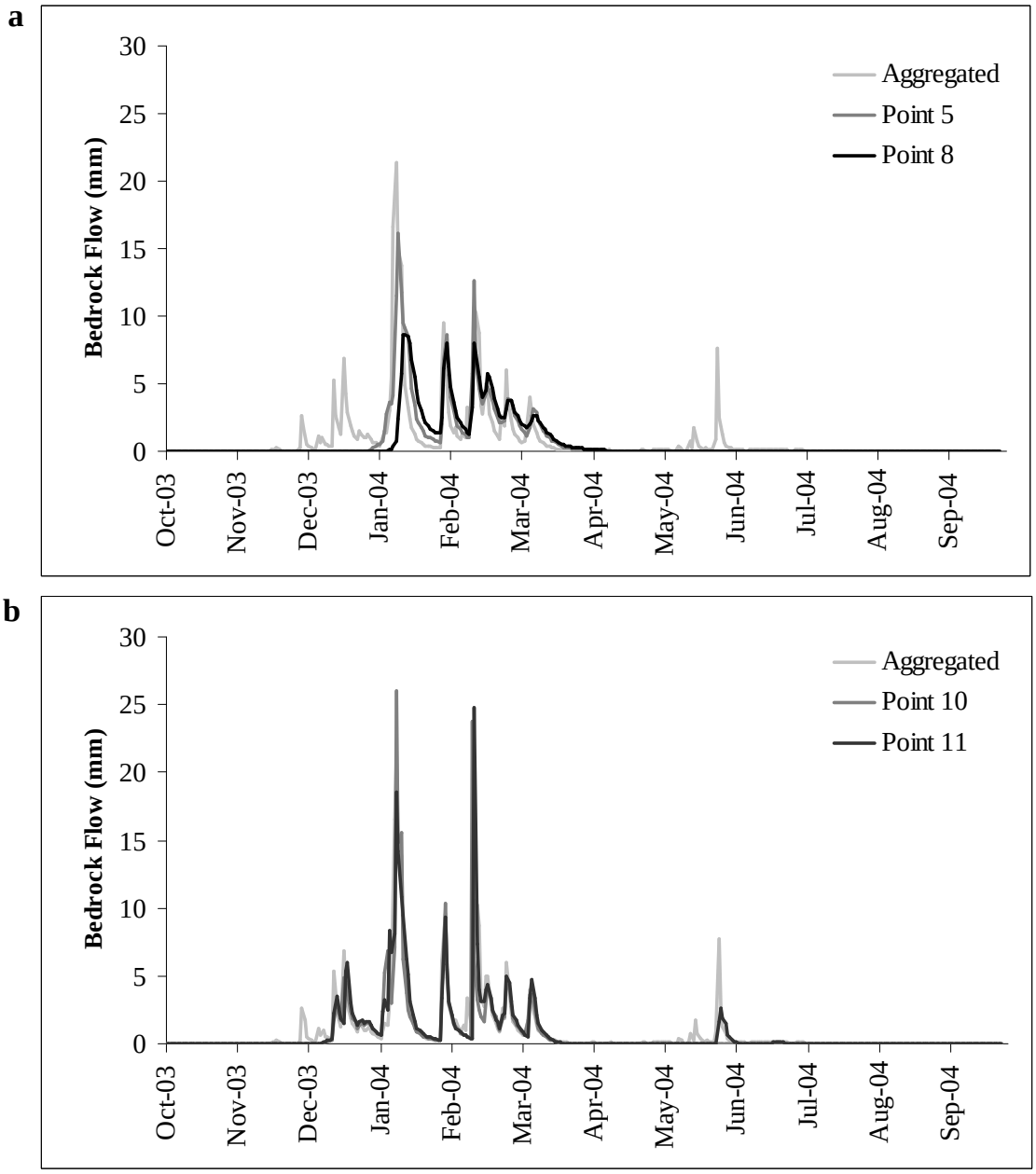

Figure 5.2. Differences in the timing and quantity of simulated bedrock flow at deep (a) (> 1 m) and shallow (b) (< .45 m) soil locations on the northwest facing slope between the upper and middle weir. Aggregated bedrock flow from the area weighted water using 57 sampling points is shown as the light gray line. Deep soil simulations noted in the figure are for points located in mid- to lower slope positions. Shallow soil simulations noted in the figure are for points near ridgelines immediately upslope of the deep soil simulation points (a).

portion of the basin where wet-up and early wet-low flux water input is high (oscillating snowmelt events occur due to aspect) and infiltration to the soil-bedrock interface is rapid through shallow, coarse soils. Lateral connection subsequently develops and transports soil water downslope to a growing variable subsurface source area. Similar processes occur in the remainder of the basin as the wet-high flux period approaches. There is a resulting lag in streamflow generation between weirs as these processes are spatially and temporally disconnected early in the water year.

Early streamflow through the upper weir was lost to the subsurface during the early portion of the wet-low flux period for the study year. McNamara et al. (2005) identified the development of a saturated wedge between the upper and middle weir that forms as the stream loses water to the subsurface. It is suggested here that the timing of streamflow through all three weirs is the result of hydrologic connection between the subsurface variable source area near the channel head and the upper weir and the saturated wedge identified by McNamara et al. (2005). Streamflow then through all three weirs marks the hydrologic connection (breach of the lag in spatially and temporally separated processes) of the vertical and lateral flowpaths from the slopes above the upper weir through the catchment outlet.

Late May rainfall produced a peak in streamflow concurrent with a spike in bedrock flow, suggesting full hillslope connection and the continuance of lateral flow dominance. The concurrence in streamflow, bedrock flow, and precipitation pulses may indicate translation of a pressure wave through the basin. Torres et al. (1998) found that precipitation on wet soils with steep water retention curves near the near-zero range can

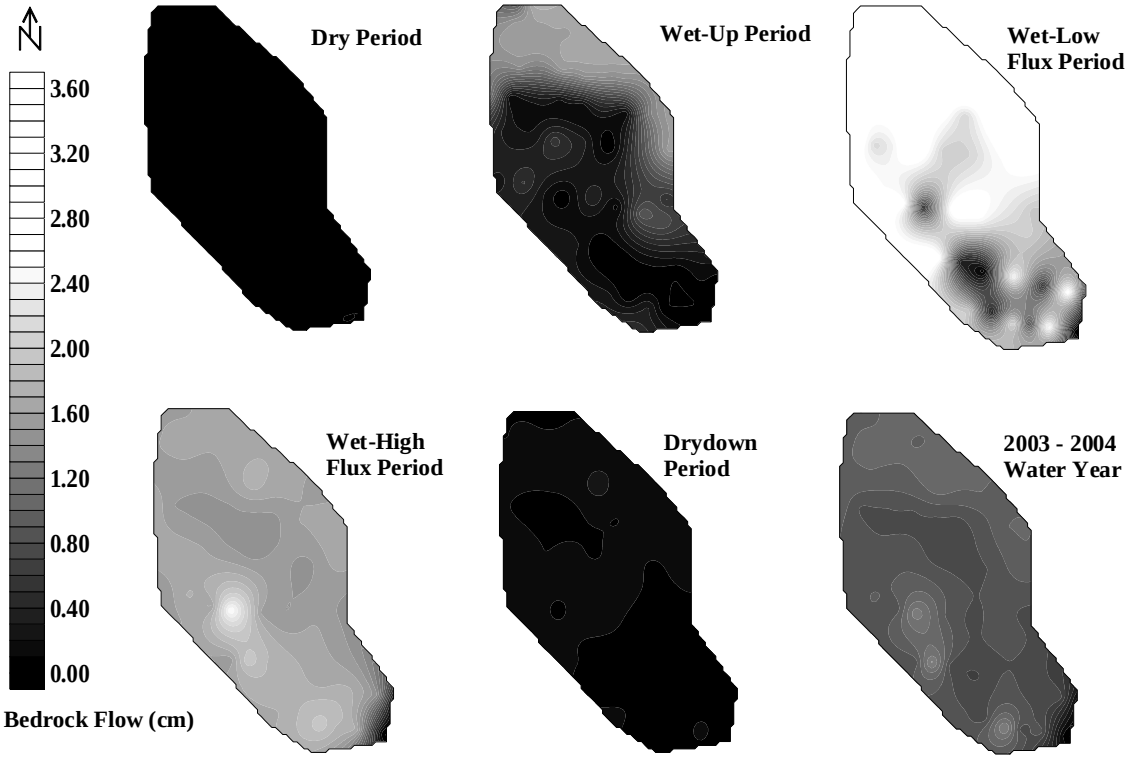

Figure 5.3. Spatial maps of mean bedrock flow (cm) for each soil moisture periods of the 2003/2004 water year. Maps identify locations of early season (wet-up and wet-low flux periods) bedrock flow production in the northern portion of the catchment where shallow soils exist. Bedrock flow production in deep soil locations (darker areas in wet-low flux map) is delayed until the wet-high flux period.

produce small pulses in hydraulic head that drive rapid draining of pre-event water. This type of event during the wet-high flux period (falling limb of the hydrograph) would support the findings of Yenko (2003) that the falling limb of the annual hydrograph is made up of pre-event water (stored early season event water).

During the drydown period for the 2003/2004 water year streamflow was lost to the subsurface between the middle and lower weirs as hydrologic connection ceased. Streamflow continued through the upper weir into June of 2004 before streamflow cessation at the site in late June. The onset of the stream losing water between the middle and lower weir indicates the dominance of vertical fluxes and the disconnect of spatially

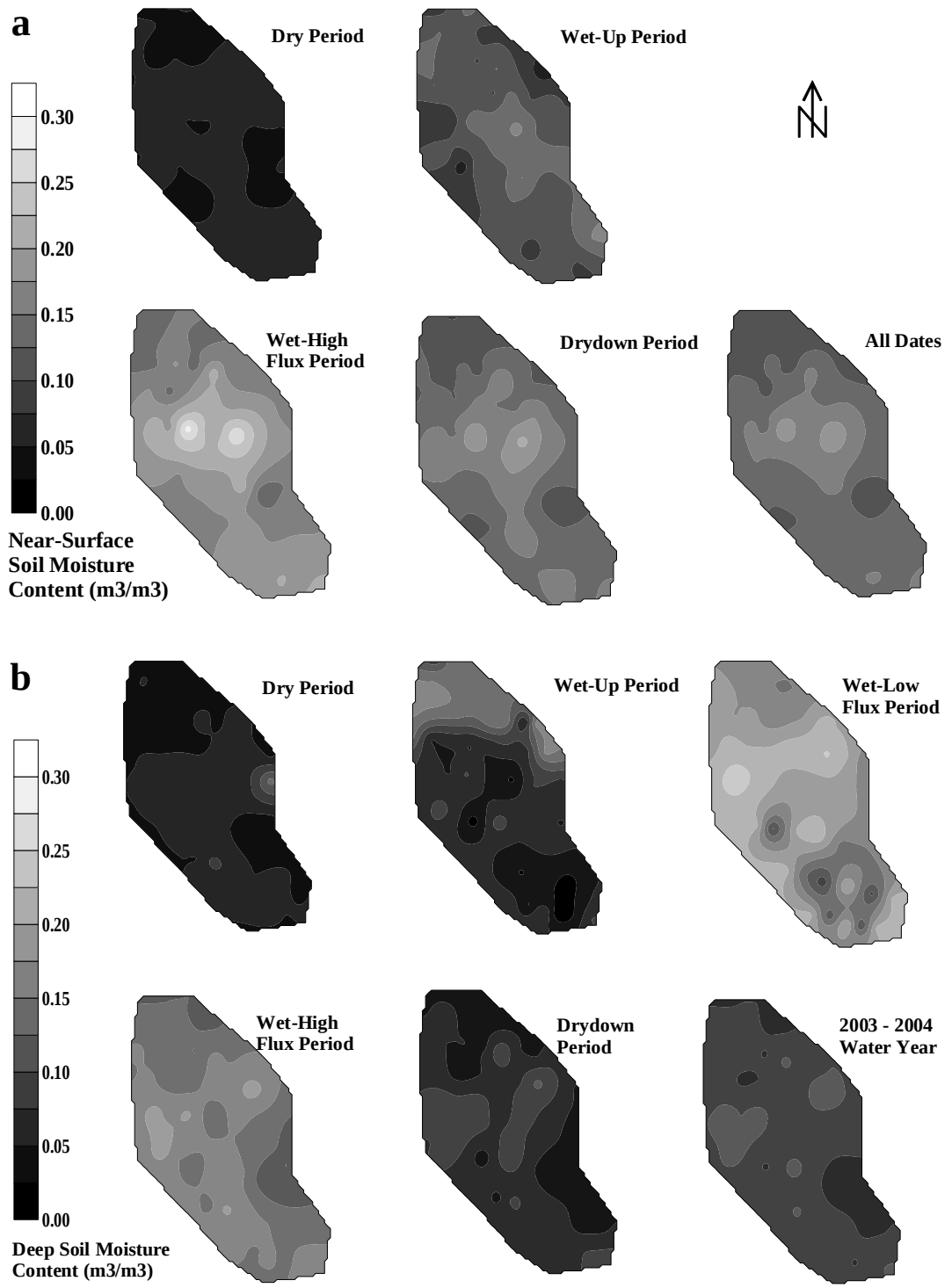

Figure 5.4. Spatial maps of mean measured near-surface (a) and simulated 1D deep (b) soil moisture contents (m^3/m^3) for respective soil moisture periods of the 2003/2004 water year. Near-surface (a) maps identify development of a subsurface variable source area in the central portion of the basin during the wet-up period.

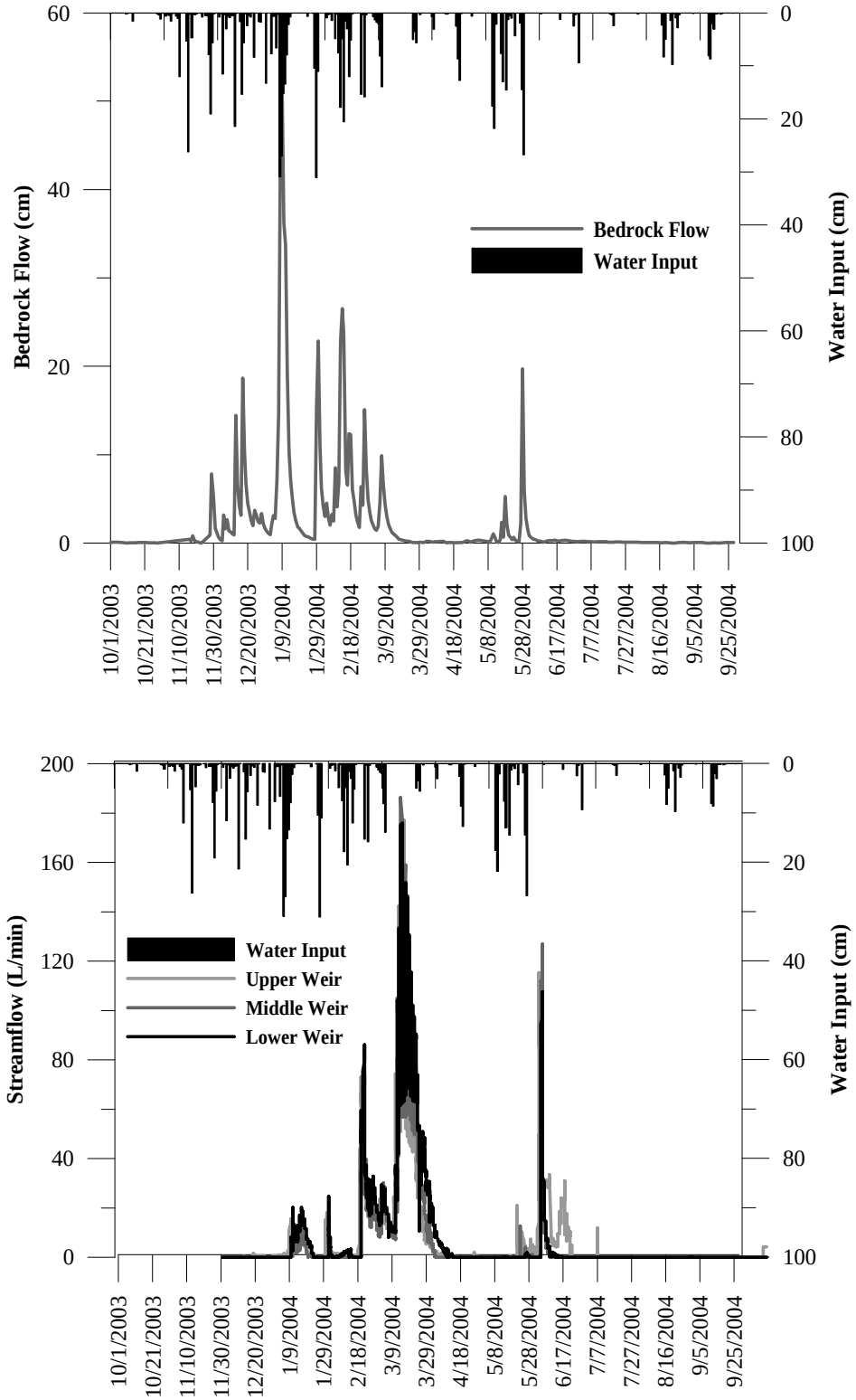

Figure 5.5. Timing of bedrock flow and streamflow with water input as simulated (bedrock flow) and observed (streamflow) during the 2003/2004 water year.

linked lateral processes. Streamflow at the site discontinues as the variable subsurface source area and saturated wedge become disconnected.

5.3 Parameterizing Controls on Soil Moisture and Streamflow Generation

The distribution of soil moisture in the UDCEW is controlled by switches between vertical and lateral processes that vary with the hydrologic regime. Testing of commonly used indices to distribute hillslope processes indicated that many wetness indices do not depict the controls identified at the UDCEW. For both the near-surface and deep soil environments, modified indices indicative of the observed controls produced improved correlation between indices and soil moisture patterns. The results indicate that wetness indices indicative of processes in humid climates are not applicable to semi-arid landscapes like the UDCEW and that the predictive capability of such indices can be improved by incorporating valid controls into the parameterization.

The varied seasonal predictive capability by the modified indices supports assumptions that the processes acting in the study area vary with soil moisture period and that indices representative of seasonal fluctuations in vertical and lateral controls are needed to simulated seasonal processes. The variables predicting vertical (local) control improved predictive capability for all periods, demonstrating that topography (non-local control) exerts less control on processes in semi-arid landscapes than in humid climates. The most significant improvement was found by including a process based index (ln[*water input – ET*]) that described the most important variable in semi-arid hydrology, water availability. The use of topographic wetness indices for hydrologic modeling in

semi-arid landscapes requires multi-index approaches that include the switches in seasonal controls on soil moisture distributions and that accurately depict the differences in the processes that differentiate semi-arid landscapes from the humid environments from which indices were originally derived.

6. CONCLUSIONS

The hypotheses in this study were that streamflow initiation and cessation at the study site are controlled by catchment soil moisture conditions and that many commonly used wetness indices do not accurately depict the processes occurring in the UDCEW. Investigation of the controls on soil moisture was combined with a water budget analysis to provide insight into hillslope processes governing streamflow at the site. Streamflow generation at the UDCEW is the result of hydrologic connection between a bedrock flow fueled subsurface variable source area near the channel head and a saturated wedge beneath the stream channel in the central portion of the basin. The hydrologic connection driving streamflow is dependent on the controls on soil moisture at the site. The controls on soil moisture are the result of the hydrologic regime. Switching of vertical to lateral controls depends on available water during the wet-up and wet-low flux periods of the year.

Parameterizing the site-specific controls on soil moisture improved the predictive capability of wetness indices. The greatest improvement was achieved by parameterizing variables representing available water input (SWE) and soil water storage (soil depth). These findings suggest that water input and the capacity of the soil to store water may be the most important variables for simulating soil moisture patterns in snow dominated semi-arid headwater catchments. The seasonal variability in the controls on soil moisture observed at the UDCEW suggests that the complexity of processes dictating catchment

responses in semi-arid climates requires parameterization of seasonal components. Many commonly derived indices parameterize steady state processes indicative of humid climates. In semi-arid landscapes, such states only occur during brief periods of year. Thus, index approaches in semi-arid landscapes, like the UDCEW, likely require multiple indices to accurately distribute hillslope hydrologic processes. Furthermore, the low correlations (best correlation in this study was 53%) in commonly used and modified indices with soil moisture patterns suggests that controls undefined in this study may be necessary to more fully explain the variability in soil moisture distributions in semi-arid landscapes like the UDCEW.

This study provides spatial support to the findings of McNamara et al. (2005) and Yenko (2003). Further research into fracture networks and soil water residence times at the site might better explain the downward delivery and/or storage of bedrock flow source water for streamflow generation and aid improvement of parameterizing hillslope processes and distributed hydrologic modeling in the UDCEW.

REFERENCES

Anderson, S.P., Dietrich, W.E., Montgomery, D.R., Torres, R., Conrad, M.E., and Loague, K. 1997. Subsurface flow paths in a steep unchanneled catchment. Water Resources Research, 33:2637-2653.

Barling, R.D., Moore, I.D., and Grayson, R.B. 1994. A quasi-dynamic wetness index for characterizing the spatial distribution of zones of surface saturation and soil water content. Water Resources Research, 30(4):1029-1044.

Bevin, K.J. and Kirkby, M.J. 1979. A physically based, variable contributing area model of basin hydrology. Hydrological Sciences Bulletin, 24(1):43-69.

Blöschl, G. and Grayson, R. 2000. Spatial Observations and Interpolation, in: Grayson, R. and Blöschl, G. (editors), Spatial Patterns in Catchment Hydrology. Cambridge University Press, United Kingdom.

Burgess, S.O., Adams, M.A., Turner, N.C. and Ong, C.K. 1998. The redistribution of soil water by tree root systems. Oecologia, 115:306-311.

Burns, D.A., Hooper, R.P., McDonnell, J.J., Freer, J.E., Kendall, C., and Beven, K. 1998. Base cation concentrations in subsurface flow from a forested hillslope--The role of flushing frequency. Water Resources Research, 34(12):3535-3544.

Burns, D.A., McDonnell, J.J., Hooper, R.P., Peters, N.E., Freer, J.E., Kendall, C., and Beven, K. 2001. Quantifying contributions to storm runoff through end-member mixing analysis and hydrologic measurements at the Panola Mountain Research Watershed (Georgia, USA). Hydrological Processes, 15:1903-1924.

Burt, T. P. and Butcher, B. P. 1985. Topographic controls of soil moisture distributions. Journal of Soil Science, 36:469– 486.

Buttle, J.M. and McDonald, D.J. 2002. Coupled vertical and lateral preferential flow on a forested slope. Water Resources Research, 38(5):1029.

Caldwell, M.M., Dawson, T.E., and Richards, J.H. 1998. Hydraulic lift: consequences of water efflux from the roots of plants. Oecologia, 113:151-161.

Chamran, F., Gessler, P.E., and Chadwick, O.A. 2002. Spatially explicit treatment of soil-water dynamics along a semi-arid catena. Soil Science Society of America Journal, 66: 1571-1583.

Daubenmire, R. 1959. A canopy-coverage method of vegetation analysis. Northwest Scientist, 33:43-64.

Davis, J.C. 2002. Statistics and Data Analysis in Geology. John Wiley Sons, United States.

Dawson, T.E. 1993. Hydraulic lift and water use by plants: implications for water balance, performance and plant-plant interactions. Oecologia, 95:565-574.

Dingman, S.L. 2002. Physical Hydrology. Prentice Hall, United States.

Famiglietti, J.S., Devereaux, J.A., Laymon, C.A., Tsegaye, T., Houser, P.R., Jackson, T.J., Graham, S.T., Rodell, M., and van Oevelen, P.J. 1999. Ground-based investigation of soil moisture variability within remote sensing footprints during the Southern Great Plains. (SGP97) Hydrology Experiment. Water Resources Research, 35:1839-1851.

Famiglietti, J.S., Rudniki, J.W., and Rodell, M. 1998. Variability in surface moisture content along a hillslope transect: Rattlesnake Hill, Texas. Journal of Hydrology, 210:259–281.

Flerchinger, G. N. and Hanson, C.L. 1989. Modeling soil freezing and thawing on a rangeland watershed. Transactions of the ASAE, 32:1551–1554.

Flerchinger, G.N. and Pierson, F.B. 1991. Modeling plant canopy effects on variability of soil temperature and water. Agricultural and Forest Meteorology, 56:227-246.

Flerchinger, G.N. and Clark, P.E., 2003. Hypothesized hydrological response to a prescribed fire on a small mountainous watershed. Abstract H32C-0585 In: EOS Transactions, Vol. 84(46) supplement, American Geophysical Union, CD-ROM.

Flerchinger, G.N. and Saxton, K.E. 1989a. Simultaneous heat and water model of a freezing snow-residue-soil system I. Theory and development. Transactions of the ASAE, 32(2):565-571.

Flerchinger, G.N. and Saxton, K.E. 1989b. Simultaneous heat and water model of a freezing snow-residue-soil system II. Field verification. Transactions of the ASAE, 32(2):573-578.

Flerchinger, G.N., Cooley, K.R., and Deng, Y. 1994. Impacts of spatially and temporally varying snowmelt on subsurface flow in a mountainous watershed: 1. Snowmelt simulation. Hydrologic Science Journal, 39(5):507-520.

Flerchinger, G.N., Cooley, K.R., Hanson, C.L., and Seyfried, M.S. 1998. A uniform versus an aggregated water balance of a semi-arid watershed. Hydrological Processes, 12:331-342. 1998.

Flerchinger, G.L., Hanson, C.L., and Wright, J.R. 1996. Modeling evapotranspiration and surface energy budgets across a watershed. Water Resources Research, 32(8): 2539-2548.

Francis, C. F., Thornes, J.B., Romero Diaz, A., Lopez Bermudez, F., and Fisher, G.C. 1986. Topographic control of soil moisture, vegetation cover and land degradation in a moisture stressed Mediterranean environment. Catena, 13:211–225.

Freer, J., McDonnell, J.J., Beven, K.J., Peters, N.E., Burns, D.A., Hooper, R., Aulenbach, B., and Kendall, C. 2002. The role of bedrock topography on subsurface storm flow. Water Resources Research, 38(12):1269.

Gomez-Plaza, A., Martinez-Mena, M., Albaladejo, J., and Castillo, V.M. 2001. Factors regulating spatial distribution of soil water content in small semi-arid catchments. Journal of Hydrology, 253:211-226.

Grant, L., Seyfried, M., and McNamara, J. 2004. Spatial variation and temporal stability of soil water in a snow-dominated, mountain catchment. Hydrologic Processes, 18(18): 3493-3511.

Grayson, R.B., and Western, A.W. 1998. Towards aerial estimation of soil water content from point measurements: time and space stability of mean response. Journal of Hydrology, 207:68-82.

Grayson, R.B., Western, A.W., Chiew, F.H.S., and Blöschl, G. 1997. Preferred states in spatial soil moisture patterns: local and nonlocal controls. Water Resources Research, 33(12): 2897– 2908.

Hawley, M.E., Jackson, T.J., and McCuen, R.H. 1983. Surface soil moisture variation on small agricultural watershed. Journal of Hydrology, 62:179–200.

Hillel, D. 1998. Environmental Soil Physics. Academic Press, United States.

Hornberger, G.M., Raffensperger, J.P., Wiberg, P.A., and Eshleman, K.N. 1998. Elements of Physical Hydrology. John Hopkins University Press, United States.

Huisman, J.A., Snepvangers, J.J.J.C., Bouten, W., and Heuvelink, G.B.M. 2002. Mapping spatial variation in surface soil water content: comparison of ground-penetrating radar and time domain reflectometry. Journal of Hydrology, 269:194-207.

Huisman, J.A., Sperl, C., Bouten, W., and Verstraten, J.M.. 2001. Soil water content measurements at different scales: accuracy of time domain reflectometry and ground-penetrating radar. Journal of Hydrology, 245(1–4):48–58.

Johnson, K.M., Lewis, R.S., Bennett, E.H., and Kiilsgaard, T.H. 1988. Cretaceous and Tertiary intrusive rocks of south-central Idaho. In: Link, P.K. and Hackett, W.R. (editors), Guidebook to the Geology of Central and Southern Idaho. Idaho Geologic Survey, Bulletin 27, pp. 55-86.

Jones, S.B., Wraith, J.M., and Or, D. 2002. Time domain reflectometry (TDR) measurement principles and applications. Hydrologic Processes, 16:141-153.

Kachanoski, R.G. and de Jong, E. 1988. Scale dependence and the temporal persistence of spatial patterns of soil water storage. Water Resources Research, 24:85–91.

Kattelmann, R. and Elder, K. 1991. Hydrologic characteristics and water balance of an alpine basin in the Sierra Nevada. Water Resources Research, 27:1553-1562.

Ledieu, J., De Ridder, P., De Clerck, P., and Dautrebande, S. 1986. A method of measuring soil moisture by time domain reflectometry. Journal of Hydrology, 88:319-328.

Lewis, R.S., Kiilsgaard, T.H., Bennett, E.H., and Hall, W.H. 1987. Lithologic and chemical characteristics of the central and southeastern part of the southern lobe of the Idaho Batholith. In: Vallier, T.L. and Brooks, H.C. (editors), Geology of the Blue Mountains region of Oregon, Idaho, and Washington – the Idaho Batholith and its border zone: U.S. Geologic Survey, Professional Paper 1436, pp. 171-196.

Maidment, D.R. 1993. Handbook of Hydrology. McGraw Hill, United States.

Matherorn, G. 1963. Traité de Géostatistique Appliquée, Tome II: Mémoires du Bureau de Recherches Géologiques et Miniéres. Editions Technip, Paris.

McNamara, J.P., Chandler, D.G., and Seyfried, M. 2005. The role of a snowpack on relationships between preferred soil moisture states, lateral flow, and streamflow generation in a small catchment. Hydrological Processes, in press.

Moore, R.D. and Thompson, J.C. 1996. Are water table variations in a shallow forest soil consistent with the TOPMODEL concept? Water Resources Research, 32:663-669.

Moore, I.D., Burch, G.J., and Mackenzie, D.H. 1988. Topographic effects on the distribution of surfaces soil water and the location of ephemeral gullies. Transactions of the ASAE, 31(4):1098-1107.

Moore, I.D., Grayson, R.B. and Ladson, A.R. 1991. Digital Terrain Modeling: A review of hydrological, geomorphological, and biological applications. Hydrological Processes, 5:3-30.

Newman, B.D., Campbell, A.R., and Wilcox. B.P. 1998. Interflow pathways in a semi-arid ponderosa pine hillslope. Water Resources Research 34(12):3485-3496.

Olea, R.A. 1999. Geostatistics for Engineers and Earth Scientists. Kluwer Academic Publishers, United States.

O'Loughlin, E.M. 1986. Prediction of surface saturation zones in natural catchments by topographic analysis. Water Resources Research, 22(5): 794–804.

Quinn, P.F., Beven, K.J., and Lamb, R. 1995. The ln(a/tanb) index: How to calculate it and how to use it within the TOPMODEL framework Hydrologic Processes, 9:161– 182.

Richards, J.H. and Caldwell, M.M. 1987. Hydraulic lift: substantial nocturnal water transport between soil layers by *Artemisia tridentata* roots. Oecologia, 73:486-489.

Ridolfi, L., D'Odorico, P., Porporato, A., and Rodriquez-Iturbe, I. 2003. Stochastic soil moisture dynamics along a hillslope. Journal of Hydrology, 272:264-275.

Ryel, R.J., Caldwell, M.M., Leffler, A.J., and Yoder, C.K. 2003. Rapid soil moisture recharge to depth by roots in a stand of Artemisia tridentata. Ecology, 84:757–764.

Ryel, R.J., Leffler, A.J., Peek, M.S., Ivans, C.Y., and Caldwell, M.M. 2004. Water conservation in Artemisia tridentata through redistribution of precipitation. Oecologia, 141:335-345.

Seyfried, M. 1998. Spatial variability constraints to modeling soil water at different scales. Geoderma, 85:231-254.

Schenk, H.J., and Jackson, R.B. 2002. Rooting depths, lateral root spreads, and belowground/aboveground allometries of plants in water limited ecosystems. Journal of Ecology, 90:480-494.

Sherlock, M.D., Chappell, N.A., and McDonnell, J.J. 2000. Effects of experimental uncertainty on the calculation of hillslope flow paths. Hydrological Processes, 14:2457-2471.

Siddiqui, S.I., Drnevich, V.P., and Deschamps, R.J. 2000. Time domain reflectometry development for use in geotechnical engineering. Geotechnical Testing Journal, 23(1):9-20.

Simunek, J., Sejna, M., and van Genuchten, M. 1999. The HYDRUS-2D software package for simulating two-dimensional movement of water, heat, and multiple solutes in variably saturated media. Riverside, California, U.S. Salinity Laboratory, ARS, USDA.

Skoien, J.O., Blöschl, G., and Western, A.W. 2003. Characteristic space scales and timescales in hydrology . Water Resources Research, 39(1):1-19.

Spence, L.E. 1937. Root studies of important range plants of the Boise River Watershed. Journal of Forestry, 35:747-754.

Sperry, J.S., Hacke, U.G., Oren, R., and Comstock, J.P. 2002. Water deficits and hydraulic limits to leaf water supply. Plant, Cell and Environment, 25:251-263.

Stieglitz, M., Shaman, J., McNamara, J., Kling, G. and Engel, V. 2003. An approach to understanding hydrologic connectivity on the hillslope and the implications for nutrient transport. Global Biogeochemical Cycles, 17(4):1105.

Tarboton, D.G. 2003. Terrain Analysis Using Digital Elevation Models in Hydrology, 23rd ESRI International Users Conference, San Diego, California, July 7-11.

Tarboton, D.G. 1997. A New Method for the Determination of Flow Directions and Contributing Areas in Grid Digital Elevation Models. Water Resources Research, 33(2):309-319.

Topp, G.C., Davis, J.L., and Annan, A.P. 1980. Electromagnetic determination of soil water content: Measurements in coaxial transmission lines. Water Resources Research, 16:574-582.

Torres, R., Dietrich, W.E., Montgomery, D.R., Anderson, S.P., and Loague, K. 1998. Unsaturated zone processes and the hydrologic response of a steep, unchanneled catchment. Water Resources Research, 34(8):1865.

Troch, P.A, Mancini, M., Paniconi, C., and Wood, E.F. 1993. Evaluation of a distributed catchment-scale water balance model. Water Resources Research, 29(6): 1805-1818.

USDA. 2005. Fire Effects Information System Plant Database. Available at: <http://www.fs.fed.us/database/feis/plants/>

USDA. 1997. Soil survey of the Boise Front: Interim and supplemental report, Natural Resource Conservation Service, Boise, Idaho.

Vachaud, G., Passerat de Silans, A., Balabanis, P., and Vauclin, M. 1985. Temporal persistence of spatially measured soil water probability density function. Soil Science Society of America. Journal, 49:822–828.

van Overmeeren, R.A., Sariowan, S.V., and Gehrels, J.C. 1997. Ground penetrating radar for determining volumetric water content; results of comparative measurements at two test sites. Journal of Hydrology, 197:316–338.

Walter, H. 1939. Grasland, Savanne und Busch der arideren Teile Afrikas in ihrer ökologischen Bedingtheit. Jahrbücher für wissenschaftliche Botanik, 87:750–860.

Webster, R. and Oliver, M.A. 2001. Geostatistics for Environmental Scientists. Wiley Press, Chichester.

Western, A.W., Blöschl, G., and Grayson, R.B. 1998a. Geostatistical characterization of soil moisture patterns in the Tarrawarra Catchment. Journal of Hydrology, 205:20-37.

Western, A.W., Blöschl, G., and Grayson, R.B. 1998b. How well do indicator variograms capture the spatial connectivity of soil moisture? Hydrological Processes, 12:1851-1868.

Western, A.W., Grayson, R.B., Blöschl, G., Willgoose, G.R., and McMahon, T.A. 1999. Observed spatial organisation of soil moisture and its relation to terrain indices. Water Resources Research, 35(3): 797-810.

Western, A.W., Zhou, S-L., Grayson, R.B., McMahon, T.A., Blöschl, G., and Wilson, D.J. 2004. Spatial correlation of soil moisture in small catchments and its relationship to dominant spatial hydrological processes. Journal of Hydrology, 286:113-134.

Williams, K., Caldwell, M.M., and Richards, J.H. 1993. The influence of shade and clouds on soil water potential: The buffered behavior of hydraulic lift. Plant and Soil, 157: 83-95.

Wood, J.D. 1996. The geomorphological characterization of digital elevation models. Ph.D. Thesis, the University of Leicester, Leicester, United Kingdom.

Yenko, M. 2003. Hydrometric and geochemical evidence of streamflow sources in the Upper Dry Creek Experimental Watershed, southwestern Idaho. Masters Thesis, Boise State University, Boise, Idaho, United States.

APPENDIX A

Characterization of UDCEW Sampling Locations

Point	UTM NAD 1927 Northing (m)	UTM NAD 1927 Easting (m)	Elevation (m)	Aspect (°)	Slope (°)	Soil Depth (m)	Upper 30 cm of Soil Profile % Coarse	Upper 30 cm of Soil Profile % Sand	Upper 30 cm of Soil Profile % Fines	Upslope Contributing Area (m^2)	Slope Distance to Divide (m)	Distance to Stream (m)	Wetness Index
1	4842070.870	569374.071	1600	91.53	30.20	0.61	11	81	8	26.87	63.32	10.00	4.28
2	4842087.093	569381.715	1602	133.21	16.12	0.46	17	76	7	104.96	39.80	45.00	6.65
3	4842089.761	569371.579	1603	146.76	22.96	0.40	17	77	6	5.09	32.77	31.21	2.27
4	4842072.865	569361.985	1606	69.32	30.34	0.46	18	74	7	13.67	49.99	20.00	2.82
5	4842074.042	569352.580	1609	66.70	22.04	0.91	14	81	6	33.53	41.65	19.14	4.43
6	4842092.870	569359.380	1606	114.12	14.59	0.56	19	74	7	2774.68	40.78	2.00	9.86
7	4842097.210	569344.620	1606	105.73	8.52	0.21	26	69	5	567.56	41.76	12.07	8.44
8	4842099.802	569330.510	1611	75.36	26.14	1.25	17	75	7	45.13	44.93	27.07	4.34
9	4842104.604	569318.342	1615	67.34	19.92	0.94	22	76	2	36.15	40.23	12.07	4.64
10	4842106.391	569308.825	1619	74.96	17.18	0.34	16	78	6	5.00	32.09	17.07	2.26
11	4842106.753	569300.665	1623	69.98	20.08	0.34	19	74	7	10.17	21.04	19.14	3.66
12	4842080.649	569323.334	1619	48.32	13.32	0.55	16	77	6	5.00	17.61	42.07	2.53
13	4842079.603	569334.274	1615	66.40	21.92	1.04	19	77	4	29.99	27.47	34.14	4.03
14	4842058.372	569335.299	1617	88.40	18.79	0.43	12	83	5	11.99	18.80	48.28	3.25
15	4842074.651	569344.583	1612	65.82	24.60	0.64	15	79	6	38.50	33.47	29.14	4.58
16	4842132.975	569291.298	1623	108.60	22.53	0.34	18	77	5	7.83	40.40	24.14	2.57
17	4842130.965	569300.776	1620	112.50	16.14	1.07	15	79	6	5.00	52.70	14.14	2.42
18	4842129.947	569316.211	1616	186.93	14.77	0.30	28	69	3	528.24	56.23	17.07	7.76
19	4842125.860	569328.560	1620	215.06	28.58	0.64	17	80	3	11.12	40.29	17.07	3.11
20	4842122.392	569341.008	1620	203.61	12.90	0.43	19	75	6	47.65	30.14	19.14	5.19
21	4842118.131	569352.345	1618	164.26	25.00	0.43	16	75	8	5.68	14.60	43.28	1.79
23	4842153.248	569337.940	1628	225.68	15.73	0.37	20	74	5	9.31	33.47	50.36	3.10
24	4842156.425	569324.995	1626	208.85	20.81	0.70	25	71	4	71.73	39.51	21.21	5.13
25	4842158.787	569310.970	1627	174.55	23.03	0.46	14	76	10	20.82	54.44	15.00	3.60
26	4842160.025	569296.516	1627	157.28	20.04	0.37	22	75	4	467.38	62.30	0.00	7.33
27	4842160.858	569285.839	1622	116.17	22.89	0.46	14	79	7	69.19	51.92	40.36	5.35
28	4842161.380	569277.397	1635	111.04	15.73	0.46	12	80	8	5.00	44.39	47.43	2.24
29	4842164.148	569268.839	1638	101.33	18.68	0.37	17	76	7	64.64	35.70	59.50	5.51
30	4842181.957	569274.249	1639	131.22	18.37	0.70	21	75	5	11.71	46.79	52.43	3.32
31	4842180.837	569286.184	1636	127.51	14.07	0.27	19	76	5	5.00	57.41	7.07	2.47
32	4842180.435	569299.050	1634	191.24	15.58	0.34	11	83	6	134.86	45.82	20.00	5.92
33	4842177.541	569310.615	1635	198.45	18.52	0.30	15	80	5	17.00	40.57	39.14	3.67
34	4842175.503	569321.258	1635	180.28	20.92	0.46	12	82	6	30.24	37.22	39.14	4.34
35	4842173.963	569333.273	1634	207.24	24.37	0.67	21	74	5	22.21	34.38	38.28	3.56
36	4842173.204	569345.341	1636	204.65	15.52	0.34	16	80	4	11.08	21.31	74.50	3.46
37	4842170.455	569354.847	1636	169.40	13.19	0.38	16	78	7	5.00	3.53	81.00	2.50
38	4842190.696	569339.194	1641	161.86	9.44	0.27	14	81	5	9.68	10.38	74.50	3.77
39	4842191.638	569332.218	1641	178.38	7.66	0.76	19	78	3	49.75	16.27	58.28	5.70
40	4842192.258	569320.724	1642	170.70	12.94	0.24	17	78	4	5.00	23.08	54.14	2.58
41	4842192.839	569312.037	1642	207.82	20.25	0.24	18	77	5	5.00	34.39	39.14	1.90
42	4842196.620	569300.350	1646	198.02	25.83	0.24	21	73	6	24.93	38.27	37.07	3.94
43	4842197.622	569290.077	1645	173.88	31.61	0.24	25	69	6	91.16	41.64	15.00	4.85
44	4842197.443	569278.634	1645	146.75	39.50	0.24	24	71	5	32.50	34.44	21.21	3.84
45	4842218.897	569276.329	1653	152.60	10.57	0.24	17	77	6	6.88	16.88	41.21	3.22
46	4842217.453	569290.452	1651	172.99	16.45	0.30	21	76	3	19.26	22.84	35.00	3.97
47	4842215.699	569302.085	1650	152.93	19.49	0.24	23	74	4	9.13	21.24	61.21	3.36
48	4842212.859	569312.638	1649	153.57	15.98	0.27	21	74	5	5.00	7.73	59.14	2.25
50	4842228.780	569296.335	1655	158.35	10.90	0.27	19	74	6	8.21	6.14	65.00	3.41
51	4842230.455	569284.921	1657	140.87	11.82	0.24	43	53	4	5.00	7.68	52.07	2.83
52	4842230.733	569277.708	1656	160.66	14.82	0.49	24	71	4	15.00	0.64	56.21	5.49
54	4842197.134	569266.376	1648	153.65	25.52	0.27	27	67	6	11.13	29.39	66.57	2.63
55	4842217.009	569266.813	1653	154.79	9.67	0.27	19	76	5	14.57	11.43	45.36	5.17
56	4842182.966	569261.766	1643	125.58	21.65	0.46	25	69	6	27.57	29.19	59.50	3.76
57	4842138.050	569280.432	1631	107.20	33.38	0.49	12	80	8	5.00	30.54	34.14	1.60
58	4842138.840	569268.619	1637	108.49	17.35	0.46	14	81	4	5.00	16.77	51.21	2.30
22A	4842154.622	569354.463	1632	196.10	15.11	0.35	18	77	6	10.43	3.15	53.28	3.47
22B	4842129.618	569354.111	1625	188.69	26.58	0.58	30	65	6	5.90	4.87	50.00	2.17

Point	Profile Curvature	Planar Curvature	Mean Curvature	Longitudinal Curvature	Cross Section Curvature	Concavity	Convexity	Percent Cover Summer	Percent Cover Spring	Percent Cover Winter	Maximum Snow Depth (cm)	Snow Density at Max Snow Depth	SWE (cm) at Max Snow Depth
1	-0.69	0.42	-1.49	-1.21	-0.28	-2.47	-0.50	50	41	20	58.4	0.311	7.17
2	-0.54	0.32	-0.75	-0.64	-0.11	-1.30	-0.20	70	60	16	56.4	0.334	7.42
3	0.19	3.48	-0.70	0.21	-0.91	-2.00	0.61	51	26	0	57.3	0.299	6.73
4	0.09	0.70	-0.16	0.11	-0.27	-0.56	0.23	96	86	35	59.4	0.302	7.10
5	-0.11	0.71	-0.44	-0.14	-0.29	-0.61	-0.26	70	56	31	60.5	0.303	7.24
6	-0.24	2.61	-0.94	-0.26	-0.68	-1.40	-0.48	96	69	11	61.4	0.276	6.66
7	-0.46	1.93	-0.98	-0.50	-0.48	-1.20	-0.77	15	10	0	64.2	0.315	8.00
8	-0.11	0.31	-0.29	-0.15	-0.14	-0.34	-0.24	55	40	6	68.3	0.340	9.17
9	-0.02	0.89	-0.34	-0.02	-0.32	-0.66	-0.03	100	100	100	68.5	0.327	8.89
10	0.37	1.27	0.01	0.44	-0.44	-1.25	1.27	65	60	12	65.1	0.310	7.98
11	0.37	-0.14	0.46	0.42	0.04	-0.02	0.94	75	26	6	62.2	0.310	7.56
12	0.65	-1.00	0.88	0.69	0.19	0.33	1.43	36	31	4	63.8	0.321	8.09
13	0.71	-0.47	1.08	0.89	0.19	0.35	1.81	60	45	20	63.0	0.315	7.89
14	0.05	-2.24	0.61	0.05	0.55	0.09	1.12	55	41	5	61.1	0.312	7.56
15	-0.15	0.62	-0.48	-0.20	-0.28	-0.73	-0.23	75	75	5	61.4	0.308	7.48
16	-0.83	0.32	-1.45	-1.27	-0.18	-2.58	-0.32	100	100	100	41.9	0.329	5.43
17	-0.45	0.34	-0.68	-0.55	-0.13	-1.30	-0.06	60	60	10	46.1	0.347	6.17
18	-0.26	1.80	-0.75	-0.28	-0.46	-1.06	-0.43	5	5	0	57.8	0.307	6.87
19	0.14	0.32	0.03	0.19	-0.16	-0.52	0.58	30	21	5	54.6	0.325	7.03
20	0.53	-0.62	1.04	0.73	0.31	0.54	1.54	25	25	0	55.7	0.330	7.31
21	1.05	-0.55	1.73	1.46	0.27	-0.22	3.68	30	27	1	52.9	0.303	6.41
23	0.26	-0.37	0.41	0.30	0.11	0.03	0.78	20	20	5	50.6	0.325	6.48
24	-0.10	1.25	-0.62	-0.12	-0.50	-1.07	-0.18	30	10	0	51.4	0.320	6.45
25	0.29	-0.27	0.47	0.37	0.11	0.07	0.87	25	20	0	51.6	0.311	6.29
26	0.13	0.55	-0.05	0.16	-0.21	-0.48	0.38	42	22	1	49.6	0.293	5.73
27	-0.20	-0.23	-0.16	-0.28	0.12	-0.57	0.24	21	11	1	49.3	0.282	5.52
28	0.79	-0.32	1.12	0.99	0.13	0.25	1.99	40	30	0	48.5	0.279	5.39
29	-0.21	1.27	-0.68	-0.25	-0.43	-0.87	-0.48	55	55	1	47.4	0.279	5.28
30	0.21	0.45	0.09	0.25	-0.16	-0.76	0.94	55	55	15	47.4	0.262	4.94
31	0.08	0.13	0.05	0.09	-0.05	-0.10	0.19	5	5	0	41.4	0.197	3.21
32	-0.09	1.29	-0.51	-0.10	-0.41	-0.90	-0.12	30	26	5	52.9	0.287	5.91
33	0.34	-0.92	0.74	0.41	0.34	0.62	0.87	25	25	1	64.2	0.309	7.89
34	0.69	-0.52	1.34	1.05	0.29	0.56	2.13	36	16	5	55.9	0.309	6.86
35	0.45	1.14	0.07	0.60	-0.54	-1.23	1.36	15	10	0	46.2	0.311	5.67
36	0.38	-0.45	0.62	0.46	0.16	0.29	0.95	26	26	1	54.2	0.300	6.43
37	0.16	-0.48	0.36	0.19	0.17	0.17	0.55	36	36	6	52.0	0.289	5.97
38	0.52	-2.15	1.05	0.56	0.49	0.43	1.67	16	6	0	51.4	0.311	6.29
39	0.67	0.36	0.65	0.76	-0.11	-0.22	1.52	21	6	1	48.5	0.307	5.86
40	0.04	-0.47	0.31	0.06	0.25	-0.20	0.82	65	16	3	50.8	0.295	5.94
41	0.87	-0.63	1.40	1.13	0.27	0.06	2.74	42	8	2	52.7	0.287	6.01
42	-0.43	1.58	-1.31	-0.58	-0.73	-1.66	-0.96	5	5	0	48.5	0.270	5.20
43	0.10	0.39	-0.09	0.16	-0.25	-0.67	0.48	20	10	2	45.4	0.259	4.68
44	-0.55	0.13	-1.01	-0.93	-0.09	-1.88	-0.14	15	10	1	45.4	0.257	4.64
45	-0.15	0.93	-0.29	-0.15	-0.14	-0.43	-0.16	45	16	4	43.2	0.254	4.33
46	1.00	0.55	1.27	1.61	-0.34	-1.05	3.59	65	41	5	37.2	0.262	3.83
47	1.07	-0.09	1.65	1.60	0.05	-0.04	3.35	5	1	0	44.8	0.265	4.65
48	0.64	-1.20	1.07	0.72	0.35	0.40	1.74	36	41	6	55.4	0.265	5.75
50	0.30	0.17	0.29	0.34	-0.05	-0.79	1.38	66	36	10	43.5	0.265	4.51
51	0.74	-1.35	1.22	0.84	0.39	0.67	1.77	51	51	10	42.0	0.261	4.32
52	0.60	1.02	0.40	0.65	-0.25	-0.55	1.35	70	61	15	43.0	0.259	4.40
54	0.33	-0.15	0.58	0.50	0.08	-0.02	1.18	5	5	0	46.2	0.262	4.80
55	1.04	-0.45	1.23	1.12	0.10	0.15	2.30	55	55	10	49.6	0.251	4.91
56	-0.14	0.46	-0.30	-0.16	-0.14	-0.90	0.30	81	71	15	44.2	0.283	4.98
57	-0.14	-1.03	0.31	-0.20	0.52	-0.80	1.43	55	45	0	60.7	0.319	7.63
58	0.68	-0.80	1.04	0.79	0.26	0.51	1.58	40	40	0	59.0	0.315	7.32
22A	0.06	-1.36	0.44	0.06	0.38	0.09	0.80	50	32	5	51.2	0.303	6.08
22B	0.09	-1.61	0.91	0.13	0.78	0.04	1.77	70	70	5	43.6	0.291	5.06

APPENDIX B

Summary of Near-Surface Soil Moisture Contents Measured at the UDCEW

	Sample Date									
Sample Point	**4/6/03**	**4/7/03**	**4/9/03**	**4/10/03**	**4/11/03**	**4/17/03**	**6/24/03**	**7/11/03**	**8/1/03**	**8/23/03**
1	0.208	0.263	0.201	0.133	0.193	0.135	0.077	0.054	0.065	0.120
2	0.200	0.225	0.192	0.094	0.160	0.109	0.070	0.064	0.049	0.102
3	0.196	0.219	0.143	0.134	0.182	0.090	0.066	0.071	0.048	0.100
4	0.191	0.179	0.187	0.175	0.159	0.114	0.061	0.050	0.046	0.087
5	0.195	0.224	0.186	0.120	0.187	0.125	0.065	0.051	0.062	0.084
6	0.238	0.213	0.138	0.182	0.145	0.125	0.054	0.077	0.042	0.082
7	0.130	0.204	0.116	0.125	0.239	0.111	0.045	0.063	0.041	0.080
8	0.176	0.180	0.175	0.165	0.161	0.155	0.065	0.050	0.042	0.074
9	0.188	0.197	0.145	0.110	0.161	0.103	0.056	0.062	0.054	0.108
10	0.198	0.214	0.147	0.107	0.142	0.115	0.038	0.048	0.055	0.047
11	0.135	0.192	0.135	0.124	0.139	0.110	0.049	0.036	0.036	0.056
12	0.185	0.199	0.155	0.090	0.169	0.135	0.054	0.062	0.051	0.135
13	0.187	0.230	0.182	0.114	0.177	0.135	0.100	0.074	0.057	0.110
14	0.194	0.234	0.192	0.096	0.158	0.142	0.053	0.051	0.057	0.075
15	0.194	0.211	0.201	0.149	0.182	0.151	0.073	0.056	0.055	0.060
16	0.168	0.206	0.190	0.081	0.160	0.109	0.080	0.045	0.052	0.034
17	0.198	0.227	0.164	0.120	0.167	0.111	0.054	0.032	0.060	0.060
18	0.178	0.207	0.129	0.126	0.124	0.110	0.051	0.052	0.046	0.061
19	0.205	0.215	0.186	0.159	0.186	0.131	0.066	0.060	0.055	0.060
20	0.126	0.122	0.116	0.086	0.114	0.082	0.050	0.040	0.053	0.041
21	0.182	0.201	0.118	0.111	0.150	0.092	0.045	0.036	0.034	0.052
23	0.235	0.238	0.147	0.185	0.119	0.138	0.054	0.026	0.052	0.046
24	0.278	0.278	0.289	0.233	0.289	0.189	0.075	0.069	0.052	0.072
25	0.201	0.169	0.157	0.160	0.172	0.092	0.050	0.046	0.035	0.040
26	0.256	0.281	0.262	0.260	0.119	0.220	0.061	0.043	0.031	0.037
27	0.196	0.231	0.160	0.145	0.118	0.108	0.086	0.073	0.046	0.062
28	0.240	0.325	0.231	0.147	0.253	0.126	0.086	0.061	0.048	0.063
29	0.194	0.229	0.220	0.066	0.134	0.132	0.038	0.062	0.052	0.066
30	0.184	0.176	0.152	0.172	0.154	0.108	0.070	0.056	0.041	0.066
31	0.203	0.127	0.152	0.095	0.085	0.090	0.058	0.060	0.049	0.060
32	0.202	0.192	0.190	0.137	0.144	0.126	0.055	0.042	0.050	0.063
33	0.229	0.229	0.167	0.215	0.193	0.152	0.064	0.071	0.047	0.058
34	0.236	0.200	0.174	0.170	0.112	0.099	0.061	0.072	0.057	0.056
35	0.116	0.143	0.162	0.185	0.207	0.132	0.072	0.059	0.046	0.052
36	0.179	0.134	0.161	0.142	0.112	0.144	0.111	0.057	0.062	0.121
37	0.166	0.106	0.153	0.152	0.145	0.113	0.055	0.062	0.045	0.062
38	0.143	0.121	0.171	0.067	0.084	0.112	0.039	0.046	0.045	0.081
39	0.162	0.159	0.148	0.108	0.136	0.114	0.040	0.053	0.049	0.072
40	0.118	0.136	0.147	0.119	0.094	0.114	0.045	0.067	0.041	0.066
41	0.143	0.177	0.099	0.180	0.140	0.148	0.054	0.043	0.053	0.067
42	0.118	0.121	0.118	0.105	0.087	0.110	0.045	0.069	0.043	0.054
43	0.153	0.203	0.159	0.149	0.125	0.132	0.051	0.064	0.049	0.062
44	0.095	0.189	0.114	0.120	0.108	0.114	0.047	0.063	0.045	0.052
45	0.171	0.122	0.165	0.084	0.088	0.090	0.054	0.049	0.033	0.049
46	0.157	0.143	0.150	0.113	0.099	0.079	0.010	0.047	0.055	0.052
47	0.132	0.152	0.124	0.069	0.112	0.104	0.046	0.045	0.050	0.052
48	0.140	0.157	0.135	0.093	0.096	0.088	0.050	0.038	0.046	0.056
50	0.143	0.172	0.142	0.139	0.078	0.128	0.050	0.042	0.042	0.065
51	0.146	0.132	0.102	0.117	0.173	0.066	0.047	0.046	0.039	0.082
52	0.135	0.131	0.128	0.085	0.096	0.067	0.041	0.045	0.038	0.055
54	0.119	0.123	0.126	0.105	0.080	0.144	0.058	0.045	0.039	0.067
55	0.129	0.172	0.121	0.117	0.129	0.113	0.055	0.060	0.034	0.072
56	0.189	0.168	0.133	0.149	0.139	0.092	0.063	0.059	0.043	0.039
57	0.211	0.198	0.146	0.098	0.198	0.133	0.069	0.064	0.069	0.048
58	0.188	0.134	0.159	0.151	0.173	0.104	0.059	0.041	0.054	0.056
22A	0.200	0.145	0.154	0.121	0.128	0.127	0.055	0.057	0.046	0.047
22B	0.186	0.147	0.118	0.107	0.108	0.085	0.047	0.042	0.073	0.062
Statistics	**4/6/03**	**4/7/03**	**4/9/03**	**4/10/03**	**4/11/03**	**4/17/03**	**6/24/03**	**7/11/03**	**8/1/03**	**8/23/03**
Mean	0.178	0.186	0.158	0.131	0.145	0.118	0.058	0.054	0.048	0.067
SD	0.039	0.047	0.037	0.040	0.044	0.027	0.016	0.012	0.009	0.022
CV	4.607	4.000	4.339	3.262	3.320	4.379	3.615	4.619	5.488	3.080
Maximum	0.278	0.325	0.289	0.260	0.289	0.220	0.111	0.077	0.073	0.135
Minimum	0.095	0.106	0.099	0.066	0.078	0.066	0.010	0.026	0.031	0.034
Range	0.183	0.219	0.190	0.194	0.211	0.154	0.154	0.101	0.051	0.042	0.101
Observations	57	57	57	57	57	57	57	57	57	57

	Sample Date									
Sample Point	**9/11/03**	**10/28/03**	**11/11/03**	**11/18/03**	**11/23/03**	**12/19/03**	**3/4/04**	**3/9/04**	**3/11/04**	**3/16/04**
1	0.049	0.049	0.052	0.073	0.074	0.165	0.197	0.200	0.249	0.257
2	0.050	0.050	0.086	0.135	0.149	0.243	0.187	0.212	0.309	0.223
3	0.041	0.052	0.049	0.129	0.142	0.252	0.190	0.208	0.290	0.188
4	0.037	0.050	0.053	0.100	0.069	0.122	0.192	0.197	0.230	0.256
5	0.033	0.040	0.055	0.095	0.091	0.159	0.187	0.192	0.222	0.289
6	0.051	0.040	0.054	0.091	0.128	0.185	0.197	0.212	0.206	0.199
7	0.051	0.050	0.068	0.115	0.063	0.157	0.192	0.217	0.272	0.165
8	0.049	0.037	0.057	0.085	0.090	0.160	0.187	0.188	0.224	0.258
9	0.043	0.034	0.052	0.136	0.117	0.157	0.190	0.192	0.212	0.181
10	0.026	0.041	0.038	0.112	0.069	0.150	0.190	0.190	0.236	0.207
11	0.037	0.051	0.068	0.068	0.107	0.129	0.189	0.191	0.222	0.231
12	0.064	0.049	0.059	0.092	0.102	0.128	0.188	0.192	0.189	0.201
13	0.049	0.047	0.066	0.076	0.056	0.159	0.186	0.190	0.246	0.235
14	0.053	0.061	0.048	0.104	0.116	0.181	0.188	0.188	0.251	0.249
15	0.050	0.053	0.082	0.071	0.100	0.179	0.187	0.188	0.245	0.232
16	0.043	0.062	0.034	0.051	0.070	0.095	0.117	0.128	0.252	0.207
17	0.054	0.049	0.047	0.094	0.110	0.174	0.193	0.197	0.239	0.261
18	0.057	0.044	0.067	0.088	0.064	0.180	0.232	0.242	0.302	0.242
19	0.057	0.048	0.041	0.190	0.121	0.187	0.212	0.218	0.279	0.260
20	0.050	0.025	0.047	0.124	0.068	0.148	0.202	0.200	0.144	0.143
21	0.039	0.040	0.052	0.100	0.079	0.190	0.196	0.209	0.203	0.160
23	0.041	0.041	0.063	0.142	0.103	0.154	0.180	0.197	0.302	0.351
24	0.041	0.045	0.041	0.145	0.121	0.196	0.276	0.283	0.343	0.321
25	0.039	0.053	0.081	0.154	0.080	0.181	0.197	0.207	0.327	0.317
26	0.050	0.061	0.064	0.070	0.120	0.189	0.272	0.280	0.348	0.438
27	0.045	0.049	0.050	0.075	0.057	0.117	0.205	0.210	0.244	0.262
28	0.064	0.022	0.060	0.074	0.057	0.156	0.182	0.192	0.220	0.263
29	0.063	0.058	0.080	0.072	0.078	0.105	0.173	0.187	0.255	0.167
30	0.041	0.055	0.059	0.086	0.141	0.172	0.203	0.208	0.257	0.211
31	0.046	0.050	0.065	0.088	0.075	0.155	0.196	0.227	0.202	0.110
32	0.056	0.061	0.058	0.102	0.124	0.169	0.204	0.207	0.253	0.167
33	0.050	0.061	0.068	0.076	0.074	0.177	0.155	0.192	0.305	0.224
34	0.052	0.046	0.082	0.076	0.106	0.237	0.225	0.222	0.244	0.215
35	0.053	0.062	0.055	0.058	0.053	0.175	0.207	0.210	0.210	0.266
36	0.054	0.072	0.045	0.075	0.055	0.236	0.180	0.190	0.321	0.217
37	0.061	0.059	0.046	0.084	0.071	0.204	0.133	0.203	0.212	0.197
38	0.039	0.050	0.079	0.078	0.072	0.107	0.087	0.217	0.219	0.297
39	0.057	0.055	0.079	0.076	0.082	0.142	0.136	0.198	0.232	0.196
40	0.044	0.067	0.085	0.104	0.108	0.178	0.141	0.252	0.205	0.152
41	0.050	0.048	0.046	0.140	0.093	0.192	0.183	0.313	0.356	0.321
42	0.045	0.040	0.044	0.105	0.066	0.145	0.173	0.192	0.238	0.156
43	0.034	0.041	0.052	0.110	0.090	0.169	0.197	0.241	0.305	0.270
44	0.030	0.037	0.050	0.108	0.089	0.153	0.222	0.222	0.279	0.152
45	0.049	0.043	0.081	0.112	0.101	0.204	0.178	0.166	0.241	0.185
46	0.033	0.030	0.060	0.094	0.099	0.185	0.211	0.208	0.242	0.229
47	0.042	0.038	0.056	0.076	0.078	0.183	0.140	0.154	0.255	0.184
48	0.044	0.042	0.047	0.090	0.075	0.181	0.146	0.228	0.191	0.175
50	0.062	0.035	0.062	0.163	0.124	0.205	0.134	0.287	0.252	0.181
51	0.049	0.035	0.060	0.148	0.079	0.180	0.142	0.272	0.156	0.192
52	0.041	0.036	0.058	0.042	0.049	0.164	0.140	0.181	0.189	0.149
54	0.041	0.053	0.060	0.112	0.090	0.254	0.184	0.192	0.177	0.156
55	0.048	0.037	0.056	0.148	0.070	0.170	0.173	0.171	0.173	0.157
56	0.041	0.038	0.051	0.076	0.116	0.169	0.189	0.193	0.240	0.228
57	0.043	0.056	0.060	0.081	0.067	0.196	0.204	0.210	0.269	0.234
58	0.048	0.035	0.054	0.073	0.107	0.155	0.181	0.196	0.252	0.304
22A	0.047	0.030	0.062	0.103	0.115	0.135	0.223	0.252	0.289	0.212
22B	0.035	0.037	0.060	0.116	0.094	0.225	0.194	0.211	0.254	0.128
Statistics	**9/11/03**	**10/28/03**	**11/11/03**	**11/18/03**	**11/23/03**	**12/19/03**	**3/4/04**	**3/9/04**	**3/11/04**	**3/16/04**
Mean	0.047	0.046	0.059	0.099	0.091	0.172	0.185	0.209	0.247	0.222
SD	0.009	0.011	0.013	0.030	0.025	0.034	0.033	0.032	0.047	0.061
CV	5.442	4.397	4.689	3.320	3.630	5.001	5.687	6.485	5.296	3.649
Maximum	0.064	0.072	0.086	0.190	0.149	0.254	0.276	0.313	0.356	0.438
Minimum	0.026	0.022	0.034	0.042	0.049	0.095	0.087	0.128	0.144	0.110
Range	0.038	0.050	0.052	0.148	0.100	0.159	0.188	0.185	0.212	0.328
Observations	57	57	57	57	57	57	57	57	57	57

	Sample Date									
Sample Point	**3/19/04**	**3/23/04**	**3/30/04**	**4/2/04**	**4/9/04**	**4/19/04**	**4/23/04**	**5/1/04**	**5/4/04**	**5/13/04**
1	0.245	0.222	0.193	0.175	0.178	0.148	0.200	0.164	0.138	0.204
2	0.217	0.168	0.187	0.172	0.136	0.115	0.175	0.132	0.122	0.183
3	0.179	0.163	0.180	0.154	0.131	0.117	0.135	0.111	0.094	0.168
4	0.196	0.231	0.194	0.179	0.169	0.135	0.172	0.129	0.128	0.145
5	0.272	0.218	0.204	0.185	0.170	0.149	0.201	0.163	0.121	0.166
6	0.176	0.177	0.195	0.159	0.162	0.127	0.190	0.119	0.096	0.149
7	0.157	0.162	0.161	0.147	0.146	0.125	0.151	0.109	0.095	0.137
8	0.258	0.203	0.204	0.188	0.159	0.153	0.180	0.168	0.148	0.204
9	0.198	0.182	0.192	0.162	0.161	0.140	0.187	0.149	0.148	0.190
10	0.181	0.184	0.182	0.144	0.160	0.125	0.154	0.116	0.100	0.163
11	0.192	0.189	0.152	0.156	0.137	0.112	0.140	0.121	0.085	0.122
12	0.228	0.216	0.199	0.178	0.160	0.136	0.188	0.117	0.112	0.141
13	0.227	0.200	0.199	0.177	0.174	0.155	0.184	0.144	0.117	0.093
14	0.195	0.204	0.198	0.189	0.154	0.141	0.148	0.164	0.120	0.164
15	0.226	0.218	0.200	0.174	0.171	0.161	0.182	0.156	0.095	0.186
16	0.222	0.186	0.176	0.138	0.138	0.115	0.120	0.138	0.102	0.177
17	0.215	0.190	0.199	0.176	0.152	0.112	0.160	0.124	0.097	0.119
18	0.243	0.162	0.149	0.167	0.198	0.181	0.200	0.132	0.110	0.234
19	0.272	0.248	0.213	0.184	0.169	0.143	0.160	0.152	0.113	0.215
20	0.083	0.134	0.116	0.120	0.105	0.118	0.105	0.090	0.088	0.136
21	0.174	0.162	0.170	0.140	0.100	0.105	0.129	0.085	0.070	0.129
23	0.226	0.235	0.199	0.167	0.161	0.117	0.180	0.153	0.143	0.206
24	0.305	0.264	0.263	0.243	0.212	0.194	0.228	0.142	0.137	0.201
25	0.206	0.201	0.172	0.169	0.158	0.094	0.229	0.141	0.132	0.197
26	0.427	0.325	0.281	0.274	0.240	0.213	0.222	0.179	0.141	0.229
27	0.177	0.196	0.210	0.172	0.174	0.125	0.164	0.153	0.108	0.160
28	0.274	0.217	0.232	0.195	0.162	0.164	0.218	0.137	0.102	0.165
29	0.253	0.178	0.190	0.173	0.199	0.135	0.189	0.165	0.090	0.185
30	0.181	0.180	0.171	0.159	0.135	0.112	0.166	0.119	0.099	0.185
31	0.132	0.136	0.145	0.144	0.120	0.079	0.120	0.126	0.067	0.185
32	0.183	0.185	0.183	0.188	0.132	0.153	0.171	0.133	0.106	0.184
33	0.244	0.269	0.185	0.160	0.138	0.154	0.176	0.135	0.117	0.197
34	0.198	0.161	0.195	0.159	0.144	0.099	0.136	0.108	0.087	0.184
35	0.249	0.227	0.198	0.175	0.170	0.148	0.175	0.137	0.105	0.183
36	0.174	0.230	0.174	0.177	0.163	0.131	0.115	0.137	0.108	0.094
37	0.153	0.124	0.146	0.158	0.105	0.123	0.164	0.102	0.106	0.187
38	0.197	0.151	0.149	0.137	0.117	0.112	0.142	0.112	0.095	0.164
39	0.179	0.162	0.148	0.143	0.130	0.106	0.144	0.109	0.099	0.160
40	0.185	0.188	0.151	0.224	0.117	0.111	0.146	0.129	0.113	0.229
41	0.211	0.243	0.228	0.219	0.146	0.143	0.176	0.179	0.144	0.190
42	0.131	0.118	0.135	0.110	0.096	0.096	0.123	0.099	0.085	0.137
43	0.157	0.137	0.155	0.168	0.141	0.099	0.141	0.102	0.084	0.133
44	0.132	0.122	0.132	0.144	0.118	0.095	0.080	0.094	0.077	0.085
45	0.122	0.115	0.129	0.138	0.108	0.097	0.083	0.096	0.085	0.142
46	0.171	0.135	0.165	0.155	0.105	0.087	0.108	0.094	0.082	0.120
47	0.138	0.148	0.146	0.119	0.132	0.100	0.133	0.107	0.096	0.145
48	0.161	0.141	0.148	0.147	0.103	0.089	0.119	0.120	0.098	0.162
50	0.175	0.148	0.147	0.116	0.110	0.067	0.121	0.090	0.103	0.138
51	0.153	0.095	0.090	0.098	0.088	0.062	0.102	0.085	0.061	0.109
52	0.134	0.130	0.137	0.124	0.093	0.054	0.117	0.087	0.076	0.124
54	0.157	0.132	0.180	0.143	0.139	0.085	0.132	0.093	0.074	0.168
55	0.133	0.141	0.166	0.135	0.102	0.089	0.124	0.086	0.086	0.158
56	0.185	0.129	0.163	0.143	0.119	0.092	0.090	0.081	0.065	0.141
57	0.219	0.214	0.199	0.175	0.166	0.165	0.178	0.142	0.131	0.153
58	0.189	0.193	0.191	0.142	0.111	0.161	0.164	0.116	0.145	0.179
22A	0.223	0.195	0.154	0.178	0.136	0.118	0.168	0.132	0.100	0.217
22B	0.163	0.149	0.154	0.165	0.101	0.082	0.119	0.115	0.131	0.136
Statistics	**3/19/04**	**3/23/04**	**3/30/04**	**4/2/04**	**4/9/04**	**4/19/04**	**4/23/04**	**5/1/04**	**5/4/04**	**5/13/04**
Mean	0.197	0.181	0.177	0.163	0.143	0.122	0.155	0.125	0.105	0.164
SD	0.054	0.045	0.033	0.031	0.032	0.032	0.036	0.026	0.023	0.035
CV	3.664	4.062	5.283	5.336	4.500	3.806	4.297	4.838	4.628	4.736
Maximum	0.427	0.325	0.281	0.274	0.240	0.213	0.229	0.179	0.148	0.234
Minimum	0.083	0.095	0.090	0.098	0.088	0.054	0.080	0.081	0.061	0.085
Range	0.344	0.230	0.190	0.175	0.151	0.159	0.149	0.099	0.088	0.148
Observations	57	57	57	57	57	57	57	57	57	57

	Sample Date							
Sample Point	**5/20/04**	**5/25/04**	**5/30/04**	**6/2/04**	**6/13/04**	**6/17/04**	**6/24/04**	**6/30/04**
1	0.222	0.163	0.185	0.139	0.138	0.121	0.074	0.118
2	0.213	0.196	0.144	0.134	0.127	0.116	0.096	0.104
3	0.224	0.168	0.187	0.151	0.126	0.113	0.102	0.119
4	0.194	0.121	0.174	0.162	0.117	0.111	0.082	0.090
5	0.221	0.181	0.189	0.151	0.134	0.130	0.119	0.117
6	0.240	0.159	0.178	0.153	0.116	0.113	0.104	0.108
7	0.178	0.156	0.176	0.112	0.123	0.112	0.101	0.100
8	0.203	0.164	0.182	0.156	0.131	0.120	0.108	0.135
9	0.221	0.168	0.172	0.161	0.133	0.139	0.144	0.145
10	0.190	0.148	0.131	0.104	0.089	0.104	0.081	0.099
11	0.177	0.158	0.147	0.130	0.083	0.101	0.090	0.087
12	0.231	0.146	0.168	0.131	0.121	0.116	0.097	0.117
13	0.206	0.147	0.210	0.135	0.125	0.145	0.125	0.139
14	0.202	0.154	0.171	0.174	0.112	0.117	0.106	0.101
15	0.231	0.165	0.185	0.164	0.134	0.130	0.096	0.110
16	0.163	0.103	0.186	0.145	0.133	0.106	0.115	0.110
17	0.213	0.145	0.159	0.134	0.119	0.100	0.105	0.116
18	0.174	0.254	0.207	0.157	0.140	0.145	0.180	0.113
19	0.185	0.149	0.178	0.151	0.142	0.133	0.106	0.140
20	0.141	0.165	0.107	0.107	0.064	0.090	0.083	0.090
21	0.201	0.142	0.136	0.130	0.121	0.082	0.087	0.119
23	0.239	0.213	0.246	0.192	0.141	0.128	0.112	0.098
24	0.264	0.251	0.266	0.292	0.233	0.227	0.156	0.143
25	0.243	0.176	0.206	0.171	0.113	0.106	0.081	0.130
26	0.227	0.183	0.259	0.246	0.207	0.191	0.155	0.144
27	0.225	0.167	0.183	0.169	0.095	0.101	0.091	0.108
28	0.230	0.190	0.172	0.176	0.100	0.135	0.112	0.110
29	0.172	0.168	0.183	0.155	0.105	0.099	0.119	0.115
30	0.180	0.141	0.188	0.157	0.117	0.133	0.083	0.122
31	0.179	0.117	0.186	0.122	0.115	0.126	0.096	0.092
32	0.213	0.159	0.200	0.145	0.134	0.152	0.128	0.131
33	0.256	0.176	0.167	0.101	0.112	0.140	0.095	0.118
34	0.239	0.185	0.232	0.144	0.127	0.135	0.099	0.109
35	0.246	0.218	0.247	0.195	0.165	0.166	0.127	0.159
36	0.135	0.102	0.190	0.185	0.110	0.143	0.153	0.145
37	0.202	0.174	0.169	0.162	0.137	0.101	0.106	0.097
38	0.158	0.139	0.152	0.107	0.099	0.112	0.097	0.112
39	0.172	0.125	0.141	0.100	0.106	0.111	0.096	0.109
40	0.179	0.156	0.232	0.139	0.146	0.125	0.116	0.119
41	0.230	0.201	0.276	0.211	0.152	0.119	0.094	0.131
42	0.179	0.130	0.145	0.106	0.119	0.118	0.115	0.105
43	0.198	0.158	0.174	0.160	0.143	0.086	0.100	0.126
44	0.134	0.121	0.156	0.106	0.104	0.122	0.124	0.102
45	0.155	0.139	0.143	0.103	0.112	0.085	0.084	0.094
46	0.175	0.151	0.158	0.129	0.131	0.100	0.086	0.105
47	0.161	0.102	0.142	0.110	0.094	0.134	0.095	0.114
48	0.172	0.136	0.152	0.122	0.104	0.124	0.109	0.098
50	0.179	0.139	0.094	0.099	0.143	0.104	0.115	0.093
51	0.156	0.096	0.133	0.076	0.083	0.073	0.076	0.104
52	0.166	0.141	0.132	0.101	0.104	0.064	0.089	0.114
54	0.191	0.184	0.197	0.155	0.117	0.121	0.121	0.108
55	0.208	0.153	0.171	0.133	0.111	0.124	0.099	0.097
56	0.190	0.117	0.179	0.118	0.101	0.111	0.093	0.129
57	0.220	0.160	0.206	0.172	0.170	0.149	0.111	0.102
58	0.223	0.156	0.246	0.181	0.130	0.109	0.110	0.107
22A	0.252	0.181	0.182	0.142	0.119	0.115	0.086	0.097
22B	0.223	0.158	0.160	0.122	0.115	0.109	0.082	0.090
Statistics	**5/20/04**	**5/25/04**	**5/30/04**	**6/2/04**	**6/13/04**	**6/17/04**	**6/24/04**	**6/30/04**
Mean	0.200	0.158	0.180	0.146	0.124	0.120	0.105	0.113
SD	0.032	0.032	0.037	0.037	0.027	0.026	0.021	0.017
CV	6.305	4.960	4.794	3.914	4.548	4.576	4.918	6.816
Maximum	0.264	0.254	0.276	0.292	0.233	0.227	0.180	0.159
Minimum	0.134	0.096	0.094	0.076	0.064	0.064	0.076	0.087
Range	0.129	0.157	0.181	0.216	0.169	0.163	0.104	0.072
Observations	57	57	57	57	57	57	57	57

APPENDIX C

Time Series Spatial Maps of Measured Near-Surface Soil Moisture in the UDCEW During the 2003/2004 Water Year

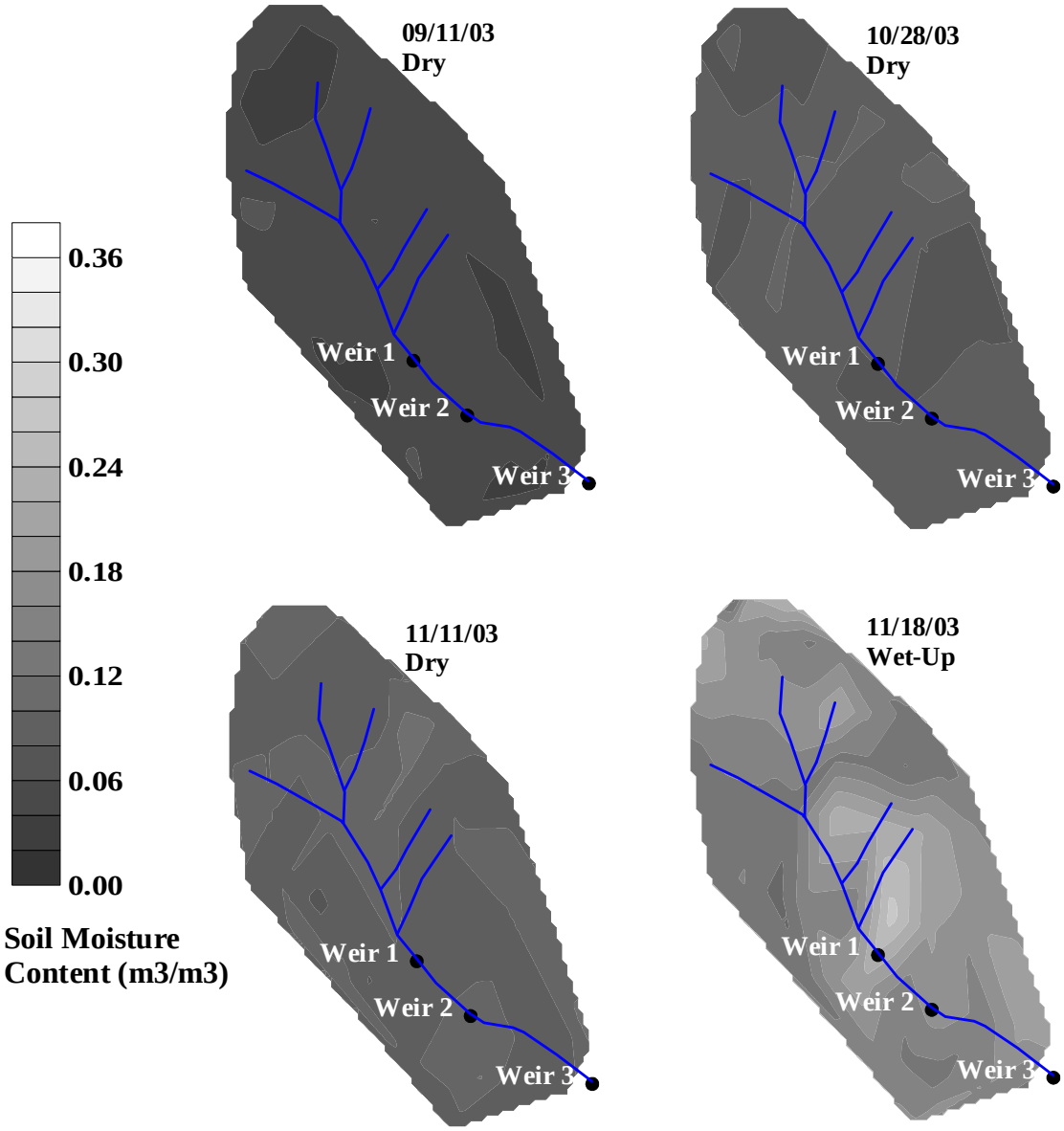
09/11/03
Dry
10/28/03
Dry
11/11/03
Dry
11/18/03
Wet-Up
Weir 1
Weir 2
Weir 3
0.36
0.30
0.24
0.18
0.12
0.06
0.00
Soil Moisture
Content (m3/m3)

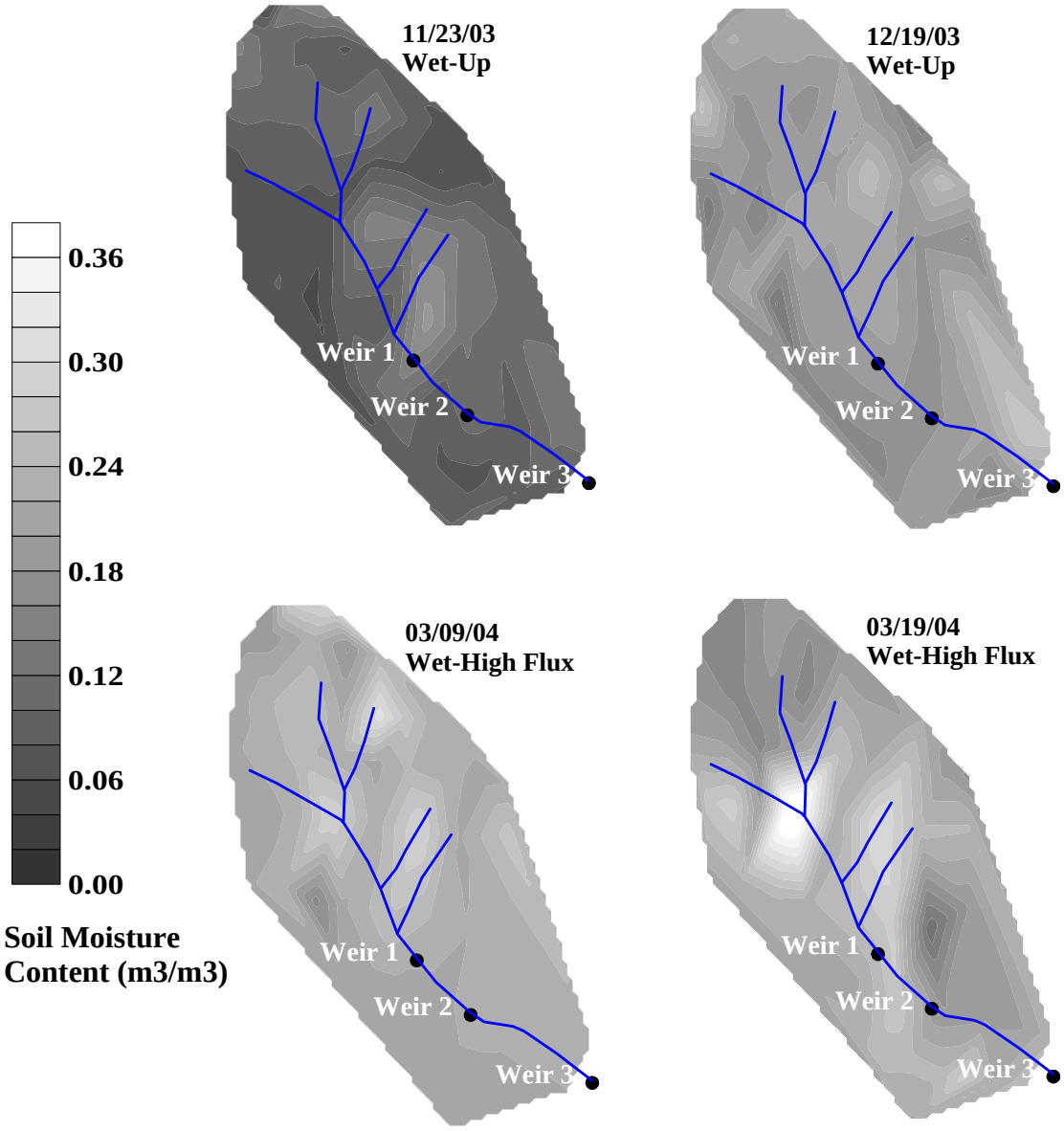
11/23/03
Wet-Up
12/19/03
Wet-Up
03/09/04
Wet-High Flux
03/19/04
Wet-High Flux
Weir 1
Weir 2
Weir 3
0.36
0.30
0.24
0.18
0.12
0.06
0.00
Soil Moisture
Content (m3/m3)

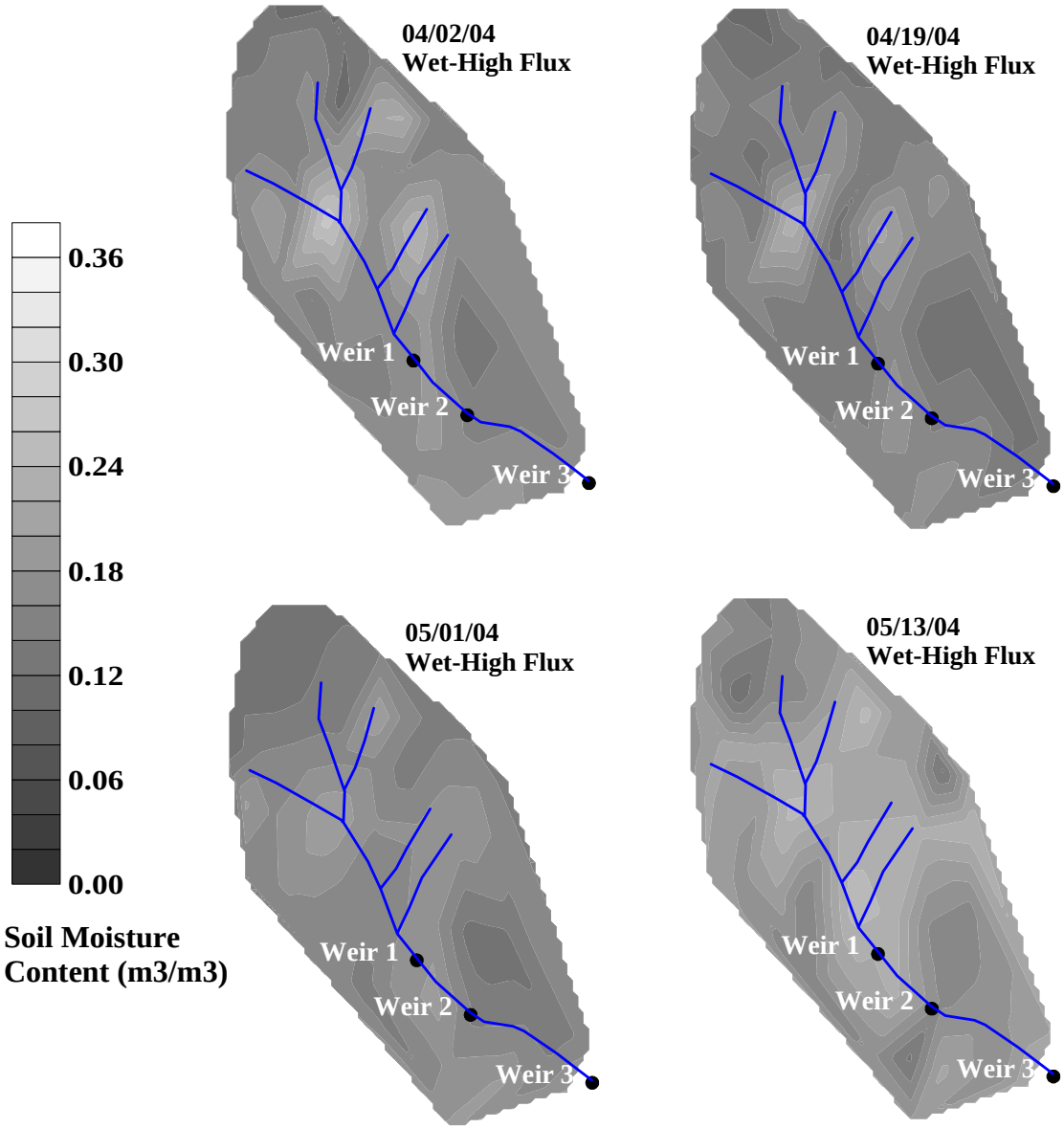
04/02/04
Wet-High Flux
04/19/04
Wet-High Flux
05/01/04
Wet-High Flux
05/13/04
Wet-High Flux
Weir 1
Weir 2
Weir 3
0.36
0.30
0.24
0.18
0.12
0.06
0.00
Soil Moisture
Content (m3/m3)

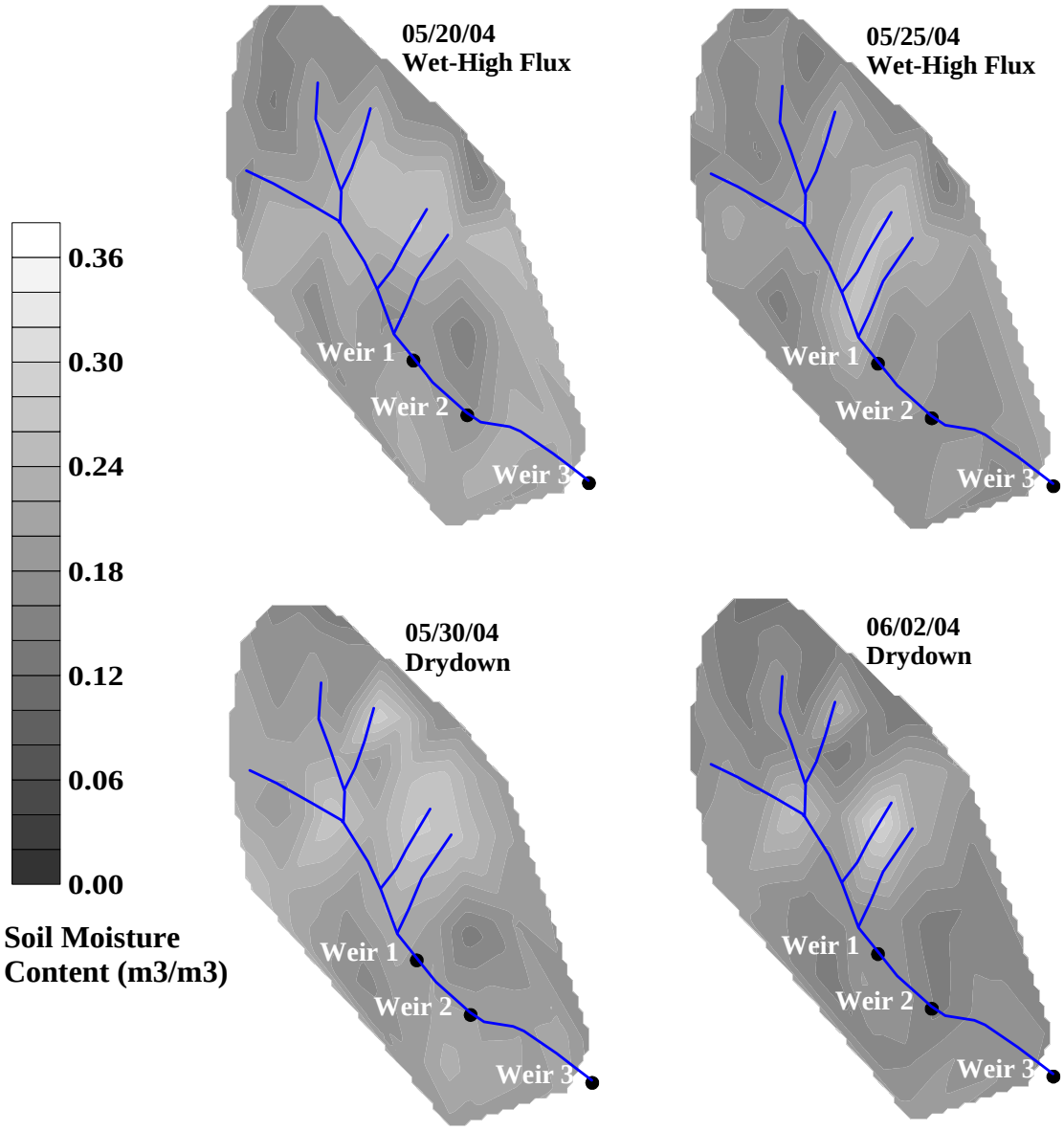
05/20/04
Wet-High Flux
05/25/04
Wet-High Flux
05/30/04
Drydown
06/02/04
Drydown
Weir 1
Weir 2
Weir 3
0.36
0.30
0.24
0.18
0.12
0.06
0.00
Soil Moisture
Content (m3/m3)

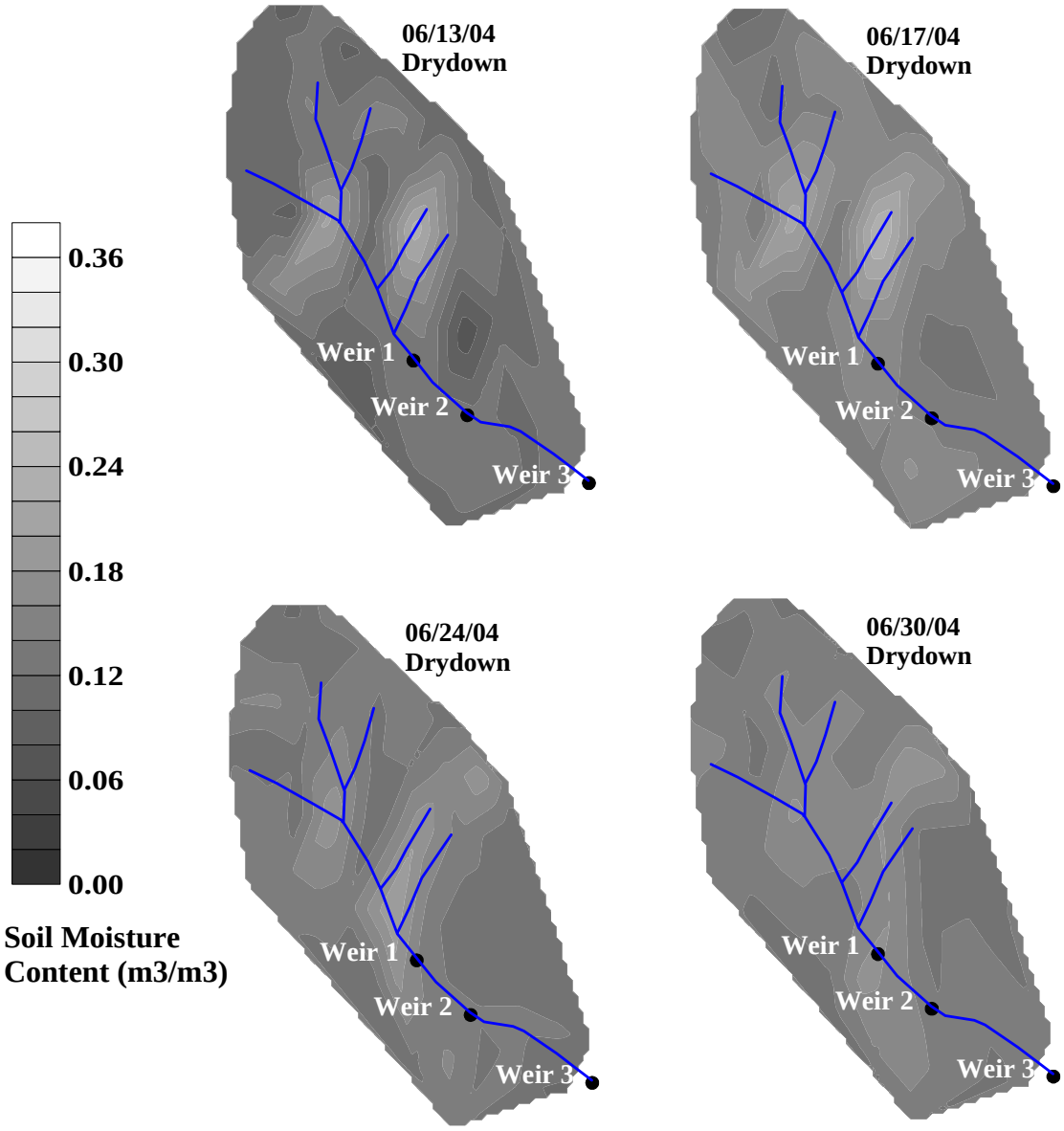
06/13/04
Drydown
06/17/04
Drydown
06/24/04
Drydown
06/30/04
Drydown
Weir 1
Weir 2
Weir 3
0.36
0.30
0.24
0.18
0.12
0.06
0.00
Soil Moisture
Content (m3/m3)

APPENDIX D

Time Series Spatial Maps of Simulated Deep Soil Moisture in the UDCEW During the 2003/2004 Water Year

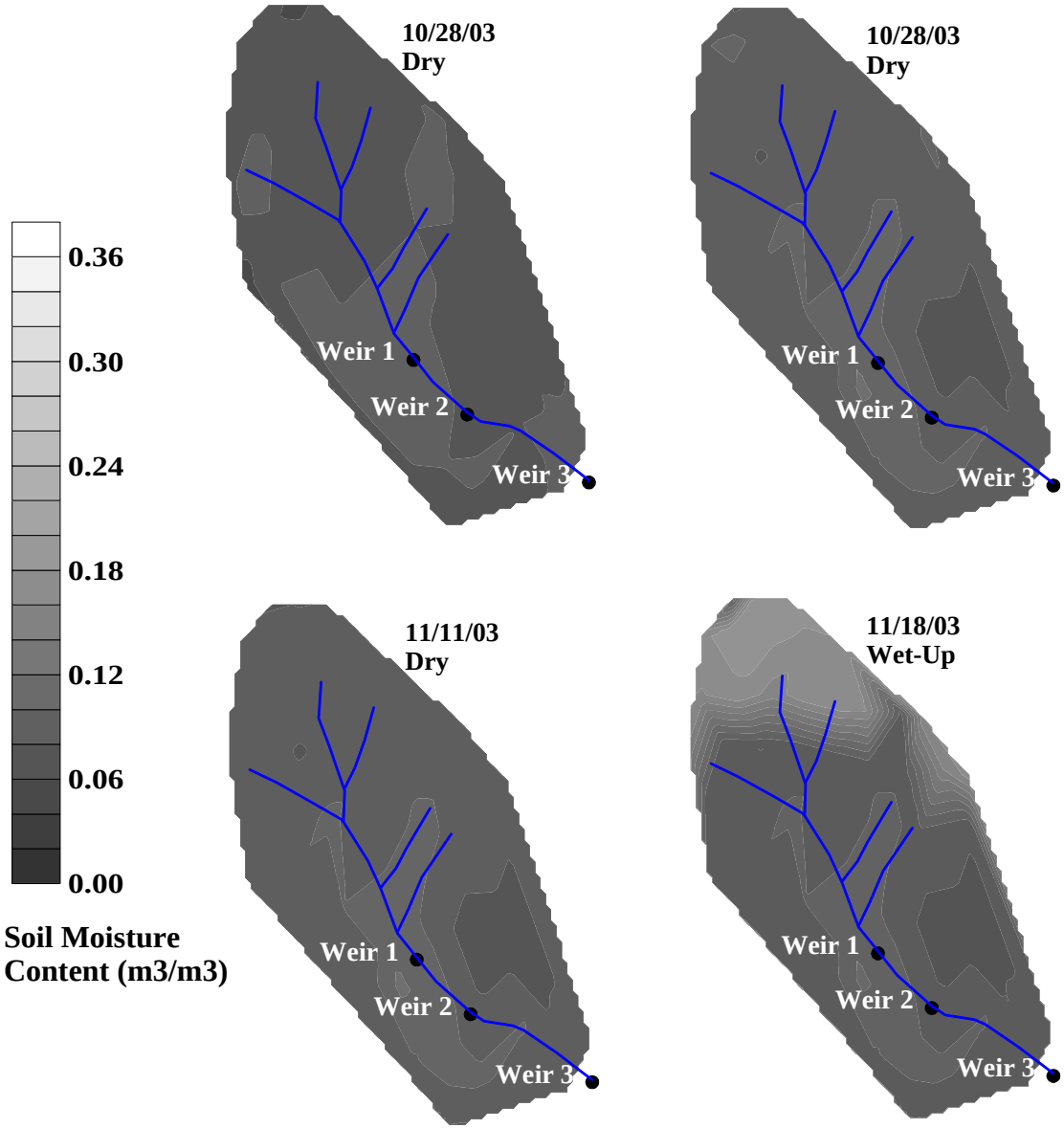
10/28/03
Dry
10/28/03
Dry
11/11/03
Dry
11/18/03
Wet-Up
Weir 1
Weir 2
Weir 3
0.36
0.30
0.24
0.18
0.12
0.06
0.00
Soil Moisture
Content (m3/m3)

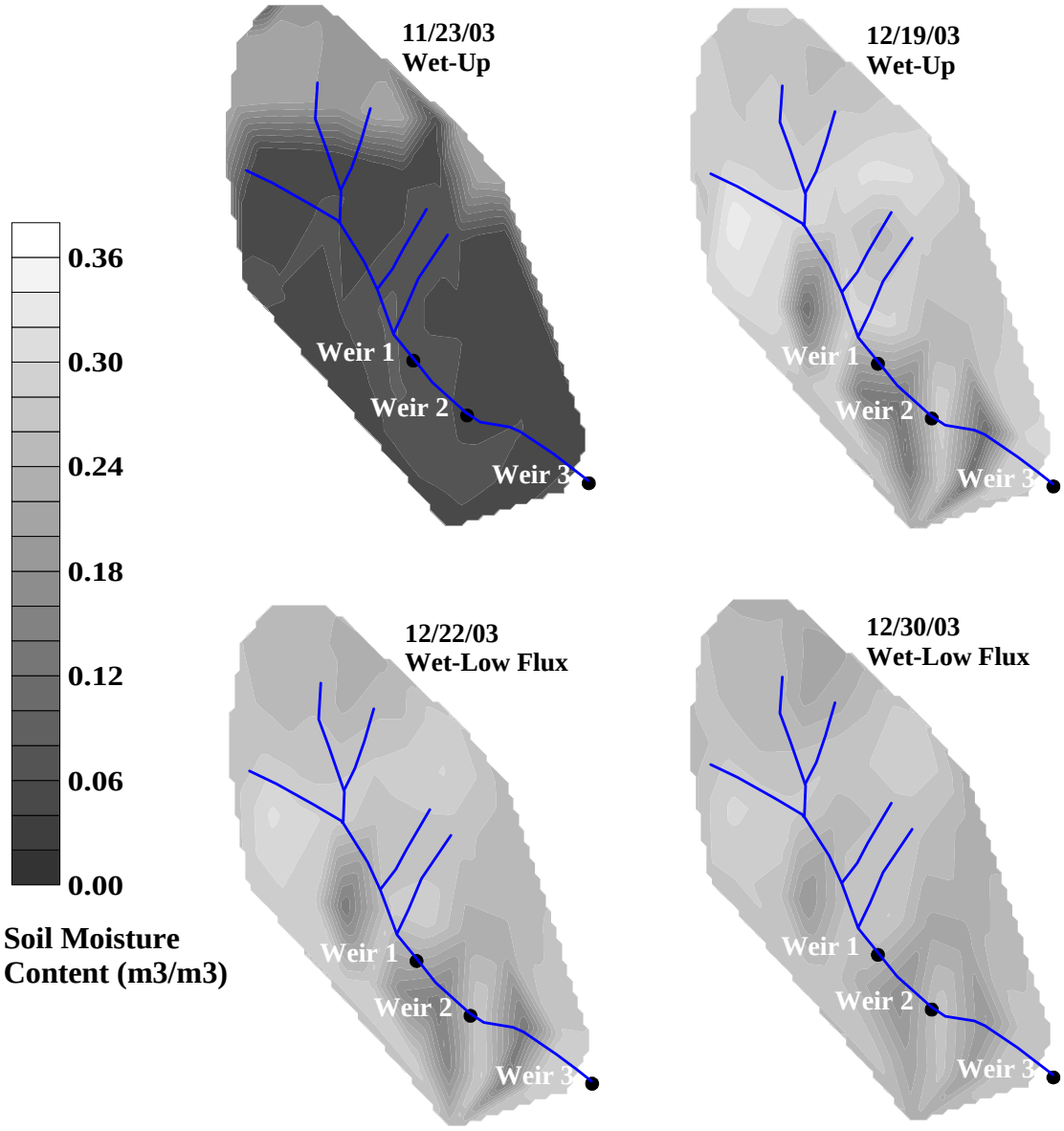
11/23/03
Wet-Up
12/19/03
Wet-Up
12/22/03
Wet-Low Flux
12/30/03
Wet-Low Flux
Weir 1
Weir 2
Weir 3
0.36
0.30
0.24
0.18
0.12
0.06
0.00
Soil Moisture
Content (m3/m3)

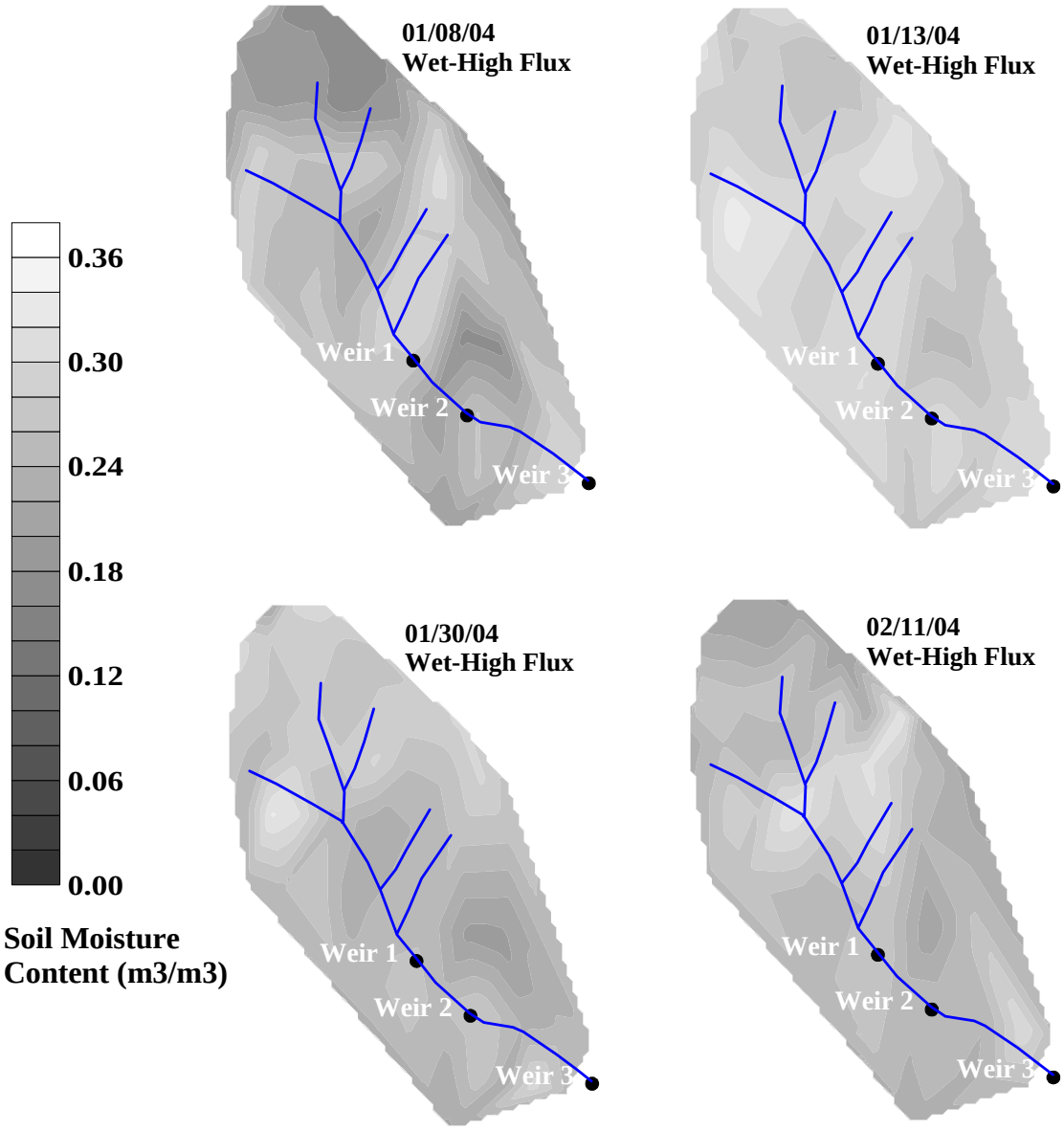
01/08/04
Wet-High Flux
01/13/04
Wet-High Flux
01/30/04
Wet-High Flux
02/11/04
Wet-High Flux
Weir 1
Weir 2
Weir 3
0.36
0.30
0.24
0.18
0.12
0.06
0.00
Soil Moisture
Content (m3/m3)

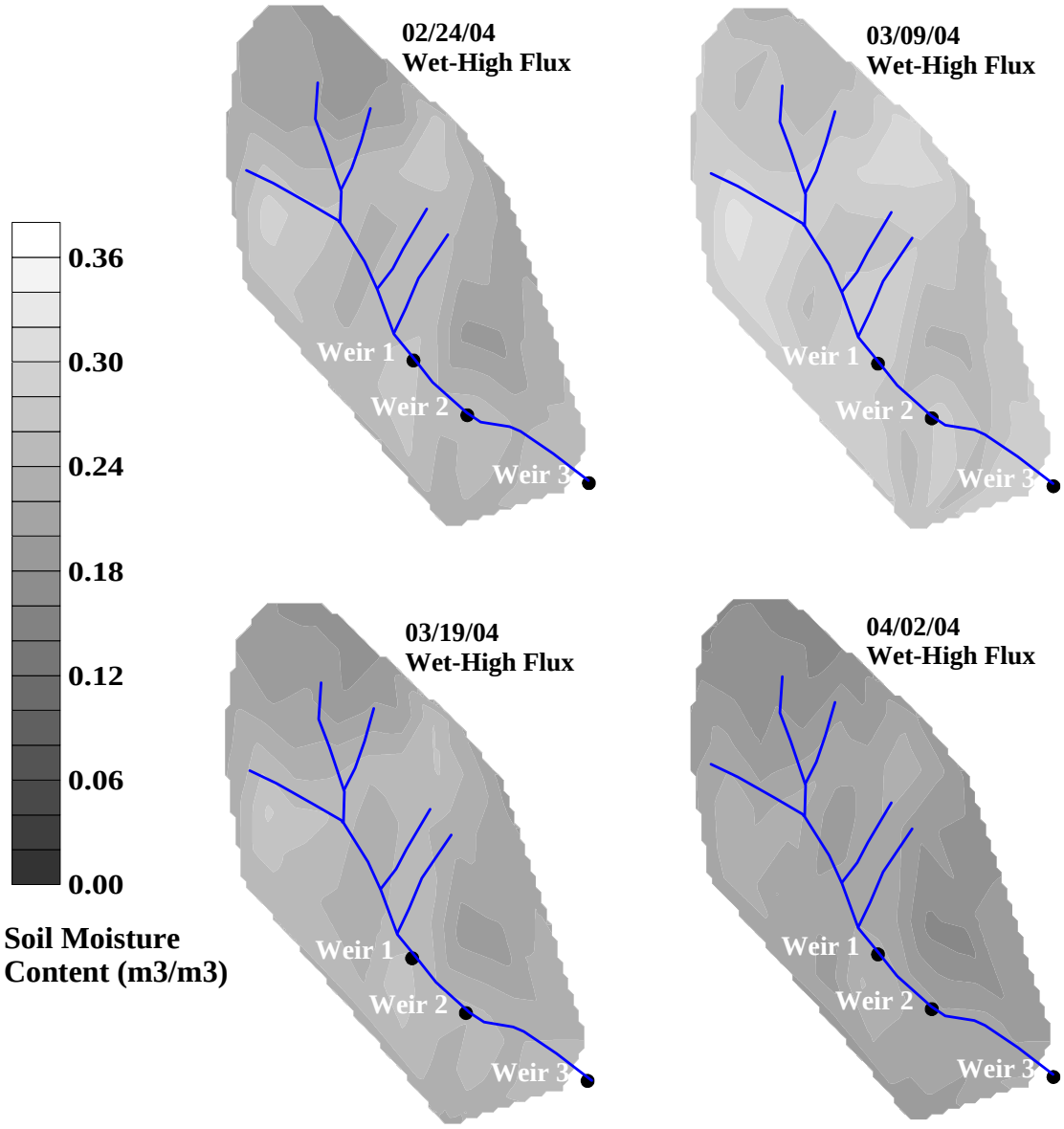
02/24/04
Wet-High Flux
03/09/04
Wet-High Flux
03/19/04
Wet-High Flux
04/02/04
Wet-High Flux
Weir 1
Weir 2
Weir 3
0.36
0.30
0.24
0.18
0.12
0.06
0.00
Soil Moisture
Content (m3/m3)

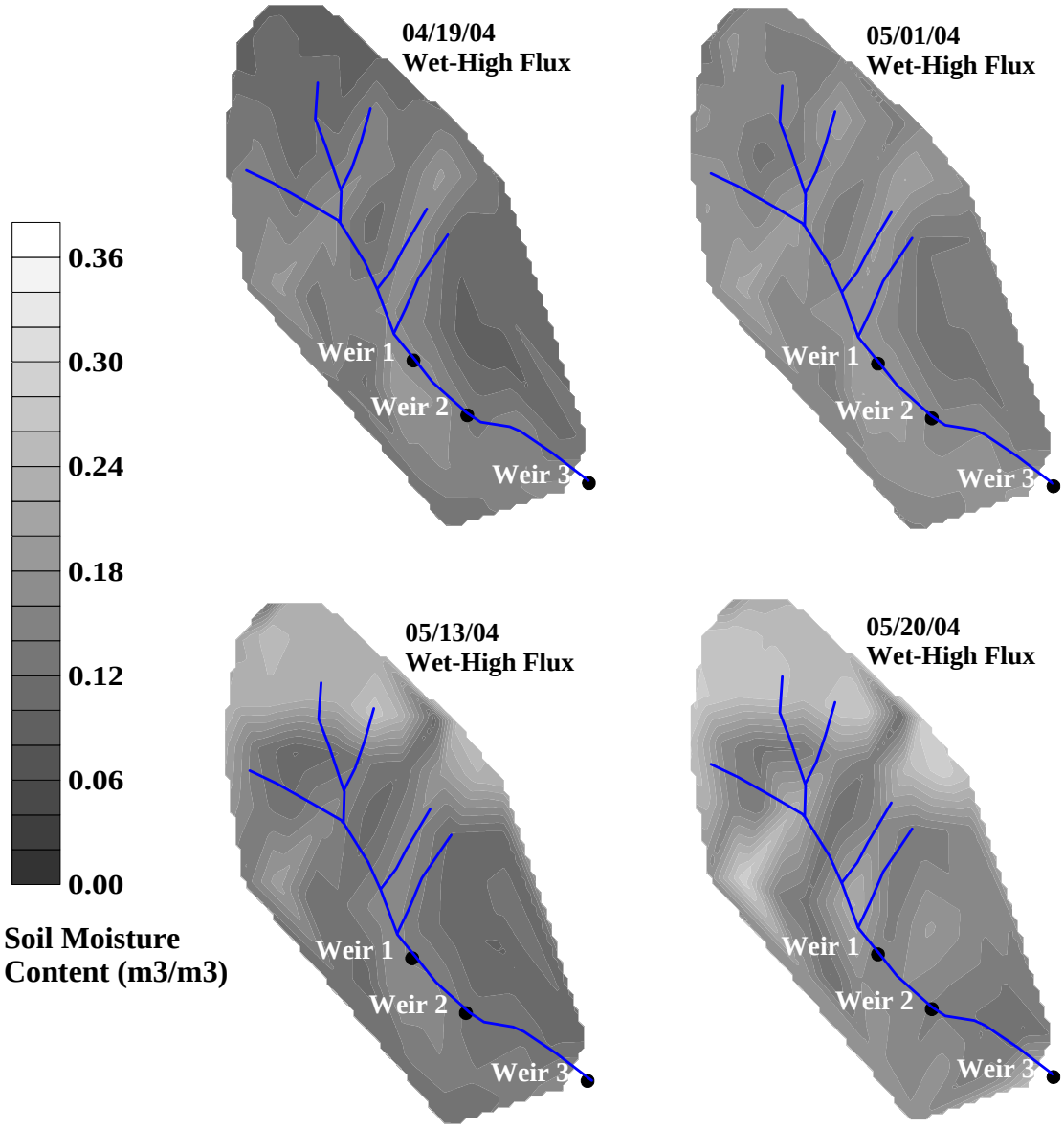
04/19/04
Wet-High Flux
05/01/04
Wet-High Flux
05/13/04
Wet-High Flux
05/20/04
Wet-High Flux
Weir 1
Weir 2
Weir 3
0.36
0.30
0.24
0.18
0.12
0.06
0.00
Soil Moisture
Content (m3/m3)

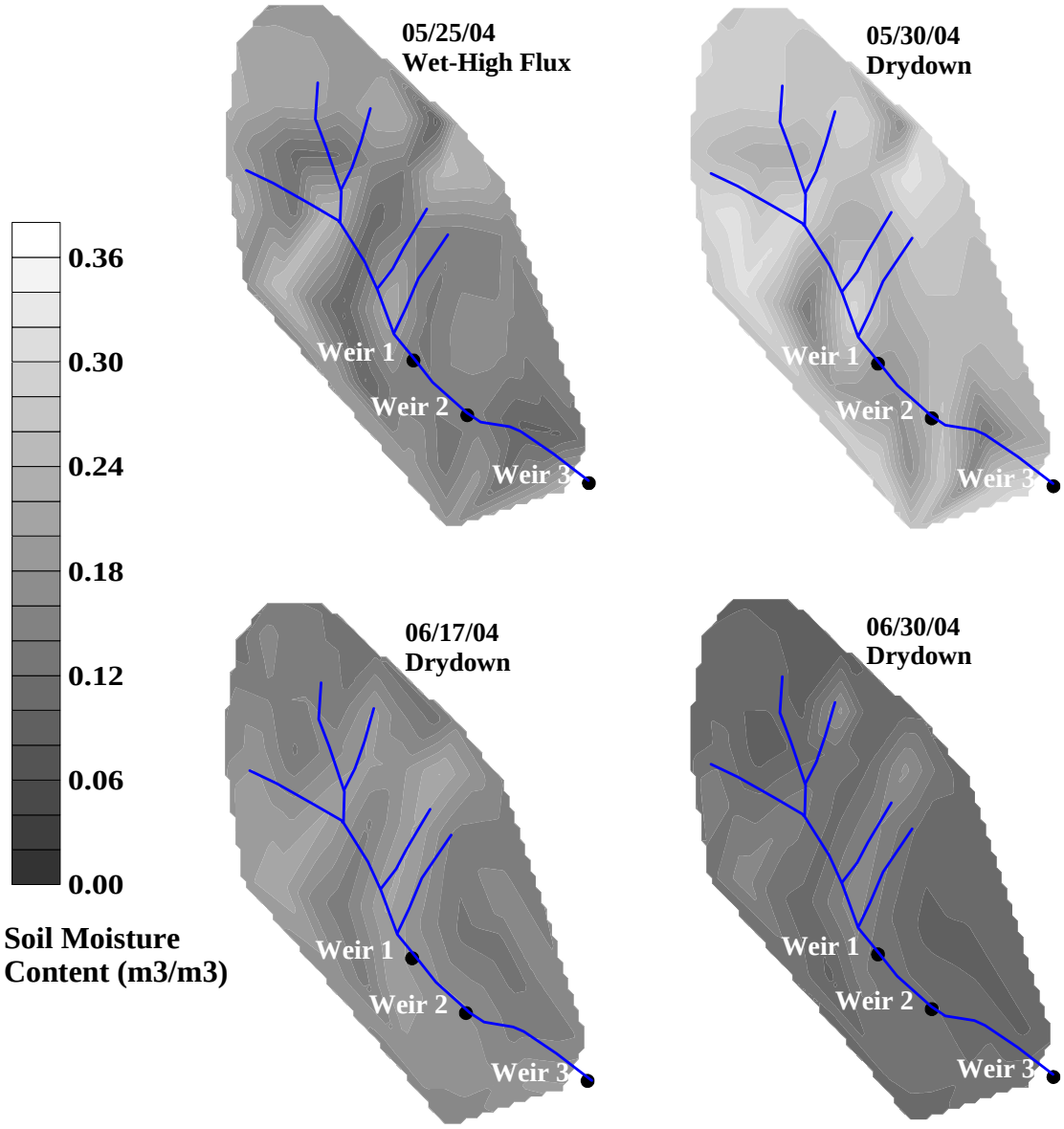
05/25/04
Wet-High Flux
05/30/04
Drydown
06/17/04
Drydown
06/30/04
Drydown
Weir 1
Weir 2
Weir 3
0.36
0.30
0.24
0.18
0.12
0.06
0.00
Soil Moisture
Content (m3/m3)